Möbius Structures on Surfaces

vorgelegt von
Diplom-Mathematiker
Claude Fabre
aus Draguignan / Frankreich

Von der Fakultät II - Mathematik und Naturwissenschaften
der Technischen Universität Berlin
zur Erlangung des akademischen Grades
Doktor der Naturwissenschaften
Dr. rer. nat.

genehmigte Dissertation

Promotionsausschuss:

Vorsitzender:	Prof. Dr. Günter M. Ziegler
Berichter:	Prof. Dr. Ulrich Pinkall
Berichter:	Prof. Dr. Konrad Polthier

Tag der wissenschaftlichen Ausprache: 18.11.2009

Berlin 2009
D 83

Contents

List of Figures

Introduction

As an alternative to TEICHMÜLLER's own compactification of Teichmüller space W. P. THURSTON elaborated a new compactification by the space of projective measured foliations, creating the operations of grafting/pruning and twisting along geodesics. In the electronic version of march 2002 of [36] Thurston's example 8.7.3 'Mickey mouse' visualizes in the Kleinian projective model the action of the quasi-Fuchsian group obtained when grafting along a single closed geodesic around a handle of a surface of genus two.

How would the picture look like in the conformal Poincaré model?
What would be the picture when using spiraling multiple leaved geodesics?

The visualizations we found do not go beyond showing multiple leaved geodesics on the 1-punctured torus without grafting/pruning or twisting. This made us curious to investigate further.

The realm we were entering covers Möbius geometry, Fuchsian groups and Cantor sets materialized as fractals. With the emergence of computer science a tremendous work has been achieved to visualize developments, where pioneers like POINCARÉ and KLEIN were handcuffed in their computations. In 2002 D. MUMFORD, C. SERIES and D. WRIGHT made the power of the 'Vision of Felix Klein' (the subtitle of *Indra's Pearls*) accessible to a public not familiar with Fuchsian groups. MANDELBROT with his fractals offered the beauty of geometry to non-mathematicians. He also tackled the visualization of Fuchsian groups. However we searched in vain for visualizations of THURSTON's new tools.

Nevertheless MANDELBROT or *Indra's Pearls* teach us that visualization is the best way to extract the beauty of geometry from its confinement in the heads of topflight mathematicians. COXETER motivated ESCHER to make infinity touchable. Maybe would artists like ESCHER or VASARELY have found some inspiration in the exploding picture of our frontispiece.

We were eager to fill a visualization gap, not to scrutinize hyperbolic three-manifolds. Two-dimensional hyperbolic and Möbius geometry applied on geodesics are enough to unveil some of the beauty hidden behind complex mathematical constructs.

The first obstacle we stumbled on was finding a widely available software. The proper choice seemed to be Mathematica®, but it offers no ready-made tools for hyperbolic geometry. This led us to elaborate a specific package, which we present in the last chapter.

In this paper accompanying the software we examine what happens when a surface of genus two – commonly a 'pretzel'– is cut along a simple closed geodesic in order to insert a small cylinder (grafting), remove it (pruning) or let both rims glide along each other (Dehn-twist or earthquake). The mathematical scissors are a Möbius transformation with variable a complex angle whose real part produces grafting/pruning and imaginary part twisting.

There are treasures to be discovered varying the parameters of our programs. Our paper can only show examples and present the software. Only self experimentation will reveal the world of grafting and twisting along geodesics.

The choice of the pretzel was motivated by the magic effects of its hyperelliptic involution, i.e. the identity map obtained when rotating the pretzel about a half turn around its axis of symmetry. The involution also operates on the 1-punctured torus, but it is much richer on the pretzel. Surfaces of higher genus, i.e. with more holes, miss these effects as they are in general not hyperelliptic.

The combination of hyperbolic and Möbius structures opens quite new fields, unsuspected in Euclidean geometry. There are infinitely many hyperbolic structures (articulated in the 6-$\mathbb{R}$- dimensional Teichmüller space). We wrote models visualizing a range of hyperbolic structures.

Grafting/pruning and twisting act on tilings of the Riemann sphere, as these operations are induced by pleating an hyperbolic plane in hyperbolic space. This leads to inflating, deflating, cleaving tessellations.

As the interest in visualization does not imply in general a profound knowledge of hyperbolic geometry we have grouped in chapter 1 the essentials on which the paper is built.

Another goal are propositions suggested by visualization, we were eager to investigate. So we fix the metrics across the grafted and pruned tile. We give a transverse measure for geodesic laminations. We study in detail the peculiar behavior of simple closed geodesics whose leaves rush swiftly against a 3-branched limit. A sequence of closed geodesics tends towards an infinite spiraling geodesic, the bending limit being a Cantor set. This is our proposition 22 on page 110.

Last but not least we take in the last chapter together with the appendices the opportunity of making available our Mathematica® package 'diskgeometry' for 2-dimensional hyperbolic and Möbius geometry.

Chapter 1.

Preliminaries

The object of this chapter is to gather statements and results we shall need across this paper. We do not only recall basic information about hyperbolic geometry, Cantor sets or fractals. We also prove propositions which not everybody might find trivial and on which later proofs are based. The intention is to avoid interrupting the flow of future demonstrations.

1.1. From a surface to its cover

The common torus with a single hole is obtained by identifying the sides of a parallelogram, e.g. a square. Copies of this tile put together give a **tessellation** (or **tiling**) of the Euclidean plane, which is the **universal cover** of the torus. This comes up to unrolling it infinitely often onto the plane. As the universal cover is simply connected the map has both advantages of being flat and without hole. Several circuits around the torus can easily be traced throughout the copies. The torus can be seen either as square tiles tessellating the plane or as a **fundamental domain** (here the canonical square) with identified edges. Flat men wandering around could not make out any difference, whether they creep along the torus or along its universal cover. This representation of the flat torus helps us visualizing, although the torus of the standard space has not constant zero curvature. In fact the flat torus lives in $\mathbb{S}^3 \subset \mathbb{R}^4$.

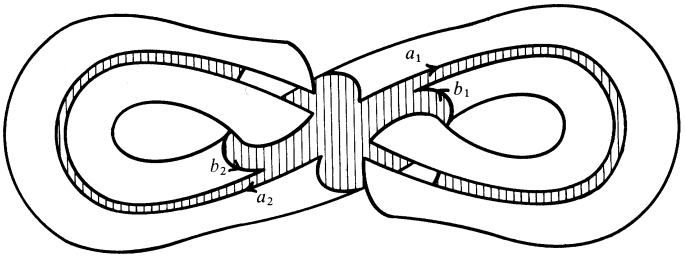

Figure 1.1.: Cutting a pretzel

The **pretzel**, more formally **double torus**, is a compact Riemann surface of genus two. Like a decoupage starting and ending in one and the same point makes the simple torus to a topologically flat square, the pretzel can be shaped from one point into an octagon as in figure 1.1 borrowed from [35, Stillwell]. This is the usual cutting, but we shall show other models with more than a single vertex and other (even not topological) polygons.

It is convenient, but not necessary as we shall see, to choose a regular hyperbolic octagon to represent the pretzel. The regular octagon cannot tessellate the Euclidean

plane and the pretzel can any way not be developed on the Euclidean but only on the hyperbolic plane, where it can be endowed with a hyperbolic metric, i.e. a metric of constant negative curvature. This means that the pretzel, as a visualization, is homeomorphic but not isometric to a hyperbolic octagon. This inconvenience can be overcome as we work with a conformal mapping distorting distances but not angles (much like flat maps of the earth). Closed geodesics or simple geodesics will remain closed or simple. This is what matters to us.

In Euclidean geometry one cannot tessellate the plane with octagons, as 135° is not a submultiple of 360°. Not much the same in hyperbolic geometry, where you can shrink angles just by enlarging the polygon, until they fit nicely around a vertex.

This is, what we show in figure 1.2, using the **Poincaré-disc** as a model for the hyperbolic plane $\mathbb{H}^2$. The tessellated hyperbolic plane is the universal cover of the pretzel, like the Euclidean plane is the universal cover of the torus. Like the torus inherits the flat metric of its cover, the tori of genus ≥ 2 can be endowed with a hyperbolic metric (not only one as we shall see).

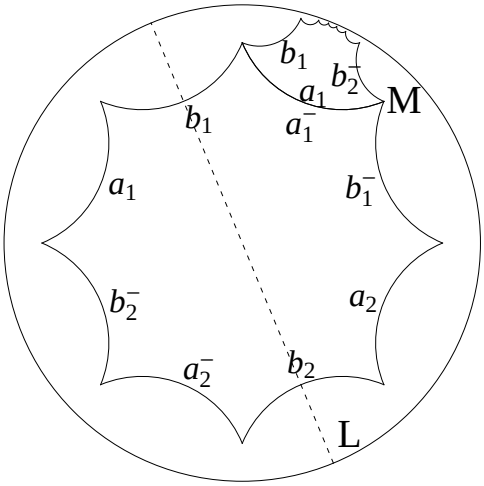

Figure 1.2.: Moving the fundamental tile

Figure 1.2 shows an octagon following the cuts of the pretzel along the four **generators** a_1, b_1, a_2, b_2 of the **fundamental group**. In the notation of the figure a_i^- is the edge a_i with reversed orientation. Later on we shall write $A_i := a_i$ instead of this classical notation. This proves to be much more convenient especially for programming.

The 'smaller' octagon is hyperbolically congruent to the central one, even if it does not seem so to our Euclidean eye. With a slight abuse of notation we also call a_1, b_1, a_2, b_2 and their inverses the **deck transformations**, which as automorphisms of the cover (*Decke* in German) map the fundamental domain across its edges to isometric copies.

All octagons of a tessellation are obtained by composing deck transformations across the edges. Using letters for the generators of the fundamental group we call **word** a composition of letters mapping the canonical octagon to an isometric copy somewhere in the disc.

Due to symmetry the small octagon seems to be obtained by mirroring the large one against the edge a_1^-. This does the job only visually, because reflecting inverses orientation. Our moves should not have an odd number of reflections, as we want to express them as Möbius transformations. Therefore we first mirror the large octagon

along its axis of symmetry L so as to exchange a_1^- and a_1. Two reflections lead back to the original orientation to be preserved in order to get a true moved copy.

Applying longer and longer words we would obtain a tessellation of the unit disc with regular 45°-angles octagons, i.e. eight octagons fit nicely around a vertex.

As we can choose the angles of the main hyperbolic octagon in the range 0°-135°, there are other ways to pave the disc with regular octagons. But we have to care for the proper match: due to the identifications the same edge has to be a_i on one side and A_i (this means now a_i^-) on the other. We therefore need a cycle of period 8, which can be achieved by no else tessellation than this one.

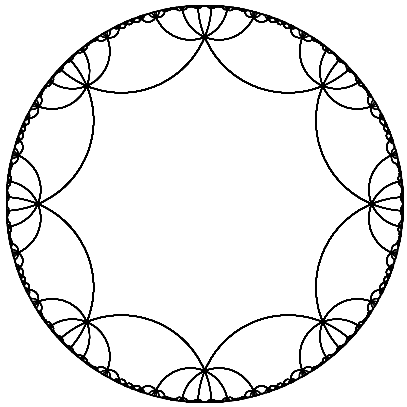

Figure 1.3.: Tessellation by octagons

Figure 1.3 shows the tessellation, which we now shall examine from a formal point of view.

The generators a_i, b_i and their inverses A_i, B_i can be taken as matrices of SL(2,$\mathbb{C}$). This is the group of 2×2 complex matrices with determinant $= 1$, so as to make the matrix unique (up to multiplication with -1) when it encodes a Möbius move. We also call these matrices a_i and b_i with a slight abuse of notation.

These mappings form a transformation group, the action of which on the canonical octagon generates the tessellation of the disc.

To move from the central canonical octagon to any copy, one has to compose the mappings to a word : $w = (x_{i_1}, \ldots, x_{i_k})$ with $x_i \in \{a_1, b_1, a_2, b_2, A_1 B_1, A_2, B_2\}$ according to orientation. Such a word is usually not commutative.

We call **relation** a constraint $w = 1$ for a word w. The neutral element, i.e. the path shrunk to a point, is notated 1. The trivial relations $a_i A_i = b_i B_i = 1$ are always satisfied. When there are no further relations the group is called a **free group**. For instance the group of the punctured torus is free.

When a group is not free the **commutator** $[a, b] := abAB$ gives a hint, how much ab differs from ba, because $[a, b]ba = abABba = ab \rightsquigarrow ba = ab$ for $[a, b] = 1$. We shall see that the group generating the tessellation for the pretzel is *not* a free group. But it is a **discrete** (or **discontinuous**) group, which means that the orbits, i.e. the sequences of images of a point of the octagon under the action of the group, form a discrete set. In other words there is around every image of a point in the orbit a neighbourhood containing no other point of the orbit. In the present case this is obvious as all the octagons are congruent.

Discrete groups which act on the sphere $\mathbb{S}^2$ by Möbius transformations, are called **Kleinian** groups. The Möbius transformations lie in $PSL(2,\mathbb{C})$, the projective subgroup of $SL(2,\mathbb{C})$. This action can be extended to all of $\mathbb{H}^3$. Poincaré proved that this is the group of orientation preserving isometries of $\mathbb{H}^3$ identified via the action on the sphere at infinity $S^2 \cong \mathbb{C}P^1$.

Kleinian groups with a (round) circle $\mathbb{S}^1$ as limit set are called **Fuchsian** groups. The unit circle being the limit set of the octagonal tiling this group is Fuchsian.

Briefly again: the transformation group of Möbius transformations generated by the a_i and b_i is a non-free discrete Fuchsian group acting on the points of the canonical octagon.

1.2. Möbius transformations

A **Möbius transformation** is a bijective conformal mapping of the **Riemann sphere** $\mathbb{C}P^1$, i.e. the complex plane extended by a point ∞.

They have the form of linear fractional complex transformations $z \mapsto \frac{az+b}{cz+d}$, where a, b, c, d are complex numbers and $ad - bc \neq 0$.

They can be expressed as a composition of inversions and form then a group, the **Möbius group**, acting on the Riemann sphere. The Möbius group is the automorphism group of $\mathbb{C}P^1$.

Being conformal Möbius transformations preserve angles, i.e. shapes but for the deformations of length. They also preserve the cross ratio, but we shall not use explicitly this property. They send extended circles to extended circles, an extended circle being indifferently a circle or a line.

$\mathbb{C}P^1$ can be seen as the set of complex lines (1-dimensional complex subspaces) into which the complex plane embeds naturally. The embedding maps a point $z \in \mathbb{C}$ to the complex line, i.e. a point of $\mathbb{C}P^1$, spanned by $(z, 1)$. We can define a point by its **inhomogeneous coordinates** z as well as by its **homogeneous coordinates** (zt, t), t being a non zero complex number. The subspace spanned by $(1, 0)$ is the point ∞.

The idea behind this is to see the Möbius transformations as projective transformations of $\mathbb{C}P^1$, obtained from an invertible linear map of $\mathbb{C}^2$. Then Möbius transformations are complex 2×2 matrices which can be composed by multiplication. Instead of using fractions the matrices act on the homogeneous coordinates and the result is passed to the quotient, so returning the complex number representing a point of the orbit.

Identifying scalar multiples and choosing determinant $= 1$ the matrices of Möbius transformations form the group $PSL(2,\mathbb{C})$, i.e. projective, complex, unit determinant, we shall work with throughout this paper.

Poincaré proved that $PGL(2,\mathbb{C}) \supset PSL(2,\mathbb{C})$ is the group of orientation preserving isometries of $\mathbb{H}^3$ identified via their action on $\mathbb{C}P^1$. This means that the tessellations we shall construct on the Riemann sphere reveal the behavior of the transformations of the underlying hyperbolic space. This will be the link between the lunes of grafting and pruning on $\mathbb{C}P^1$ and the pleating of hyperbolic planes in hyperbolic space.

We are much obliged to Charles Gunn of TU-Berlin for the views of figure 1.14 on page 18, a wonderful rendition of our 4-colored dodecagon model.

Four different colors are given to the front and the back of the both pairs of pants of the pretzel where three side lengths can be chosen. In this projective Kleinian ball geodesics are straight lines and planes are flat (but angles are distorted). Thus a tiling of the Kleinian disc on our sheet of paper is truly flat to the Euclidean eye. In the Poincaré disc on $\mathbb{C}P^1$ grafting produces lunes. The many lunes push away the unit circle whose boundary appears as bubbles riding on bubbles like Mickey Mouse ears. $\mathbb{C}P^1$ is the sphere at infinity of the hyperbolic ball. The lunes on $\mathbb{C}P^1$ correspond to the bends of the hyperbolic plane supporting the tessellation. Also the cleaving earthquake along the geodesic is good to see thanks to the tile having been cut into four colored parts.

1.3. Hyperbolic geometry

1.3.1. Hyperbolic metric of $\mathbb{H}^2$

Beltrami made hyperbolic geometry easier to grasp by presenting a surface locally isometric to the hyperbolic plane: the **pseudosphere**. The isometry is only local because the pseudophere (i) is a cylinder wrapped around an axis and (ii) ends abruptly at its border. Nonetheless it has like the hyperbolic plane constant negative curvature, i.e. one can cut out a patch and move it around. It will lie nicely on the surface without stretching or shrinking.

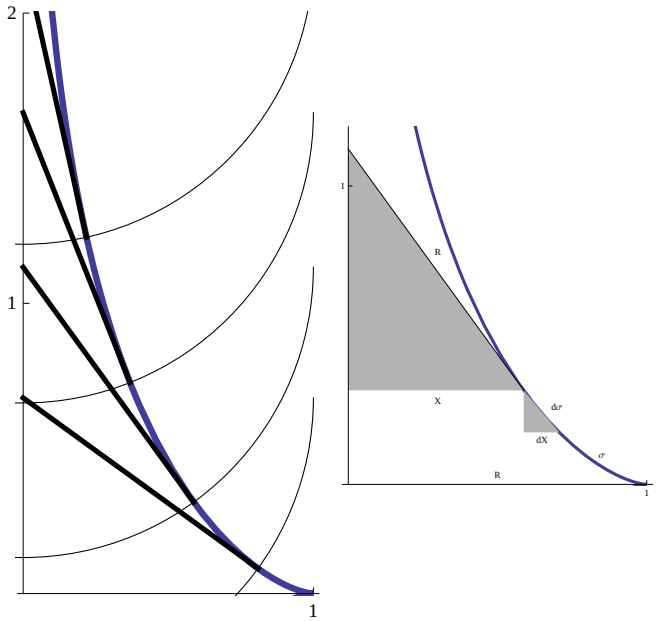

Figure 1.4.: Beltrami's pseudosphere

The pseudosphere is generated by rotating a **tractrix**, around the y-axis. The tractrix, or curve of pursuit, is the curve a toy describes, when a child drags it with a stiff shank, turning orthogonally from his initial direction. An easy way to approximate the tractrix is to take a family of circles of same radius all centered on the ordinate axis and draw the curve orthogonal to the family of circles as in figure 1.4. We can understand figure 1.4 as an orthogonal planar front projection of the pseudosphere or as a vertical cut along a meridian and the axis.

Without loss of generality we scale with unitary radius. We may also parametrize by curve length and compute the distance from the x-axis along the curve. When moving an infinitesimal distance dx along the x-axis $d\sigma$ is the linearization of the curved path σ. Due to similarity of the gray triangles:

$$\frac{dx}{d\sigma} = -\frac{x}{R} \rightsquigarrow x = Re^{\frac{-\sigma}{R}} + const$$

For the choice $R = 1$ and $const = 0$ follows $x = e^{-\sigma}$.

We now go over from the pseudosphere to the planar chart of the hyperbolic halfplane model. The points (x, σ) lies on the latitude circle of radius x at the distance σ measured along the tractrix from the boundary on the pseudosphere.

The points (x, σ) and $(x + dx, \sigma)$ make an angle dx seen from the midpoint of the latitude circle. Hence their distance on the pseudosphere is xdx. This is how hyperbolic metric shrinks Euclidean objects when they move towards the unit circle at infinity.

On the chart all points with the same latitude have the same ordinate. The chart being conformal infinitesimal lines in whatever direction are multiplied by the same factor $\frac{1}{x} = e^{\sigma}$. For some $d\hat{s}$ on the pseudosphere we get $d\hat{s} = xds$ on the chart. Consequently the chart ordinate y of the point (x, σ) on the pseudosphere is given by

$$\frac{dy}{d\sigma} = \frac{1}{x} = e^{\sigma} \rightsquigarrow y = e^{\sigma} + const$$

We are free to set $const = 0$.

This is the metric $d\hat{s} = \frac{ds}{y} = \frac{\sqrt{dx^2+dy^2}}{y}$ in the half plane model of the hyperbolic plane. With this metric we get readily the h-distance between points on a vertical geodesic:

$$d(x + iy_1, x + iy_2) = |\int_{y_2}^{y_1} \frac{dy}{y}| = |\log \frac{y_1}{y_2}| \tag{1.1}$$

1.3.2. Horocycles

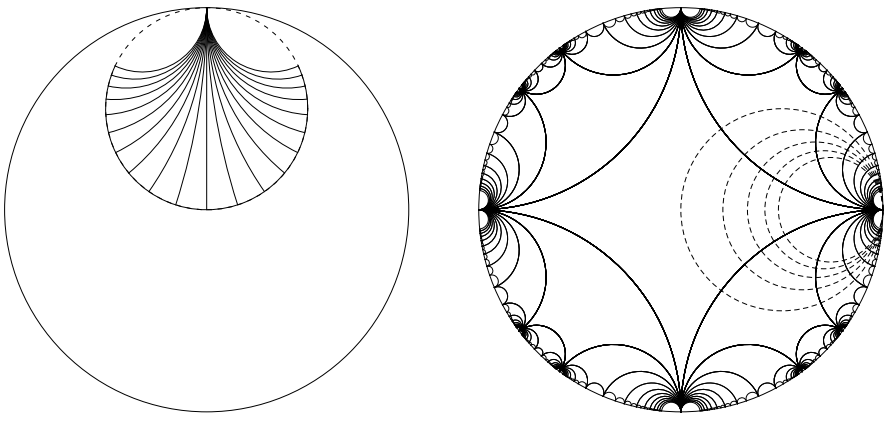

Figure 1.5.: Horocyles and 1-punctured torus

As we shall mostly use the Poincaré disc model, we now show why the open unit disc is a covering space of the pseudosphere.

David Hilbert was first to prove that it is impossible to embed the entire hyperbolic plane isometrically in Euclidean space, i.e. not only the pseudosphere has a boundary.

Recall an **horocycle** is a geometric object specific to hyperbolic geometry, a circle with its centre at ∞. In the disc model it appears as an Euclidean circle tangent to $\mathbb{S}^1_\infty$ in its centre. In the half plane model $\mathbb{H}^2$ it is an Euclidean horizontal line.

We can map isometrically the pseudopshere into $\mathbb{D}^2$, if we open it along a meridian. In the half plane model we take as horizontal coordinate the angle in $[-\pi, +\pi]$ around the axis of symmetry in order to make a full turn across the surface. The Möbius transformation $z \mapsto \frac{iz+1}{z+i}$ maps the half plane onto $\mathbb{D}^2$. It sends the horocycle supporting $\{-\pi + i, i, \pi + i\}$ to the horocycle through the origin and the cusp point i. Figure 1.5 shows the image of the pseudosphere in $\mathbb{D}^2$. We have added geodesics in steps of $\frac{\pi}{10}$ for better visibility. When mirroring against the boundaries the entire horocycle would be tiled by all layers of the pseudosphere. This makes clear how the Poincaré model extends Beltrami's pseudosphere from the interior of the horocycle to the whole interior of $\mathbb{D}^2$, i.e. beyond Hilbert's limit.

Figures 1.4 and 1.5 were made with the program Traktrix_ etc.

On the right of figure 1.5 we see a 1-punctured torus with a family of horocycles spiraling around the puncture within the horocycle through the origin. Each horocycle corresponds to the infinite sequence of neighbouring copies of latitude circles centered on the axis of the pseudosphere. Geodesic meridians and horocycles of the pseudosphere build a system of orthogonal circles. All the horocycles are orthogonal to all geodesics aiming at the point at infinity.

The image of the open end of the pseudosphere is called a **cusp**. The neighbourhood of the puncture of the 1-punctured torus in Figure 1.5 is also a cusp. The family of horocycles spirals around the puncture. This tessellation fills in the whole unit disc. The cusp is analogous to the infinite end of the pseudosphere, or more generally to a cuspy neighbourhood of a point at infinity entered by disjoint geodesics. When examining a transversal to a geodesic lamination, we shall meet again such a cuspy neighbourhood of a point at infinity entered by disjoint geodesics orthogonal to horocycles but in the half plane model.

1.3.3. Geodesic laminations

We state some important results indicating the references of the sources.

A *lamination* of a surface S is a one dimensional foliation of a closed subset of the interior of S.

The flow lines of a nowhere vanishing vector field form a **foliation**. Figure 1.6 is borrowed from *Three-Dimensional Geometry and Topology* [36, Thurston]. We see the flow lines of a constant vector field $X(x, y) = (1, \alpha)$ on the torus $T^2 = \mathbb{R}^2/\mathbb{Z}^2$, i.e. the images of straight lines $y = x + y_0$ on T^2. The two fatter leaves are circles. There are two other leaves spiralling around and accumulating onto the circles. A foliation provides a visualization of the underlying surface.

A m-geodesic lamination for a hyperbolic metric m on S can be decomposed as the union of a family of *disjoint simple geodesics*. The disjoint simple geodesics whose union constitute the lamination λ are called the **leaves** of the lamination. A **simple**

geodesic is a geodesic not intersecting itself. It is either closed or infinite. Components of the boundary ∂S are allowed but no geodesic transversal to ∂S. The decomposition of a geodesic lamination as a union of disjoint simple geodesics is unique.

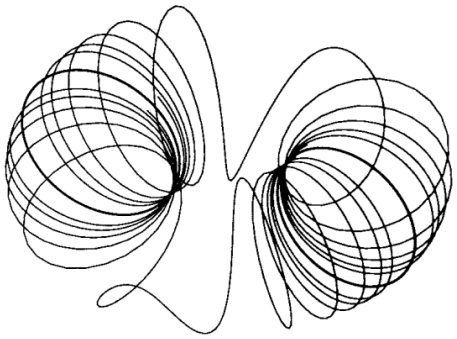

Figure 1.6.: Foliation of the torus by THURSTON

A theorem in [10] states:

Theorem 1 (Canary, Epstein, Green)**.** *There exists on the hyperbolic plane a constant C with following property. Let $d(.,.)$ be a distance function. If the geodesic g has unit tangent vector v in a point x and the geodesic h a unit tangent vector w in the point y, and g and h are disjoint, then $d(v, \pm w) \leq Cd(x, y)$.*

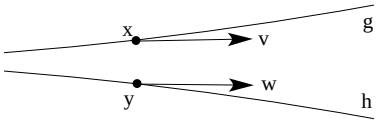

Figure 1.7.: Converging vector fields

Consequently when g and h are disjoint, the unit tangents to g and h induce a **Lipschitz direction field**. This notion of nearby parallelism allows to cover a surface with a lamination, i.e. a system of simple geodesics. More precisely:

Definition 1. *A geodesic lamination λ on a surface S is a lamination whose leaves are simple geodesics. If a closed subset λ of S is the disjoint union of simple (closed or infinite) geodesics, then λ is a geodesic lamination.*

A lamination can eventually consist of sublaminations. The geodesic lamination is called **minimal** when it does not contain any proper sublaminations.

[5, Bonahon] proves : **A geodesic lamination is the disjoint union of *finitely many* sublaminations and of *finitely many* isolated leaves.**

Each end of an infinite isolated leaf spirals along a unique minimal sublamination.The existence of only a finite number of sublaminations will prevent from pleating for ever. Simple closed geodesics are uncomplicated laminations.

Contrary to what intuition might suggest simple geodesics on a surface are not common. F BONAHON proves in [5] : **If the geodesic lamination λ has no isolated**

leaves, then for every arc k transverse to λ the intersection $k \cap \lambda$ is a Cantor set.

The proof uses a result of [Bi,Se2]: **The union of all simple geodesics has Hausdorff dimension 1.** In other words, it is countable. Consequently the union of all geodesic laminations has Hausdorff dimension 1 as well.

Measuring laminations

Consider a lamination of the pretzel. We already stated a result of BONAHON: A geodesic lamination is the disjoint union of *finitely many* sublaminations and of *finitely many* isolated leaves. The simplest example of a transverse measure is counting the number of intersections of a transversal τ with λ. We know that grafting/pruning inserts a wedge which is the spur on $\mathbb{C}P^1$ of bending the plane in $\mathbb{H}^3$ along a geodesic lamination. As the lamination λ has finitely many leaves there are finitely many bends.

Consider a bend between two flat pieces (in the projective model of $\mathbb{H}^3$). When two planes meet along a geodesic, the angle α they form is constant along that geodesic. The angle α of meeting of two such planes is a **transverse bending measure**, say $\mathfrak{B}$, for the lamination λ . Then $\mathfrak{B}(\tau)$, transverse to λ, is the total angle of turning of the normal to the plane along τ. When three planes have pairwise intersections in $\mathbb{H}^3$

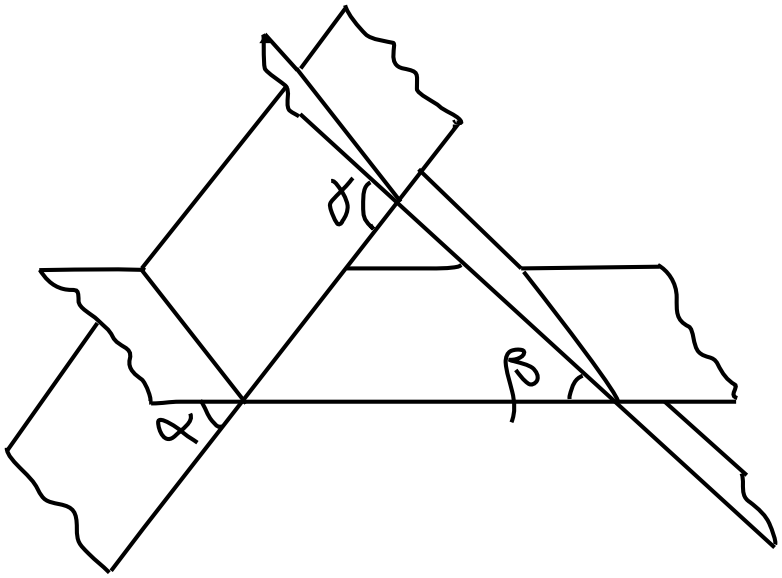

Figure 1.8.: Intersecting three planes

but no triple intersection the three dihedral bending angles are such that $\alpha + \beta \leq \gamma$, because in hyperbolic geometry $\gamma - \alpha - \beta$ is the area of the triangle. Indeed let A be the area of the triangle, then $\pi - \gamma$ is the interior angle, thus $A = \pi - \alpha - \beta - (\pi - \gamma) \rightsquigarrow A = \gamma - (\alpha + \beta)$.

As there is only one and the same bending angle when grafting or pruning, i.e. $\alpha = \beta$, it follows $\gamma = A + 2\alpha$. Thus taking smaller and smaller triangles $A \to 0$ and $\gamma \to 2\alpha$.

Letting the polyhedral approximation shrink to smoothness the angle sum corresponding to τ is a monotone sequence converging to a value $\mathfrak{B}(\tau)$. For short paths $\mathfrak{B}(\tau)$ is a close approximation to the angle of the tangent planes at the ends of the path.

The bending measure $\mathfrak{B}(\tau)$ is supported by the whole lamination λ. Every isolated leaf of λ must be a closed geodesic. Otherwise a transverse arc τ through any limit point of the leaf would have infinite measure. Consequently the transverse arc τ can only intersect the geodesic either in a finite set of points or in a Cantor set.

1.3.4. Space of hyperbolic structures

We want to describe the space $\mathcal{H}$ of all hyperbolic structures on the pretzel, using a quotient space for factoring out uninteresting variations. We fix a pretzel M_0 immersed in $\mathbb{R}^3$ and use the so called Fenchel Nielsen parametrization based on the pant decomposition.

We need an equivalence relation to get rid of the orientation preserving isometries which are isotopic to the identity. An **isotopy** is a homotopy between two maps, that is an homeophormism on the image at every stage. According to a theorem of Baer isotopy is the same as homotopy on surfaces, except the open disc and the annulus, so we can exchange the formulations, as we consider a pretzel.

1.3.5. Moduli space

We can take $\mathcal{H}$ and factor out the group $\mathrm{Diff}_+ M_0$ of orientation preserving diffeomorphisms on M_0. This space $\mathcal{H}/\mathrm{Diff}_+ M_0$ is called the **moduli space**, the moduli being the 6 parameters. It was Riemann, who stated in 1859, that isomorphism classes of closed Riemann surfaces of genus $g \geq 2$ are parametrized by $3(g-1)$ complex parameters. The moduli space $\mathcal{M}S := \mathcal{H}/\mathrm{Diff}_+ M_0$ has therefore real dimension $6(g-1)$. The moduli space is not as easy to handle with as the finer topology of the so called **Teichmüller space**.

1.3.6. Teichmüller space

The representation of tori with multiple holes by a 1-vertex regular 4-gon, i.e. an octagon for the pretzel, is so widespread that one could think, this model might be the only hyperbolic structure, so to say the only pretzel endowed with a hyperbolic structure, i.e. which can be shown in the Poincaré disc or any other model of the hyperbolic plane. It is one of the intentions of this paper to visualize that there are many pretzels that can be shown in the Poincaré disc. Of course all these pretzels are homeomorphic to each other, but we want to study the variations inside an homeomorphy class. The Teichmüller space is the space, where all the pretzel shapes live.

Let S be a surface admitting a hyperbolic structure, i.e. a metric of constant negative curvature, and let $\mathcal{S}_S$ be the space of such structures. Then the moduli (or Riemann) space is the quotient of $\mathcal{S}_S$ by the action of the group of diffeomorphism of S, $\mathrm{Diff}\, S$. Briefly the moduli space is the set of equivalence classes of Riemann surfaces, whereby two such surfaces are considered equivalent if there exists a holomorphic homeomorphism between them.

Simpler to study is the Teichmüller space $\mathcal{T}S$, the universal cover of the moduli space $\mathcal{M}S$. It is the quotient of $\mathcal{S}_S$ by $\mathrm{Diff}_0\, S$, i.e. the group of diffeomorphisms homotopic to the identity by a homotopy that takes the boundary into itself. So the Teichmüller space $\mathcal{T}S$ is the space of conformal structures on the surface S whereby the uninteresting conformal automorphisms which are isotopic to the identity are disregarded.

The fundamental group of the moduli space is called **mapping class group**. The mapping class group of a surface S, $\mathrm{mcg}\, S$, relates the moduli space to the Teichmüller space through the relation $\mathcal{M}S = \mathcal{T}S/\mathrm{mcg}\, S$, implying $\mathrm{mcg}\, S = \mathrm{Diff}\, S/\mathrm{Diff}_0\, S$. The mapping class group is a discrete group, the group of automorphisms up to isotopy. It is an algebraic invariant, briefly a discrete group of symmetries of the surface S.

The Teichmüller space has the structure of a manifold because it has a natural topology in which it is homeomorphic to the open ball in $\mathbb{R}^{6g-6+2e}$, g being the genus and e the number of punctures. This topology may be defined by the **Teichmüller metric**, a complete metric with respect to which the mapping class group acts as a group of isometries. This non Riemannian metric provides some of the geometry usually associated to Riemannian metrics and behaves better in some respects.

The uniformization theorem states that every compact surface S admits a hyperbolic, Euclidean or elliptic structure that makes S into a complete metric space. Since all differentiable structures can be given a Riemannian metric (using eventually a partition of the unity) every orientable surface has a complete metric of constant curvature. Thus the Teichmüller space can be identified with the space of isotopy classes of Riemannian metrics of constant curvature and the study of complex structures on a surface can be seen as the study of its hyperbolic structures.

Considering the pretzel, which is our main object of attention, we shall study several tessellations obtained by cutting it into **pairs of pants**. Constructing these pairs of pants and gluing them together defines points in Teichmüller space. Each Riemann surface is a point in Teichmüller space given by at least one tessellation in hyperbolic space. Thus there is a tessellation for each conformal structure on the surface. There are many of them and always one is a hyperbolic structure, i.e. of constant negative curvature $= -1$.

Noting the Teichmüller space $\mathcal{T}_g$ (g being the genus), the orientation preserving moduli space μ_g^+ is the quotient:

$$\mu_g^+ M_0 = \tau_g M_0 / mcg^+ M_0$$

mcg stands for mapping class group, or homeotopy group. It is the quotient of the group of self-homeophormisms of M_0 by the normal subgroup of isotopies (or here homotopies due to Baers theorem). mcg^+ is the orientation preserving component. The connected component of the identity in Diff is a normal subgroup Diff_0, the group of diffeomorphisms homotopic to the identity by the homotopies which always take the boundary to itself. Then the Teichmüller space can alternatively be defined as:

$$\mathcal{T}_g M_0 = \mathcal{H} M_0 / \mathrm{Diff}_0 M_0$$

Each structure in $\mathcal{T}_g M_0$ is an ordered triplet of positive parameters, the lengths of the boundary components. Note that the triplet would be unordered in the moduli space, since there are elements of the mapping class group that permute the boundary components. We can talk about the length of the shortest representative of a loop of a homotopy class. The result, for measuring the lengths $L(\delta_i)$ of the boundaries of the pant holes, will be a bijective length map $L : \mathcal{T}_g M_0 \to \mathbb{R}^{6(g-1)}$, thus $\mathcal{T}_2 M_0 \to \mathbb{R}^6$ for a pretzel.

As stated in [36] two elements of μ_g are equivalent in moduli space if and only if they have the same holonomy group, whereas they need to be equivalent in Teichmüller space to have the same holonomy map.

The **holonomy** is the group homeomorphism between the fundamental group $\pi_1(M)$ of a (G, X)-manifold M and its action group G.

1.3.7. Inserting a Dehn-twist

Inserting a **Dehn-twist** along a geodesic is what THURSTON calls an **earthquake**.

THURSTON remarks that in order to determine a point in Teichmüller space we need to consider how many times the leg of a pyjama suit is twisted before it fits onto the baby's foot.

The idea of the Dehn-twist is to cut out a narrow cylinder from the suit, twist it, then sew it anew. This alters the pyjama suit but solves the problem of putting in the baby's leg!

This twisting does not affect the perimeter of the suit's leg. We take a small cylindric slice and twist both circular ends against each other before regluing. A short longitudinal geodesic becomes a helix with any number of full turns. Inserting this slice before regluing is the twisting of the pants hole! Only both points on the rims stay in place, the rest of the short geodesic spirals now around.

To implement this, we have to extract the short cylinder. So we cut one pair of pants open using a Möbius transformation.

Figure 1.9.: Inserting a DEHN-twist

This operation along a geodesic is quite different from grafting or pruning. No cylinder is inserted or removed, the same cylinder is cut away and twisted before reinserting. The unit circle bordering the Poincaré disc still borders the new tessellation. It is just a gliding within the disc along the geodesic. This creates different hyperbolic metrics when crossing the Dehn-twist, only the metric along the geodesic gets confused. When grafting or pruning the Möbius transformation deforms the Poincaré disc, i.e. the hyperbolic structure. When crossing a graft or a prune we enter into a new Poincaré disc with a different radius. We shall investigate in chapter 4 the incidence on the metric.

1.4. Elliptic and hyperelliptic involution

Every punctured torus can be rotated to the identity by a half turn around an axis passing through three fixed points called Weierstrass points. This is the **elliptic involution**. All the same a pretzel has an **hyperelliptic involution** with six Weierstrass fixed points on the axis of rotation.

These involutions induce a specific behavior of simple closed geodesics on the punctured torus and the pretzel. *The automorphism group for surfaces of genus* ≥ 3 *has only trivial involution.* This is what motivates studying the specificity of the 1-punctured torus and the pretzel.

1.5. Surfaces in hyperbolic space

A set of geodesics in the Poincaré disc have their endpoints on the unit circle. When asking us whether a many leaved geodesic has self intersections, we only need to examine whether their endpoints on the circle intertwine or not. POINCARÉ first proved that something analogous happens one dimension higher:

Theorem 2 (Poincaré)**.** *The group of orientation preserving isometries of* $\mathbb{H}^3$ *is* $PGL(2,\mathbb{C})$ *via its action on the boundary* $\mathbb{S}^2 \cong \mathbb{C}P^1$*.*

A consequence is that the Möbius structure we shall use for inserting or cutting off a small cylinder reflects what happens in hyperbolic space: the plane gets pleated i.e. crinkled. To better understand this we step down one dimension lower. First we need the concept of orthogonality in projective geometry.

1.6. Orthogonality in the Kleinian disc

Constructions in the Poincaré disc use straightedge and compass (see f.i. [16]), hence the importance of orthogonality. Due to conformality a right edge on the pseudosphere or on $\mathbb{H}^2$ will always still be a right edge in Poincaré's disc, but not so in Klein's disc. Contrary to what intuition suggests the notion of orthogonality gets thanks to a small wonder even easier when geodesics are transfered from Poincaré's into Klein's model.

We first state an important theorem of projective geometry, very easy to prove when the conic is a circle.

Theorem 3 (La Hire)**.** *If a point* A *lies on the polar* b *of a point* B*, so the polar* a *of* A *goes through* B*.*

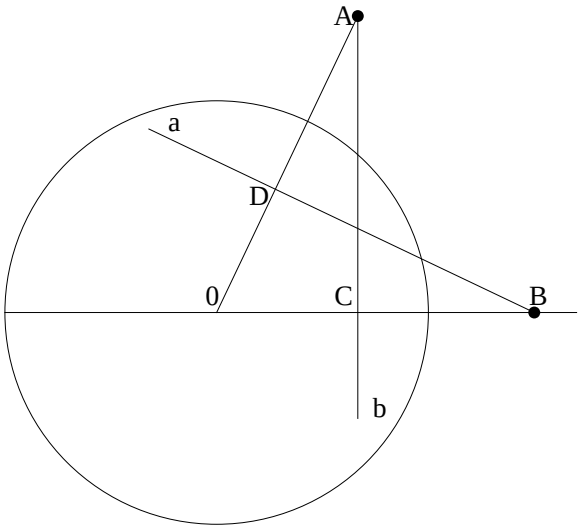

Figure 1.10.: La Hire's theorem

Proof. Let C be the inverse of B with regard to a circle of radius R centered on the origin and let A be a point on the polar b of B. Then $AC \perp OB$ and $OC\ OB = R^2$ by construction.

Let D be the foot of the perpendicular from B to OA. the triangles OAC and OBD are similar as they are right and share the angle at the origin. Thus

$$\frac{OA}{OB} = \frac{OC}{OD} \rightsquigarrow OA\,OD = OC\,OB = R^2$$

It follows that D is the inverse of A and a is the polar of A.

In the degenerate case $A = C$, $OA\,OD = OC\,OB = R^2$ still holds, as $D = B$. □

Proposition 1. *The family orthogonal to a geodesic RS in Klein's disc is a pencil of lines through the pol P of the geodesic RS.*

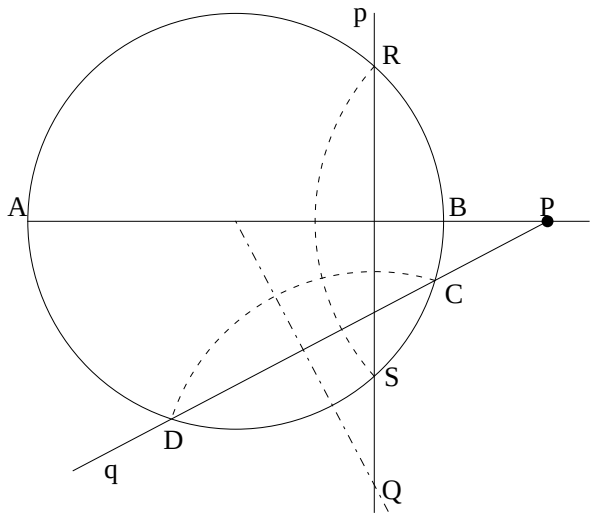

Figure 1.11.: Pencil of perpendiculars

Proof. We call P-geodesic a geodesic in Poincaré's model and K-geodesic the straight line joining the endpoints, i.e. the same geodesic in Klein's model.

Let, without loss of generality, RS be a vertical P-geodesic and P be its pol with regard to the unit circle.

Then the family of P-geodesics orthogonal to RS builds an Apollonian system with point circles R and S.

An arc of circle DC of the family will have centre the intersection Q of the support p of RS and the perpendicular bisector of DC. Thus Q is the pol of the K-geodesic DC, which joins the intersections of orthogonal circles.

It follows with La Hire that P lies on the support of DC.

□

Geodesics being Euclidean lines in Klein's disc is often very convenient. To pass from the arc of circle supporting a geodesic in the Poincaré model it suffices to join the endpoints on the unit circle. Not less useful is the property, that the family of perpendiculars is most easily obtained using the pole of the geodesic.

Figure 1.12 shows the Apollonian array of the perpendiculars to an arc and the pencil of lines through the pole in the Kleinian model.

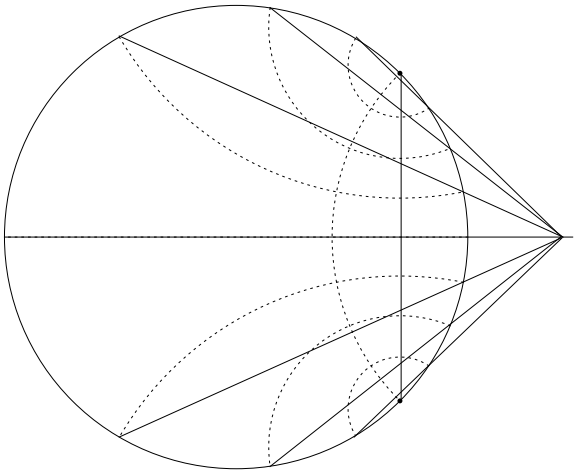

Figure 1.12.: Orthogonality in the Klein disc

All the geodesics of the Poincaré disc are supported by circles with centre on the polar. The geodesics in Klein's disc join through straight lines the endpoints of Poincaré's geodesics. As J. Stillwell remarks in [34] Klein's disc lets us understand that in a certain sense hyperbolic moves all are rotations, because a limit rotation is a rotation about a point at ∞ and a translation is a rotation about a point beyond ∞.

1.7. Pleatings in the Kleinian ball

Figure 1.13 is a planar cut through the centre of Klein's ball (a model of the projective space $\mathbb{H}^3$). The broken fat line is the track of a pleated hyperbolic plane orthogonal to the section.

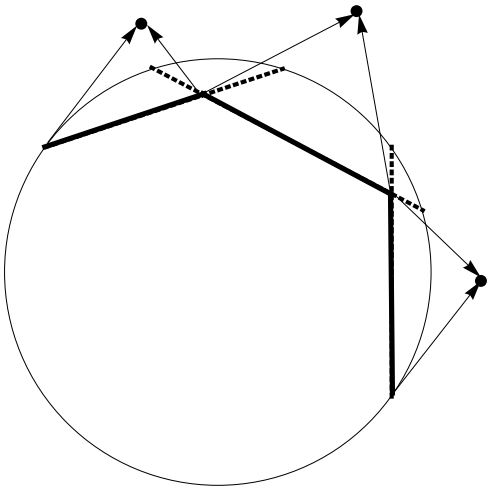

Figure 1.13.: Pleating in $\mathbb{H}^3$

The angle between the flat pieces of the pleated plane is also the angle of the arrows, i.e. the normals which intersect at the three poles.

Recall BELTRAMI obtained the hyperbolic half ball model through stereographic projection, from a pole into the opposite half ball, of the Poincaré disc bordered by the equator. He then made an orthogonal projection of the half ball back into $\mathbb{D}^2$, which is Klein's disc. Thus we can switch from one disc to the other using the half ball.

Imagine the arrows of figure 1.13 would be light rays projecting orthogonally. The image of the bended fat line would be made of three disjoint arcs on $\mathbb{S}^1_\infty$. Inverse stereographic projection from the south pole would transfer the disjoints arcs into Poincaré's disc, which again can be transferred on the ball $\mathbb{C}P^1 \cong \mathbb{S}^2$ by adding a point ∞.

This journey through the models makes plausible why the gaps between the disjoint arcs on the $\mathbb{S}^1_\infty$ (cut through $\mathbb{C}P^1$) correspond to the lunes obtained when grafting in the conformal model. Should we have send the arrows in the opposite direction, the image of the bended fat line would have been made of overlapping arcs. This results from the fact that grafting in the inner Poincaré disc has counterpart pruning in the outer Poincaré disc on $\mathbb{C}P^1$.

Grafting, pruning and twisting are not just a play along geodesics as this paper centered on visualization might suggest. They are important tools created by THURSTON for studying hyperbolic three-manifolds. He developed the concept of **uncrumpled** (or **pleated**) **surface**, which associates to a complete hyperbolic surface S of finite area in a three-manifold N an isometry $f : S \to N$ such that every point $x \in S$ in the interior of a straight line segment is mapped by f to a straight line segment. Basics to this work far beyond the scope of our paper are given in the electronic version of [36]. Also [4, Bonahon] gives very precious insights.

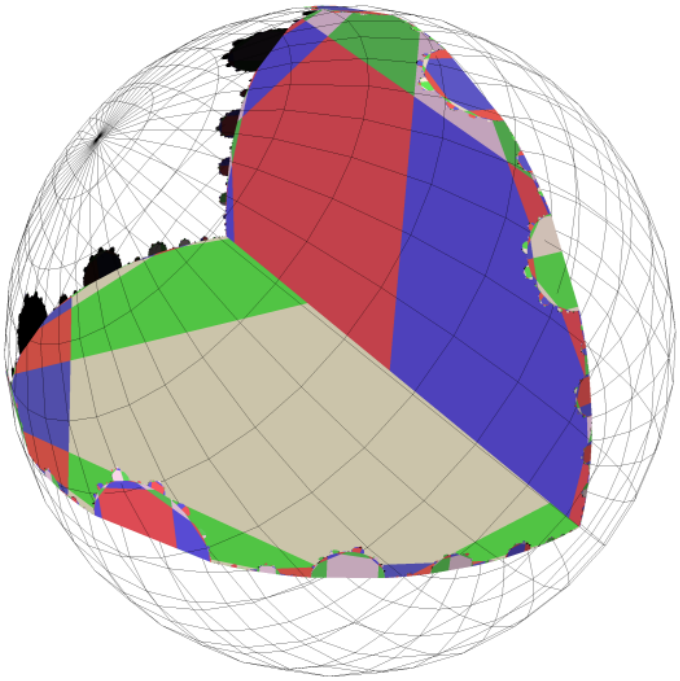

Figure 1.14.: Möbius moves in the Kleinian ball

We shall not go any deeper into the **pleatings** of hyperbolic planes in hyperbolic space. We only wanted to give a hint at what grafting, pruning and twisting are good for. Beyond the moves in Teichmüller space, they inform about bends in $\mathbb{H}^3$. This also makes plausible, why it is always possible to bend finitely often, when the bending

angle is chosen small enough. For infinitely many bends, the angle must be zero, i.e. no bending any more. This is what will happen along infinite geodesics on the punctured torus or on the pretzel.

We are much indebted to Charles Gunn of TU-Berlin for figure 1.14, a wonderful rendition of our 4-colored dodecagon model. Our flat grafted tiling has been transported into the Kleinian ball as a crumpled tessellation. 4 different colors are given to the front and the back of the both pairs of pants of the pretzel where 3 side lengths can be chosen.

In the projective Kleinian model the tiling before grafting is like a sheet of paper, i.e. flat to the Euclidean eye. In our 2 dimensional Poincaré disc on $\mathbb{C}P^1$ grafting produces lunes. The many lunes push away the unit circle whose boundary appears as bubbles riding on bubbles like Mickey Mouse ears. The lunes on $\mathbb{C}P^1$ correspond to the bends of the hyperbolic plane supporting the grafted tessellation. Also the cleaving of the earthquake along the geodesic is good to see thanks to the tile having been cut into four colored parts.

1.8. Cantor sets

1.8.1. Definition

A **Cantor set** is obtained by repeatedly removing from the interval $[0, 1]$ open intervals of length some fixed percentage $0\% < q < 100\%$ of $[0, 1]$. Any percentage may be removed around the midpoints of the intervals in each stage. The removed percentage must not be the same on the right and on the left. Figure 1.15 shows a Cantor set where an interval of length $\frac{7}{12}$ is removed around the middle but asymmetricly, $\frac{1}{4}$ from the left and $\frac{1}{3}$ from the right.

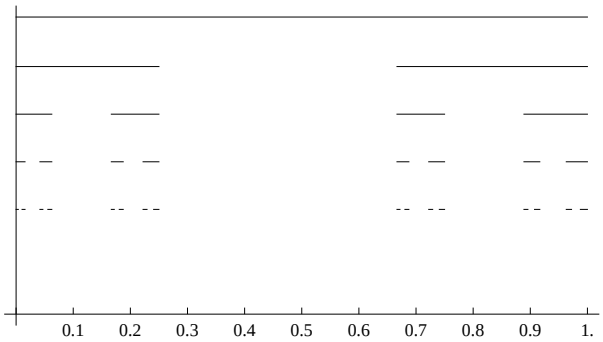

Figure 1.15.: Asymmetric Cantor set

It is possible to construct Cantor sets removing less and less at each stage, so that not only dust is left at the end. Really of interest are the sets with Lebesgue measure 0 like the classical middle third set.

Proposition 2. *All Cantor sets with Lebesgue measure zero are homeomorphic.*

Proof. The proof is immediate, as it is easy to find a bijection between any Cantor set of measure zero and the classical middle third set. □

Thus we can without loss of generality concentrate on the middle third Cantor set.

1.8.2. The Cantor function

A good visualization of the Cantor set is given by the **Cantor function** or 'devil's staircase'.

This function considers not what is left, but maps the removed intervals in the successive n stages. The height of the steps is uniformly 2^{-n}. The gaps in the definition domain correspond to the 'dust' of not removed segments.

D. R. Chalice has proved that the Cantor function is the only monotone increasing real-valued function satisfying

i) f(0) = 0,
ii) f(x/3) = f(x)/2
iii) f(1-x) = 1 - f(x).

Due to this property the function values can be computed recursively. This is how this graph was constructed.

So far n is finite, there are gaps in the definition domain of x, where $f(x)$ is not defined.

Figures 1.15 and 1.16 have been obtained from the program About_Cantor, which is a compilation we made from Stan Wagon's Mathematica® in Aktion [37].

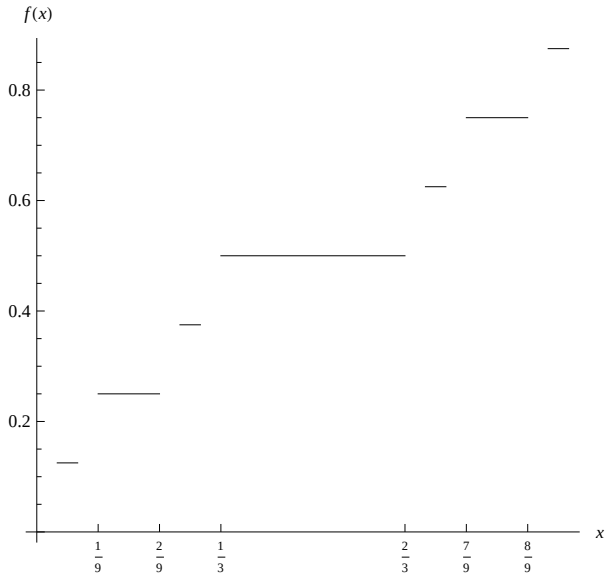

Figure 1.16.: The Cantor function

1.8.3. How to measure a Cantor set

Proposition 3. *The classical Cantor set has Lebesgue measure zero.*

Proof. Let R_k denote the removed intervals and m their Lebesgue measure. Then

$$m(R_1) = \frac{2}{3} - \frac{1}{3} = \frac{1}{3} = \frac{2^0}{3^1}$$
$$m(R_2) = \left(\frac{2}{9} - \frac{1}{9}\right) + \left(\frac{8}{9} - \frac{7}{9}\right) = \frac{2}{9} = \frac{2^1}{3^2}$$
$$m(R_3) = \left(\frac{2}{27} - \frac{1}{27}\right) + \left(\frac{8}{27} - \frac{7}{27}\right) + \left(\frac{20}{27} - \frac{19}{27}\right) + \left(\frac{26}{27} - \frac{25}{27}\right) = \frac{4}{27} = \frac{2^2}{3^3}$$

It follows

$$m\left(R_n\right) = \frac{2^{n-1}}{3^n}$$

The intervals being disjoint $m\left(\bigcup_{n=1}^{\infty} R_n\right) = 1$. Consequently the Cantor set, which is the set of what has not been removed, has by difference Lebesque-measure null. □

The problem with the Cantor function are the gaps, i.e. the not removed intervals. Instead of measuring intervals we would like now to associate a continuous measure with each point of the interval $[0,1]$. To get rid of the gaps we use the **Dirac's measure** and the **Dirac's delta function** defined as follows.

Let X be a non empty set, $\mathfrak{P}\left(X\right)$ its power set, then $\left(X, \mathfrak{P}\left(X\right)\right)$ is a measurable space. For $x \in X$ and any $E \subset X$, the **Dirac measure** at x is $\delta_x : \mathfrak{P}\left(X\right) \to \{0,1\}$ defined by $x\left(X\right) = 1$ if $x \in E$ and $x\left(X\right) = 0$ otherwise.

This is a measure because $\delta_x\left(\emptyset\right) = 0$ (as $x \in X$) and further for a sequence $\left\{A_n\right\}_{n\in\mathbb{N}}$ of disjoint subsets of X :

- Either $x \notin \bigcup_n A_n \rightsquigarrow \delta_x\left(\bigcup_n A_n\right) = 0$ hence $\delta_x\left(A_n\right) = 0$ for all $n \in \mathbb{N}$
- Or $x \in \bigcup_n A_n$ then there exists exactly one $n_0 \in \mathbb{N}$ such that $x \in A_{n_0}$, with $\delta_x\left(A_{n_0}\right) = 1$ and $= 0$ for all $n \neq n_0$. It follows $\delta_x\left(\bigcup_n A_n\right) = 1$

For any function $f : X \to \mathbb{R} \cup \{\infty\}$ the integral $\int_x f\delta_x = f\left(x\right)$ evaluates f at x.

Let m be the Lebesgue measure, $A \in \mathbb{R}$ a measurable subset and δ (without subscript!) the Dirac delta function, then for any measurable function $f : \mathbb{R} \to \mathbb{R}$, $x \in \mathbb{R}$ fixed and $t \in \mathbb{R}$ variable:

$$\int_A \delta\left(t - x\right) f\left(t\right) dm\left(t\right) = \int_A f d\delta_x = f\left(x\right) \delta_x\left(A\right)$$

If f is defined so that $f\left(t\right) = 1$ for all $t \in A$, then

$$\int_A \delta\left(t - x\right) dm\left(t\right) = \int_A d\delta_x = \delta_x\left(A\right)$$

Consider now on an interval $[a,b]$ an infinite sequence of functions $f_n\left(x\right)$ (n will then be identified with the number of stairs of the staircase) such that :

$$\int_a^b f_n = \begin{cases} 1 & \text{if } x \in [a,b] \\ 0 & \text{if } x \notin [a,b] \end{cases}$$

Recentering the removed intervals of the Cantor set around their midpoints it follows:

$$f_1(x) = \delta\left(x - \frac{1}{2}\right)$$
$$f_2(x) = \left(\delta\left(x - \frac{1}{6}\right) + \delta\left(x - \frac{5}{6}\right)\right)$$
$$\dots$$
$$f_n(x) = \frac{1}{n}\sum_{i=1}^{n} \delta(x - x_i)$$
$$\dots$$

Here the x_i are the x-values of the midpoints of the intervals.

For $n \to \infty$ we have $\int_0^1 f_n(x) = \frac{1}{n}\sum_{i=1}^{n} \delta(x - x_i) = 1$ and we get the measure

$$\mu(x) = \int_0^1 \frac{1}{n}\sum_{i=1}^{n} \delta(\xi - x_i) = \frac{1}{n}\sharp\{i | x_i \leq x\}$$

As an example in the range of x-values from 0 to 1 in steps of 0.1 the measures will be for $n = 3$
$\{0, \frac{1}{4}, \frac{1}{4}, \frac{1}{2}, \frac{1}{2}, \frac{1}{2}, \frac{1}{2}, \frac{5}{8}, \frac{3}{4}, \frac{7}{8}, 1\}$

or for $n = 10$
$\{0, \frac{205}{1024}, \frac{1}{4}, \frac{205}{512}, \frac{1}{2}, \frac{1}{2}, \frac{1}{2}, \frac{615}{1024}, \frac{3}{4}, \frac{205}{256}, 1\}$

As n increases fewer and fewer successive measure-values are equal.

1.8.4. Visualization of the delta measure

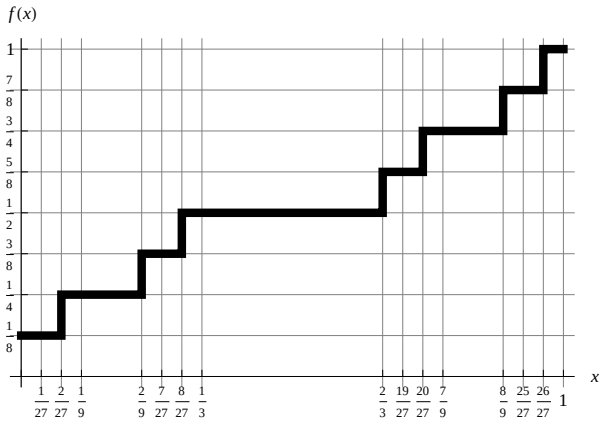

Figure 1.17.: The delta-measure of a lamination

Plotting the measures against the interval $[0, 1]$ looks very much like the Cantor function. The sole difference is that the stairs have been prolongated to the left so removing the gaps at all intermediary stages. The measure is continuous.

Figure 1.17 was obtained with our program Lamination_measure.

We can identify each intermediary stage with the number of loops of a spiralling geodesic.

Think now of somebody walking on a transversal across the Cantor set inferred by the closed geodesic. The vertical segments arise when the walker crosses the geodesic. They correspond to the bends of the pretzel in hyperbolic space. As the geodesic makes more and more loops, the vertical jumps will steadily decrease in size (but they still all have equal size).

1.8.5. Cantor sets and fractals

Cantor sets are deeply related to the world of fractals, where they can be visualized.

To start with consider the **Koch curve**, which is in some sense the contrary of the middle third Cantor set, as it grows instead of getting scarce. The middle third of a line is replaced by two segments of equal length placed as to form an equilateral triangle. Repeating this operation *ad libitum* the length of the curve increases each time by 4/3. It crinkles again and again being forced to live within a bounded area.

Note that the curve turns to the right and to the left, whereas in the pleating we shall consider in hyperbolic space the angle does not change sign. However this example enlightens the concept of Hausdorff dimension, which we note D.

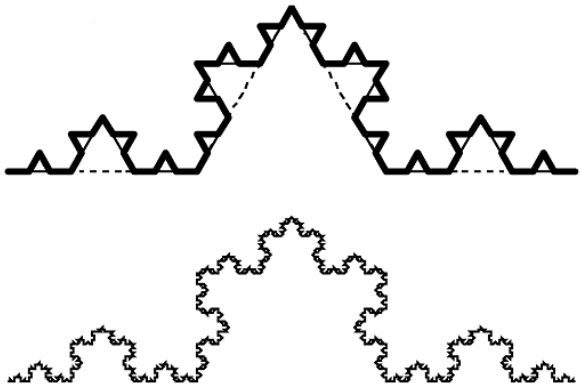

Figure 1.18.: The Koch curve

On the Koch curve the number of segment at level $n+1$ is $x_{n+1} = 4x_n$ but the length of each segment is divided by three: we have to magnify x_{n+1} by 3 to get the length we had in x_n. Thus with regard to the length and according to the definition of the Hausdorff dimension, we get another equation

$$3^D x_n = x_{n+1} \rightsquigarrow 4 = 3^D \rightsquigarrow D = \frac{\log 4}{\log 3} = 1,26186\ldots$$

This confirms the visual impression of a curve getting denser rather than longer, exploding the restraints of one-dimensionality.

The Hausdorff dimension of the middle third Cantor set arises in an opposite but analogous way.

The dust of each segment of level n fragments into the dust of 2 subsegments at level n+1, so $x_n = 2x_{n+1}$. On the other hand the dust of x_{n+1} must be expanded by three to recover the previous segment length:

$$x_n = 3^D x_{n+1} \rightsquigarrow 3^D = 2 \rightsquigarrow D = \frac{\log 2}{\log 3} = 0,63093\ldots$$

Here the Cantor dust fails to be one dimensional but the accumulation remains far from being zero dimensional.

We look now at the data of the middle third Cantor set from a slightly different but equivalent point of view.

Proposition 4. *Let d_n be a segment of dust not removed at stage n from the interval $[0,1]$. Then the limit set of the d_n for $n \to \infty$ is a Cantor set if and only if*

$$|\log(\mathit{length}(d_n))| \propto \log n$$

where $a_n \propto b_n$ means that the ratio $\frac{a_n}{b_n}$ is bounded between two positive constants for n large enough.

Proof. Let $\epsilon = \text{length}(d_n)$.

Let n_ϵ be the level under scrutiny when the segments have length ϵ. Let D be the Hausdorff dimension then,

$$D = \frac{\log n_\epsilon}{\log \frac{1}{\epsilon}} \rightsquigarrow D \log \frac{1}{\epsilon} = \log n_\epsilon$$

ϵ being infinitesimal $\log \epsilon < 0$, thus

$$\log \frac{1}{\epsilon} = -\log \epsilon = |\log \epsilon|$$
$$\rightsquigarrow \quad D \log \frac{1}{\epsilon} = D\,|\log \epsilon| = D\,|\log(\text{length}(d_n))| = \log n_\epsilon$$

This is the result which was found for the middle third set with $n_\epsilon = 2$ and $\epsilon = \frac{1}{3}$, i.e. $D = \frac{\log 2}{\log 3}$.

Consider now a Cantor set of Lebesgue measure zero, where the removed percentages are not the same at every stage. Then different limits will apply according to the sequence of percentages. These limits will have a maximum and a maximum. Then

$$|\log(\text{length}(d_n))| \propto \log n \tag{1.2}$$

□

1.9. Farey fractions

The homotopy classes of simple paths on the torus T^2 are represented by simple geodesics turning m times around the core and n times around the hole. We shall let m and n grow so that any irrational number corresponding to an infinite geodesic becomes the limit of a sequence of fractions. The **Farey fractions** produce such sequences.

Figure 1.19 shows a tessellation of the Poincaré disc generated by the modular group. The **modular group** is a subgroup of $PSL(2,\mathbb{Z}))$ whose generators have integer coefficients.

This tessellation, discovered by Gauss in a context of number theory, has the interesting property that the vertices of the ideal triangles hit the unit disc in rational points.

Note that the tessellation can be moved so that one edge of the ideal triangle becomes a diameter. Then the union of two adjacent triangles forms a 1-punctured torus.

Each fraction is obtained from its both neighbours by the peculiar Farey addition:

$$\frac{p+r}{q+s} = \frac{p}{q} \oplus \frac{r}{s}$$

for any $p, q, r, s \in \mathbb{Z}$

Two neighbouring fractions fulfill the relation: $ps - rq = 1$.

The definition of a **Farey sequence** is as follows:

Definition 2. *The Farey sequence of order n lists in order of increasing size all completely reduced fractions between 0 and 1, which have denominator $\leq n$.*

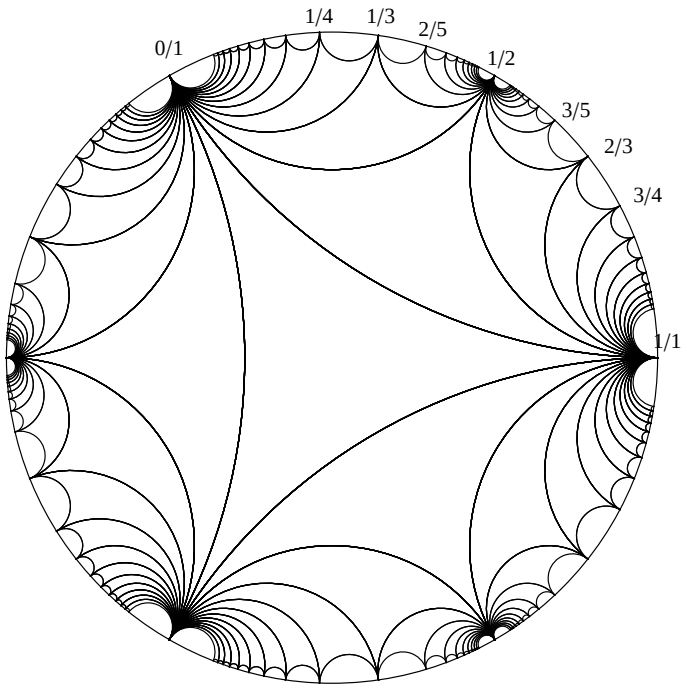

Figure 1.19.: Tessellation by modular group

So far $p, q, r, s \in \mathbb{N}$ there is a well known very simple algorithm for computing the sequence based on the property $ps - rq = 1$. It will return for example:

$$\text{farey}\,(5) = \{0, \frac{1}{5}, \frac{1}{4}, \frac{1}{3}, \frac{2}{5}, \frac{1}{2}, \frac{3}{5}, \frac{2}{3}, \frac{3}{4}, \frac{4}{5}, 1\}$$

To complete this, we have written an enlarged algorithm Farey_play which gives the neighbours of any Farey fraction without computing the whole sequence and returns a sequence of fractions which approximates a given irrational number < 1.

Let us find as an exercise the sequence of Farey fractions for $\sin \frac{\pi}{4} = \frac{\sqrt{2}}{2}$ with precision 10^{-4}. The return is the approximation $\frac{70}{99}$ together with the sequence:

$$\{0, \frac{1}{2}, \frac{2}{3}, \frac{7}{10}, \frac{12}{17}, \frac{41}{58}, \frac{70}{99}, \frac{29}{41}, \frac{17}{24}, \frac{5}{7}, \frac{3}{4}, 1\}$$

The Farey fractions can be visualized as **Ford circles** (also known as **Farey circle packing**). These are tangent circles touching the real line at points ordered as Farey fractions. For every fraction $\frac{p}{q}$, p and q coprime integers, the circle of diameter $\frac{1}{q^2}$ touches the real line at $\frac{p}{q}$. These circles can be converted into horocycles in the half

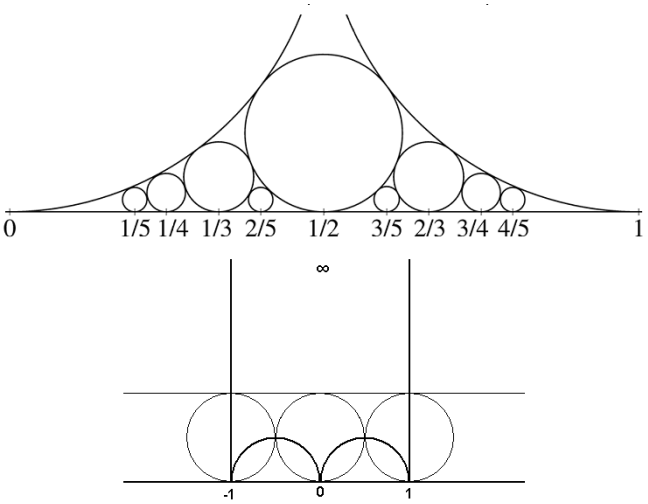

Figure 1.20.: Ford circles

plane hyperbolic model. Joining by geodesical half circles the rational points where the horocycles hit the real axis at infinity we get again the once punctured torus made of two ideal triangles. The corresponding tessellation is what we already saw in the disc model.

Let now the generators of the tessellation, say $a, b, A = a^-$ and $B = b^-$, be identified to the edges of the 1-punctured torus. The Farey fractions show how longer and longer words become aggregated into each other (figure 1.21 is borrowed from [28, Indra's Pearls].

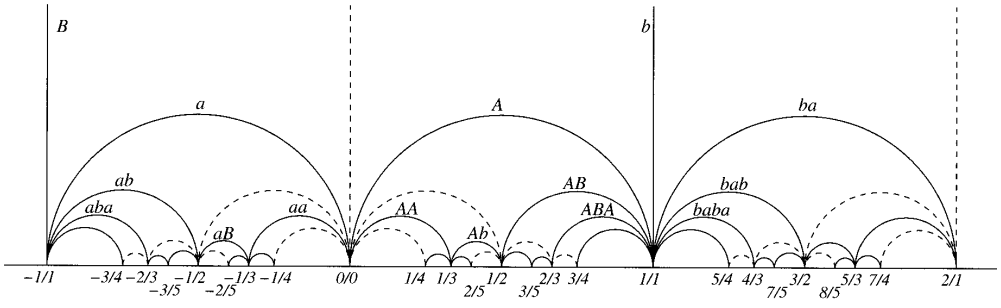

Figure 1.21.: Modular tessellation

This motivates why a converging sequence of simple closed geodesics on the punctured torus does not spread out on the surface. In the contrary the words are encased. Let for instance W_a be a word ending in a, then the three other edges of the tile, W_{ab}, W_{aB} and W_{aa} are spanned in between and hit the real axis in neighbouring Farey fractions.

Looking back at the approximation of $\sin \frac{\pi}{4}$ the fractions of the approximating sequence induce simple closed geodesics with always more spirals in a narrow stripe.

Chapter 2.

Grafting across a handle

2.1. Inserting a cylinder into the pretzel

We now endow a pretzel with a **Möbius structure**, i.e. a structure where generalized circles (circles and lines) are mapped to generalized circles.

Consider a closed geodesic around a handle. The Möbius structure works as scissors that enable us to cut the pretzel along the geodesic, so as to paste in a cylindrical wedge. This wedge is a lune between equidistant curves in the Poincaré disc.

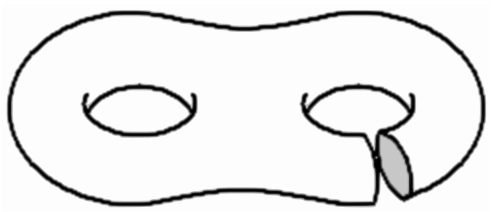

Figure 2.1.: Inserting a graft

This operation is called **grafting**, suggesting the insertion of a shoot in a branch of a tree. The inverse operation is **pruning**, also with a reference to agriculture: a cylinder is removed instead of inserted. The visualization of grafting is pleasant to the eye because a blown up tessellation is easy to interpret, whereas pruning deflates the tessellation into a messy puzzle of intricate tiles.

This paper is mainly dedicated to both operations of grafting and pruning. The Möbius matrices push stuff away (grafting) or into itself (pruning). From the point of view of programming this just means reversing the sign of the angle of the lune, or... it only seems to be so easy, because when pruning you have to get rid of the superfluous stuff, which is tedious.

An alternative operation consists in using a matrix that lets the geodesic slide against itself along the cut. This operation was known as a Dehn-twist. Thurston called it an earthquake, in this particular case.

As grafting is the imaginary counterpart of twisting, it suffices to extend the matrix in the grafting resp. pruning program. No further modifications are required to visualize earthquakes. However the tessellation of an earthquake is as messy a puzzle as the pruned tessellation, because the unit circle $\mathbb{S}^1_\infty$ is not altered.

Grafting resp. pruning can be combined with twisting into a complex earthquake, see [22, Mc Mullen]. This is again easiest to program : replace a matrix by a multiplication of two matrices.

2.2. Cutting across a handle

Proceeding step by step with the target of infinite simple geodesics running wildly across the pretzel, we start with the simplest case of the geodesic crossing a handle.

Lifting up to the universal cover, the image of the path must be a line crossing a generator, say the pair a_1/A_1, orthogonally and through all adjacent octagons.

We use the fact, that two ultraparallel lines in the disc have a unique common perpendicular (we shall prove this soon). Figure 2.2 shows tiles with the geodesic across two paired edges. For a better sight we have moved the tessellation, so that one geodesic is a diameter.

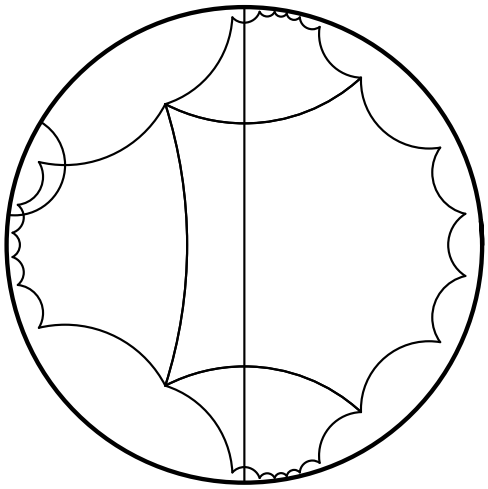

Figure 2.2.: Closed geodesic around a handle

Due to the symmetry against the real axis the perpendicular through the three adjacent octagons must be one and the same line. It follows by induction, that the perpendicular crosses all octagons throughout the tessellation.

We now recenter the octagon around the origin and consider the perpendicular through the pair a_1/A_1. On the pretzel the rims of the strip lie equidistant to the cut, as a result of a Möbius transformation pushing away in one direction, so as to form what we call a **lune**. Lifting this up, the side of the lune will be the equidistant curve to the orthogonal geodesic. A curve equidistant to a line in the disc is an arc of an Euclidean circle with the same endpoints as the line.

To fix this lune numerically we need the Möbius transformation mapping the border of the lune. To define the arc we then choose three points, the endpoints of the perpendicular and their midpoint, which we want to map to an arc with the same endpoints and a free to move midpoint, so as to open the lune at please.

We could of course take any point at a given hyperbolic distance of the cut, the midpoint is only easier to handle with (for graphic purposes we sometimes use the *diskgeometry* instruction giving the Euclidean midpoint).

To avoid a lot of computing between Euclidean an hyperbolic distances for any choice of the distance, we shall measure distance by the opening angle α of the lune, an easy to visualize parameter we can then vary at please. Due to conformality Euclidean and hyperbolic angles are the same.

2.2.1. The opening angle of the lune

The hyperbolic distance between the rims of a lune is constant throughout the lune but not the Euclidean distance that depends on where the lune lies in the disc and where the distance is measured along the lune. We must therefore characterize the opening length by its angle which determines alone the lune uniquely.

Proposition 5. *The hyperbolic distance δ from a geodesic to an equidistant curve is in one to one correspondence with the opening angle α of the lune.*

Proof. M being the Möbius pushing map, let r be the Euclidean midpoint of the arc joining p and q, $M(r)$ its image.

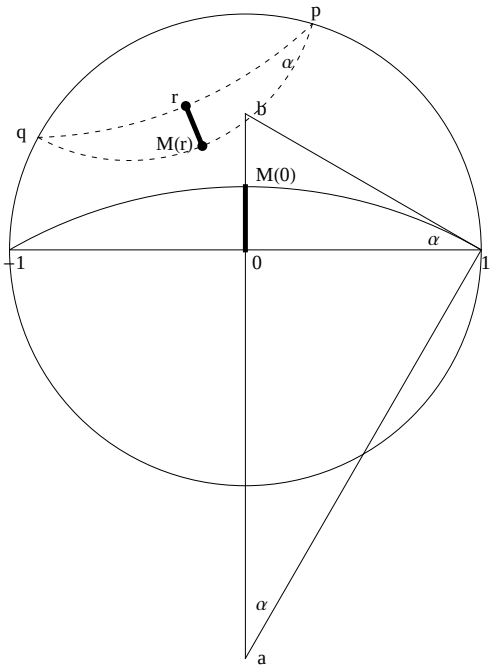

Figure 2.3.: Angle of the lune as distance

The Möbius transformation

$$z \mapsto \frac{(-z+r)(p-q)}{(p+q-2r)z - 2pq + r(p+q)}$$

maps the arc (p, r, q) to $(-1, 0, 1)$, preserving α and the hyperbolic distance $\delta := d_H(r, M(r)) = d_H(0, M(0))$.

Let R be the radius of the arc $(-1, 0, 1)$, then $R = \frac{1}{\sin\alpha}$ and $|a| = R\cos\alpha = \cot\alpha$.

Let $d := |M(0)|$ be the Euclidean distance corresponding to the hyperbolic δ

$$d = R - |a| = \frac{1}{\sin\alpha} - \cot\alpha = \tan\frac{\alpha}{2}$$

This gives the value of α for the hyperbolic distance δ

$$\delta = 2\tanh^{-1}\tan\frac{\alpha}{2} \rightsquigarrow \tan\frac{\alpha}{2} = \tanh\frac{\delta}{2}$$

So α is related to δ through

$$\alpha = 2\tan^{-1}\tanh\frac{\delta}{2} \tag{2.1}$$

□

2.2.2. Construction of the common perpendicular

We stated that two ultra-parallels have a common perpendicular along which we make a cut. We now give the construction of this perpendicular, which will also prove its existence.

Theorem 4 (common perpendicular)**.** *Two geodesics have a common perpendicular, if and only if they are ultra-parallel. This common perpendicular is then unique.*

Proof. In the Poincaré disc two geodesics that are not ultra-parallel cannot have a common perpendicular. Otherwise both geodesics would form with their perpendicular a triangle with two right angles and a third angle of at least 0° (when they are parallel), which is impossible.

Assuming now the existence of a common perpendicular for two non intersecting geodesics, it must be unique. Otherwise both perpendiculars would form either a rectangle if they do not intersect or two triangles with two right angles. This is impossible too.

In the special case, where the segments joining the endpoints of two geodesics are parallel, the diameter orthogonal to them is the common perpendicular.

In all other cases we give the construction of the common perpendicular, therefore proving its existence.

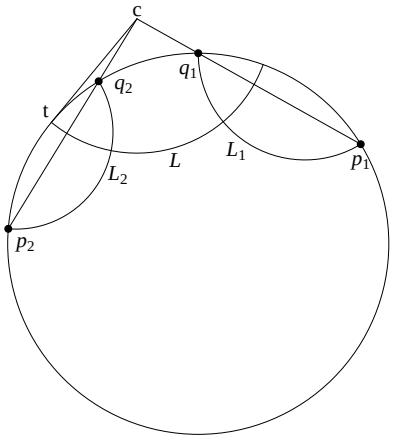

Figure 2.4.: Construction of the common perpendicular

The lines p_1q_1 and p_2q_2 joining the endpoints intersect in c. The arc of circle centered in c and orthogonal to the unit circle in t is the common perpendicular. Why?

L is an arc of the circle with center c and radius (c,t), so it is a geodesic. Inversion in L exchanges p_1 with q_1 and p_2 with q_2, as the unit circle is orthogonal to L. The intersections of L with L_1 and L_2 are invariant. As there is a unique circle through three points, the geodesics L_1 and L_2 are mapped to themselves, which infers that L is at right angles with them. □

2.3. How does grafting work?

Figure 2.5 shows the common perpendicular λ to the sides a_1 and A_1. With a grafting angle of 70° λ gets moved to the equidistant curve $\widehat{\lambda}$, which is still a common perpendicular of the edges but no geodesic any more.

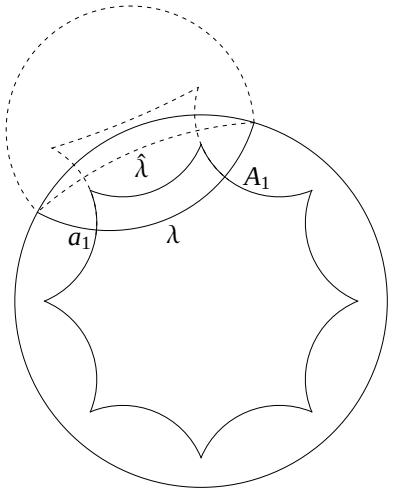

Figure 2.5.: Edge sliding by grafting

In fact all Euclidean circles through two points form an elliptic pencil. The supports of a_1 and A_1 are members of an Apollonian hyperbolic pencil orthogonal to the family of equidistant curves. Therefore the transformed of the edges a_1 and A_1 only glide along the supports.

This is rather analogous to an Euclidean orthogonal translation, but what looks like a curvy quadrangle is not a rectangle, because the equidistant curve is no geodesic. Apart from this, the process of translation is quite the same as when an Euclidean line segment is moved orthogonally to get a rectangle.

2.3.1. The word problem

The construction of a tessellation makes clear that one can move from any octagon to any other just by applying to its points the composition of the Möbius transformations on any path joining both octagons, what we called a word. How can we select such paths, so that each octagon is characterized by a unique word?

Null-homotopic paths, i.e. paths contractible to a point, correspond to words $w = 1$. The problem of deciding whether a given word is equal to 1 is indeed tough. DEHN called it 1910 the **word problem**. Novikov proved 1955 that the word problem is not solvable for some specific groups with a finite number of generators.

Let us try to start from the central octagon and move away with layers of concentric octagons.

We call the central octagon I_2 - meaning the 2×2 unit matrix - and call $a_1, \cdots, B_2$ the eight octagons around it. We then take the neighbouring octagons around each of the eight vertices and complete the wording.

We can construct the next layer, taking care to always select the shortest path starting from the center of the disc. This is done easily by comparing the lengths of the words.

One advantage of this wording is that we increase step by step the relevant tessellated area in the disc with words of quite different lengths.

However we get the problem that two paths may be of the same minimal length - see the dark gray octagons in figure 2.6.

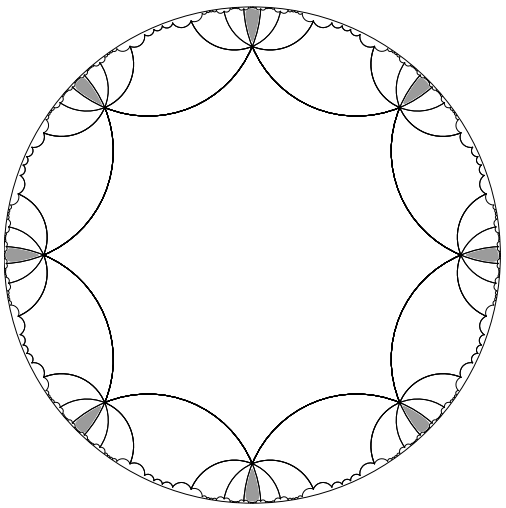

Figure 2.6.: Redundant moves

This results from the fact that we can trace a path around a vertex, so as to get back to I_2 after eight steps.

Due to $a_1.B_1.A_1.b_1.a_2.B_2.A_2.b_2 = 1$ cyclic left shifts give at once 7 other words $= 1$:

$$a_1.B_1.A_1.b_1.a_2.B_2.A_2.b_2 = 1$$
$$B_1.A_1.b_1.a_2.B_2.A_2.b_2.a_1 = 1$$
$$A_1.b_1.a_2.B_2.A_2.b_2.a_1.B_1 = 1$$
$$b_1.a_2.B_2.A_2.b_2.a_1.B_1.A_1 = 1$$
$$a_2.B_2.A_2.b_2.a_1.B_1.A_1.b_1 = 1$$
$$B_2.A_2.b_2.a_1.B_1.A_1.b_1.a_2 = 1$$
$$A_2.b_2.a_1.B_1.A_1.b_1.a_2.B_2 = 1$$
$$b_2.a_1.B_1.A_1.b_1.a_2.B_2.A_2 = 1$$

Obviously we should not waste time computing such words.

A further nasty implication is that for instance

$$a_1.B_1.A_1.b_1.a_2.B_2.A_2.b_2 = 1 \rightsquigarrow a_1.B_1.A_1.b_1 = (a_2.B_2.A_2.b_2)^{-1} = B_2.a_2.b_2.A_2$$

or as well $a_1.B_1.A_1.b_1.a_2 = B_2.a_2.b_2$ and so on. Conclusion: a single word $W = 1$ generates a lot of duplications.

In free groups the only allowed words $= 1$ are the product of an element by its inverse, here $a_i.A_i$ or $A_i.a_i$ and $b_i.B_i$ or $B_i.b_i$ with $i = \{1, 2\}$. the octagon group is unfortunately not free, hence we have to fight with the word problem.

Before looking for ways to minimize the duplications, we first have to fix an algorithm, so as to be able to write down all words. We construct such a tree, before considering redundant branches.

2.3.2. The tree of words

Before setting up the algorithm, we have to define, when we step out of this merry-go-round.

Of course we have in all models to eliminate at least the trivial pairing $a_i A_i = b_i B_i = 1$. However it is a specific problem of the octagon model that there are eight tiles around each vertex. The group not being free this implies that too many long words loop uselessly around vertices. Models with only four tiles around each vertex are much better in this respect. So we had to find a specific solution for the octagon.

One way could be to choose words up to a maximal length. This is certainly a good idea as the number of words of course grows tremendously with the number of letters. This would however let the tree waste machine time with smallest invisible tiles close to the border, whereas significant tiles with long words would be missed. Alternatively we can stop, when the Euclidean distance from the center of any octagon is sufficiently close to the radius 1 of the disc. This again would require longer words for approaching the border, but longer words for tiles far from the border means looping uselessly around vertices.

We found it best to combine both escaping instructions. We got pretty satisfactory drawings in a reasonable time by escaping when the distance between the origin and its image is over 0.999 or the number of letters is over 7. So we come close enough to the border but limit redundant copies around vertices.

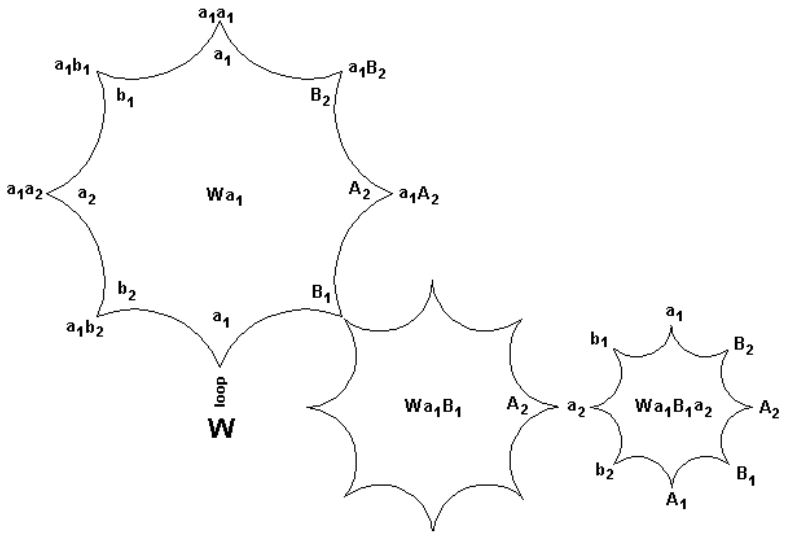

Figure 2.7.: Walking up and down the tree

The idea is to put the 8 letters in cyclic order and create new branches until the break condition is reached. The last letter under scrutiny being the inverse of the first one, there is an automatic jump back, when the cycle is completed. We examine a word W the identity at the very beginning and transform the coordinates of the octagon by the matrix a_1. We arrange the letters, so that a_1 is opposite to A_1, etc.

Turning anticlockwise we numerate the matrices, say $a_1 = i$. Then $A_1 = i + 4$. This gives us a nice trick found in [28, Indra's Pearls]!

Using numeration modulo 8 we get:

$$
\begin{array}{llll}
A_1 & = i+4 \mod 8 & = i-4 \mod 8 \\
B_1 & = i-3 \mod 8 & \\
A_2 & = i-2 \mod 8 & \\
B_2 & = i-1 \mod 8 & \\
a_1 & = i \mod 8 & \\
b_1 & = i+1 \mod 8 & \\
a_2 & = i+2 \mod 8 & \\
b_2 & = i+3 \mod 8 &
\end{array}
$$

We program a loop for $k = i - 3$ to $k = i + 3$ and get the words we are seeking for, whereas $a_1 A_1 = 1$ generates the escape out of the loop. Using recurrence we are in a position to go up the tree until the escape instruction is reached and then climb down to the previous node.

The words of 1 and 2 letters can be extracted and put at the beginning of the list. All the words are reduced words (no trivial cancellations). All octagons can be drawn, some of them are duplicates due to redundancy of the wording but reasonably few.

2.3.3. How to solve the word problem

Our ambition is not to solve the world problem, only to draw pictures fine enough for human eyes, this in a reasonable computing time. But a refinement would possible.

[28, Indra's Pearls] states that all Kleinian groups are **automatic groups** and there is a program KBMAG by Holt constructing a FSA (Finite State Automaton). An **automaton** is a table stating for the relevant word endings what happens when multiplied from the right by each generator: either a break instruction or a link to a simpler ending. Such a table is easy to insert in the program but unfortunately as the Indra's Pearls authors write: even with 2 generators and the simple relation $(abAB)^2 = 1$ it is still a substantial task to work out a suitable automaton.

Chapter 3.

Tessellating with the octagon

3.1. Constructing the octagon

The instruction *RegPoly* $\left[8, \frac{\pi}{4}\right]$ of our package *diskgeometry* returns immediately the vertices of a regular octagon with angle $\frac{\pi}{4}$. We have computed exactly the edges of the octagon and the generators in order to save all data in a nutshell without rounding errors. Of course this exact calculation has anecdotic character, we did it more for fun than for practical use.

3.1.1. Computing the vertices of the octagon

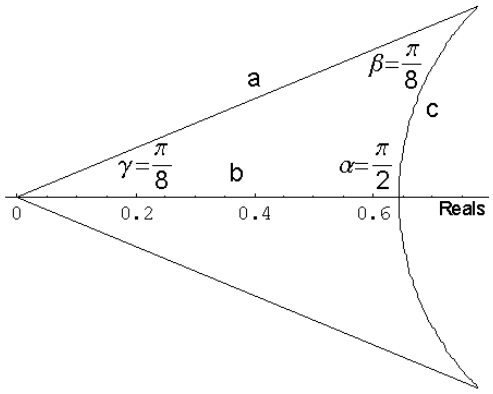

Figure 3.1.: Measuring the octagon

A hyperbolic triangle is uniquely defined by its three angles (up to a hyperbolic move). We turn the octagon so that both vertices of an edge are conjugated complex numbers. The midpoint of the edge lies then on the real axis.

As $\sin\frac{\pi}{4} = \cos\frac{\pi}{4} = \frac{\sqrt{2}}{2}$ the trigonometric functions can be entered exactly.

We use two well known hyperbolic cosine formulas:

$$\begin{cases} \frac{\sinh a}{\sin\alpha} = \frac{\sinh b}{\sin\beta} = \frac{\sinh c}{\sin\gamma} \\ \cosh c = \frac{\cos\alpha\cos\beta+\cos\gamma}{\sin\alpha\sin\beta} \end{cases}$$

Rotating through $\frac{\pi}{8}$ the first edge has endpoints $\left(\frac{1}{\sqrt[4]{2}}, 0\right)$ and $\left(\frac{1}{\sqrt[4]{8}}, \frac{1}{\sqrt[4]{8}}\right)$ and midpoint $\left(\frac{1}{\sqrt[4]{8}}, \frac{1}{2\sqrt{-4+3\sqrt{2}}}\right)$.

The other edges follow using the matrix $\frac{1}{2}\begin{pmatrix}\sqrt{2+\sqrt{2}} & -\sqrt{2-\sqrt{2}}\\ \sqrt{2-\sqrt{2}} & \sqrt{2+\sqrt{2}}\end{pmatrix}$ for rotating through $\frac{\pi}{4}$.

3.1.2. Computing the generators

We have obtained a new octagon, when first inverting the edges A_1 along the line L to get a_1 and then inverting in A_1. Three points (two vertices and the midpoint of the edge) are related by a Möbius transformation, which we give determinant $= 1$.

With $\alpha := -(1+i)\left(1+\frac{1}{\sqrt{2}}\right)$ and $\beta := -\frac{1}{\sqrt[4]{2}}\left(1+\sqrt{2}-i\right)$ we obtain:

$$a_1 = \begin{pmatrix}\bar{\alpha} & -\bar{\beta}\\ -\beta & \alpha\end{pmatrix} \quad b_1 = \begin{pmatrix}\bar{\alpha} & -\beta\\ -\bar{\beta} & \alpha\end{pmatrix} \quad a_2 = \begin{pmatrix}\bar{\alpha} & \bar{\beta}\\ \beta & \alpha\end{pmatrix} \quad b_2 = \begin{pmatrix}\bar{\alpha} & \beta\\ \bar{\beta} & \alpha\end{pmatrix}$$

$$A_1 = \begin{pmatrix}\alpha & \bar{\beta}\\ \beta & \bar{\alpha}\end{pmatrix} \quad B_1 = \begin{pmatrix}\alpha & \beta\\ \bar{\beta} & \bar{\alpha}\end{pmatrix} \quad A_2 = \begin{pmatrix}\alpha & -\bar{\beta}\\ -\beta & \bar{\alpha}\end{pmatrix} \quad B_2 = \begin{pmatrix}\alpha & -\beta\\ -\bar{\beta} & \bar{\alpha}\end{pmatrix}$$

We first computed A_1. Then B_1, A_2, B_2 follow by conjugation, i.e. rotating the homogeneous coordinates to coincide with A_1, applying the Möbius transformation A_1 and rotating back. We then used that a_i is the inverse Matrix of A_i (and b_i is inverse of B_i) as it is the same edge, i.e. the transformations on both sides must be inverse of each other.

All the generators are expressed in α and β (as defined above) and their complex conjugates. They all have the same trace $Re(\alpha) = -2-\sqrt{2} < -2$.

Such moves are called hyperbolic and have two fixed points. They are conjugate to $z \mapsto kz$ for a real $k > 1$, which means that they are scaling maps. Conjugation corresponds to a coordinate change on the Riemann sphere, it gives a different point of view but the dynamic behavior is the same.

Poincaré established in 1882 that the automorphisms of his disc, i.e. the Möbius transformation leaving the unit circle invariant, must be of the form $\begin{pmatrix}u & v\\ \bar{v} & \bar{u}\end{pmatrix}$ for $u, v \in \mathbb{C}$.

Proposition 6. *The matrices* $\begin{pmatrix}u & v\\ \bar{v} & \bar{u}\end{pmatrix}$ *with* $u, v \in \mathbb{C}$ *form a subgroup of SU2 with real trace.*

Proof. : Let $G = \left\{M \in SU2 \mid M = \begin{pmatrix}p & q\\ \bar{q} & \bar{p}\end{pmatrix}, p, q, \in \mathbb{C}\right\}$

- $M, M' \in G \rightsquigarrow MM' \in G$ because $\begin{pmatrix}p & q\\ \bar{q} & \bar{p}\end{pmatrix}\begin{pmatrix}p' & q'\\ \bar{q'} & \bar{p'}\end{pmatrix} = \begin{pmatrix}pp' + q\bar{q'} & pq' + q\bar{p'}\\ \bar{q}p' + \overline{pq'} & \bar{q}q' + \overline{pp'}\end{pmatrix}$ has real trace.
- $M \in G \rightsquigarrow M^{-1} \in G$ because $M^{-1} = \frac{1}{\det M}\begin{pmatrix}\bar{p} & -q\\ -\bar{q} & p\end{pmatrix}$ has real trace.

□

So this is a group. We can tessellate the disc by composing such matrices to words.

3.2. Cutting along a geodesic

Take an octagon mapping a pretzel and cut along the common perpendicular across two identified edges. This is a closed geodesic crossing the edge orthogonally.

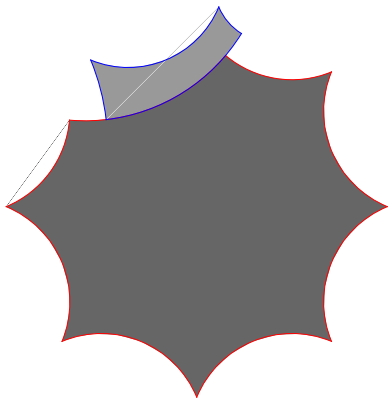

Figure 3.2.: Earthquake on the tile

Figure 3.2 shows a rim of the cut gliding along the other rim. This is the insertion of a Dehn twist which W.P. Thurston calls picturesquely an **earthquake**. The Möbius transformation doing the job leaves both the unit circle $\mathbb{S}^1_\infty$ and the closed geodesic invariant. Here we used the Möbius transformation, which fixes -1 and 1 and sends the origin along the real line to $\tanh\varphi$ for some angle φ. The transformation was applied only on the part of the octagon above the geodesic.

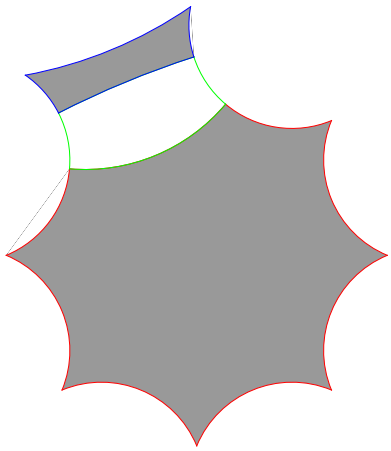

Figure 3.3.: Grafting on the tile

Figure 3.2 like figure 3.3 was made with the program Bubble_Graft_octo. The latter shows a cylinder inserted between the rims of the cut pushing away the region above the geodesic, i.e not only the geodesic but the upper part of the Poincaré disc too. This operation is called **grafting**. Its counterpart is **pruning**, when a cylinder is removed. The question arises whether this new disc still has an hyperbolic structure and what structure can be given to the lune. We shall study metric matters in the next chapter.

3.2.1. Tessellating with the modified tile

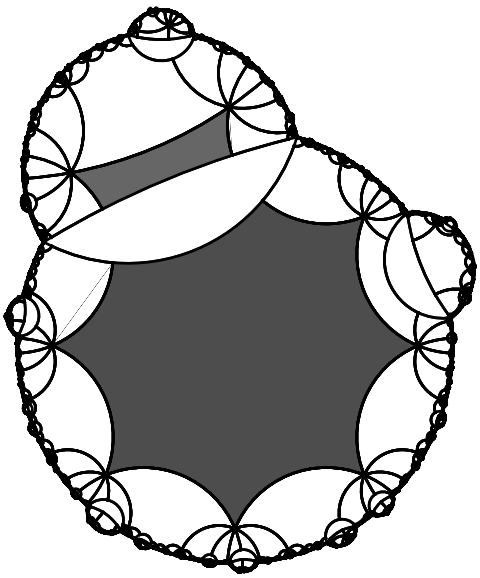

Figure 3.4.: Grafted tiling

Figure 3.4 was made with the program Bubble_Graft_octo.

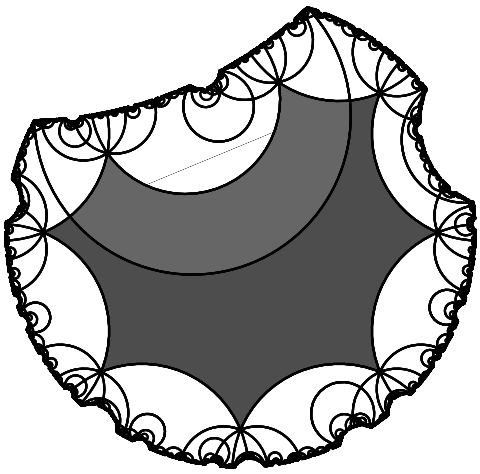

Figure 3.5.: Pruned tiling

Figure 3.5 was made with the program Bubble_Prune_octo.

Having computed the generators the temptation arises to begin tessellating before new tailoring the fundamental tile. This proves very soon to be a bad idea. The proper way is to first construct the new fundamental tile, before computing anew the generators according to what happened with the tile.

To tailor the new tile the first step is to cut the original one into domains bordered by the octagon and the geodesic. In the present case there is one part of the octagon under the geodesic which will remain unaffected and the other part above where something will happen.

This *domaining* of the tile will also be used later on, when the closed geodesic will have several leaves.

The first reason for this *modus operandi* is to take into account in which order the pieces of the puzzle get moved. Once the decomposition of the puzzle has been defined the moves are hierarchized : choose first the domain which is not affected by the moves of the others, then the domain which is only affected by the move of the first one, etc.

The second reason is that the geodesic is a single line whereas the lune created by pruning has two rims. With earthquakes or pruning there is no lune, but the segments on the support are not the same. Pruning requires one more (tedious) operation : the pruned off stuff must be cut away at the very beginning.

After the tile has been retailored and the generators tuned in accordingly, tessellating uses the same list of words, thus exactly the same instructions, as were used for the original tile.

3.2.2. An earthquake on the octagon

From the point of view of visualization the earthquake is quite ungrateful an operation. The problem, so to say, is that the boundary of the Poincaré disc shows no changes. The best we could achieve was to fill in the fundamental tile with color. Alternatively the coloration could be extended to all tiles but the small improvement is not worth the longer computing time.

The Poincaré disc remains round as ever, the metric is still everywhere the Poincaré metric of Gaussian curvature -1. Only on the geodesic itself the metric is undefined. In fact twice the same geodesic is translated along itself.

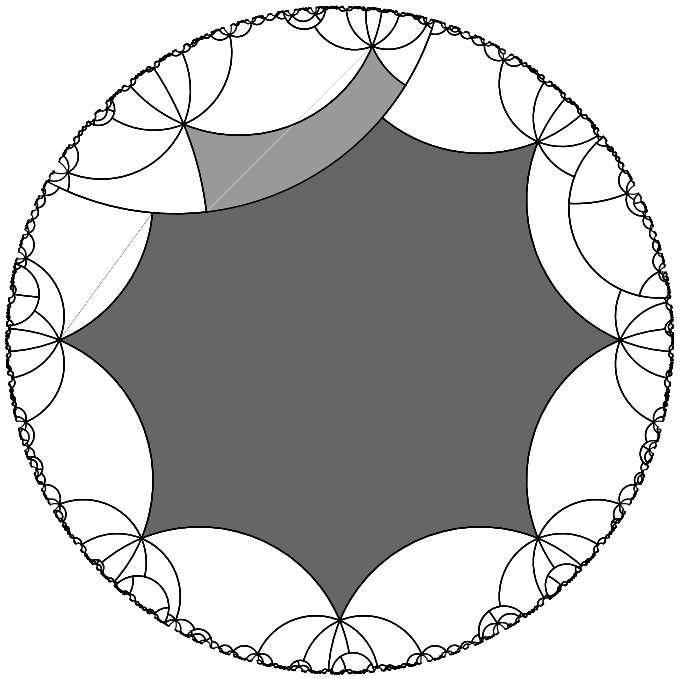

Figure 3.6.: An earthquake on the octagon

Figure 3.6 was made with Bubbles_Equake_octo.

3.2.3. Grafting and pruning on the Riemann sphere

The same angle of $\frac{\pi}{3}$ has been used for both figures 3.4 and 3.5. A close look reveals that the nooks and crannies seem to agree together... and they really do!

The reason for this becomes clear when we transport the Poincaré disc onto the Riemann sphere $\mathbb{C}P^1$. Then there are two discs. The interior disc is centered on the origin and the exterior disc centered on the point ∞. Grafting pushes outwards the border of the inner unit disc whereas pruning pushes inwards into the outer disc. The fractal limit set is the limit curve of both tessellations.

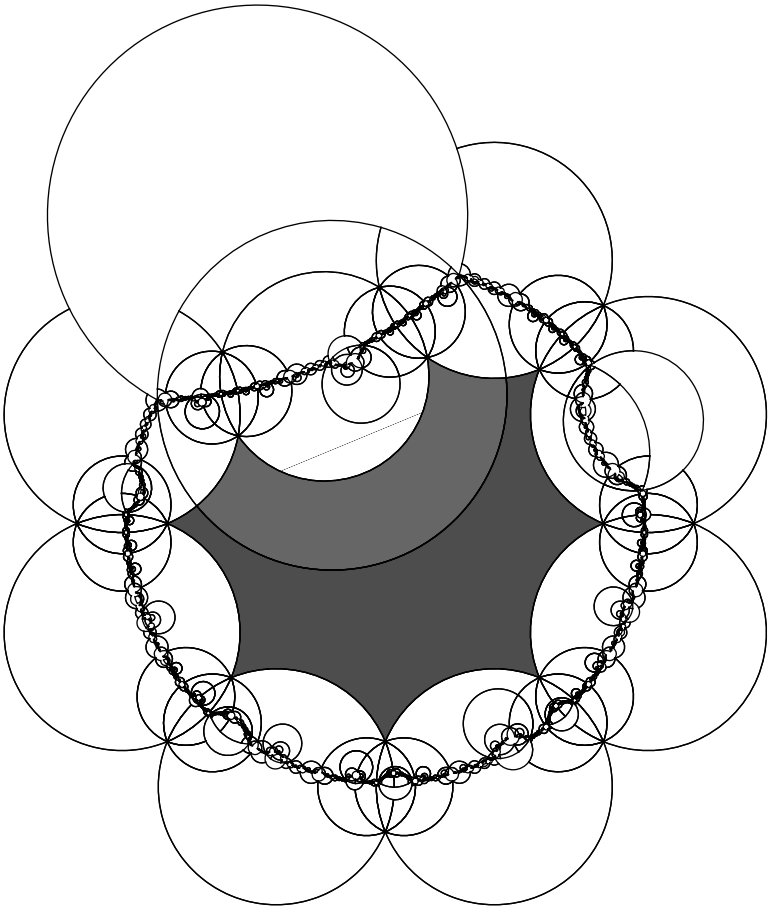

Figure 3.7.: Grafting and pruning are complementary

Figure 3.7 - made with Bubble_Prune_octo - was obtained easily by inverting the points of the grafting map against the unit circle. It reveals how the limit set gets pinched in.

This idea was originated by Benoit Mandelbrot as he proved that the curve depicting the limit set of touching Schottky circles presented by Fricke and Klein [13, fig. 156] is a misleading simplification. He created the tool of sigma-discs revealing a very intricated limit set. [28, Indra's Pearls] also use this idea.

The octagon model is not really appropriate for visualizing the limit set of grafting and pruning. This is because the non free group with 8 octagons around a vertex infers too many duplicates, thus a long computing time when approaching the limit set.

The program Pretzel_Pruning_tess using the dodecagon model returns figure 3.9 which is a zoomed extract of the limit set of the tessellation of figure 3.8.

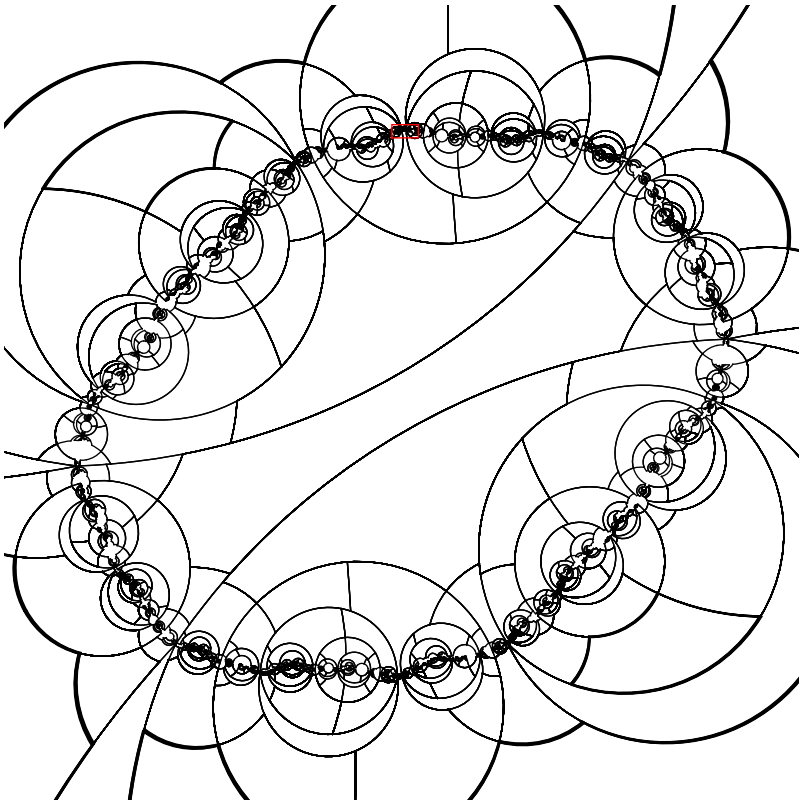

Figure 3.8.: Grafting and pruning with the dodecagon

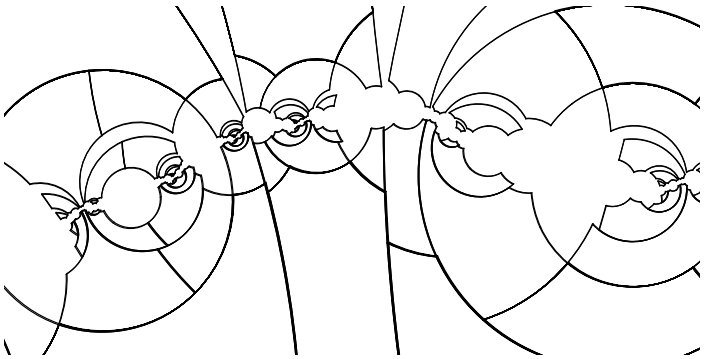

Figure 3.9.: Zooming in the limit set

3.2.4. Bubbles on bubbles

Instead of the tessellation the pictures 3.10 and 3.11 show the surrounding Poincaré circles which the tessellation fills in. Bubbles swell out riding on bubbles (Thurston speaks of Mickey Mouse ears) in the grafting picture which correspond with the erosion acted by pruning. This might give a better idea of the limit set.

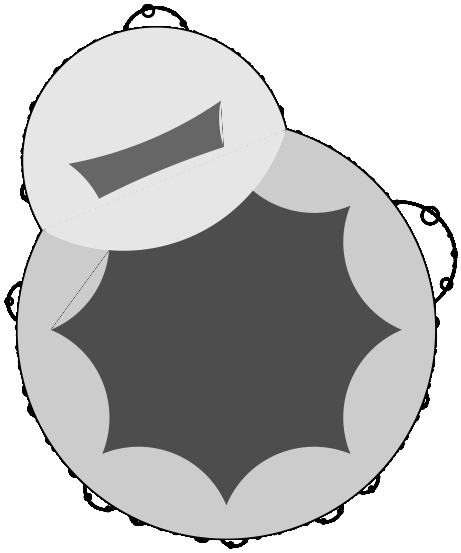

Figure 3.10.: Grafted discs

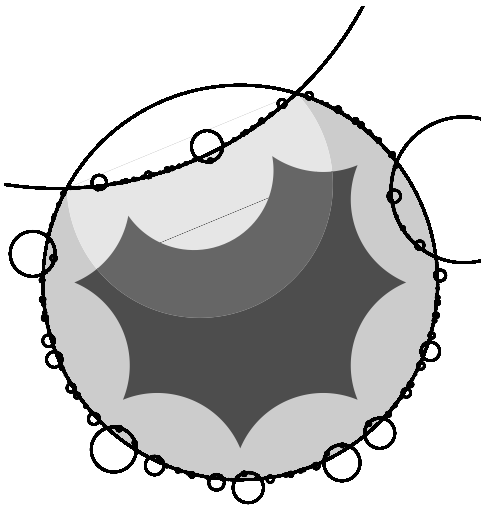

Figure 3.11.: Pruned discs

3.2.5. The maximal angle for pruning

Is is a general phenomenon that the angle of grafting or pruning is bounded. In the end infinite geodesics do not allow any pruning or grafting any more, as we shall see.

With the 1-leaf closed geodesic around the handle there is a lot of room for grafting or pruning, but there is a limit in this case too.

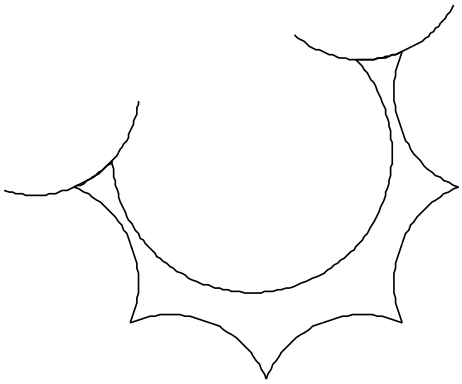

Figure 3.12.: Near the limit

Picture 3.12 shows that we can push down the edge b_1, whose endpoints glide along the identified edges a_1 and A_1. The same happens when grafting, it is a consequence of the Appolonian properties.

We can push until b_1 will kiss the pair (a_1, A_1). Then the tile would become disconnected, i.e. it would be no tile any more.

The limit angle for pruning happens to be $\alpha \approx \frac{11}{29}\pi$.

Chapter 4.

The metric of grafting and pruning

As we remarked twisting preserves the hyperbolic metric but the lunes of grafting or twisting are moves which affect the metric. We want to study the changes. First we show that the Gaussian curvature is -1 for any radius of the Poincaré disc.

4.1. Hyperbolic metric in the disc

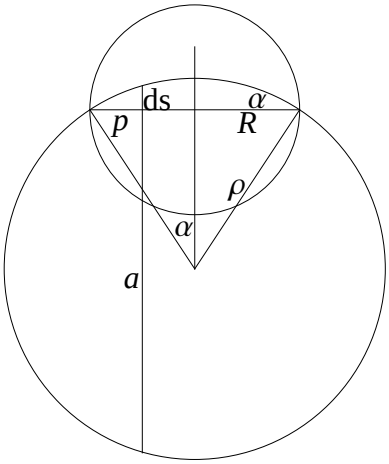

Figure 4.1.: Computing the metric

Let the smaller circle be the Poincaré disc of radius R. The arc inside the disc supported by the larger circle of radius ρ is an equidistant curve at a constant hyperbolic infinitesimal distance ds from the real line. Let a be the length of the segment under the vertical line supporting ds.

As hyperbolic moves preserve distances, all geodesics are conjugated, so there is no loss of generality to interpret the diameter as the image of any geodesic in the Poincaré disc.

Consider a point p on the diameter. Let $d\hat{s}$ be the preimage of ds on the hyperbolic plane measured through the angle α :

$$d\hat{s} = \alpha \approx \sin\alpha = \frac{R}{\rho} \rightsquigarrow \rho = \frac{R}{d\hat{s}}$$

It follows with the secants theorem $(R-p)\,(R+p) = ds\,a$.

It is easy to verify : $a = 2\sqrt{\rho^2 - R^2} + ds$. Thus for $ds \to 0$, $a \to 2\rho$ (as $\rho \to \infty$) :

$$R^2 - p^2 = (R-p)(R+p) = 2\rho \quad ds = 2\frac{R}{d\hat{s}} ds \rightsquigarrow d\hat{s} = \frac{2R}{R^2 - p^2} ds$$

For a point z conjugated to p, i.e. which was sent to p by a hyperbolic move with $|z| = p$:

$$\boxed{d\hat{s} = \frac{2R}{R^2 - |z|^2}} \tag{4.1}$$

is the metric of a Poincaré disc of radius R.

Consider on $\mathbb{D}^2$ an integration path $\gamma : \quad [0,1] \to D^2 \quad \| \quad \gamma(0) = 0, \quad \gamma(1) = w.$

The length of γ based on the metric is:

$$\boxed{L(\gamma) = \int_0^1 \frac{2R|\gamma'|}{R^2 - |\gamma|^2} dt} \tag{4.2}$$

Proposition 7. *Changing to R the unit radius of the Poincaré disc infers a scaling by $\frac{1}{R}$ of the argument of the* arctan *in the distance formula.*

Proof. Let $\gamma = r(t) e^{i\phi} \rightsquigarrow \gamma' = r' i\phi + ire^{i\phi}\phi' \rightsquigarrow |\gamma'|^2 = r^2 + r^2\phi'^2$, then

$$L(\gamma) = \int_0^1 \frac{2R}{R^2 - r^2} \sqrt{r'^2 + r^2\phi'^2} dt \geq \int_0^1 \frac{2R}{R^2 - r^2} r' dt = 2 \arctan \frac{|w|}{R}$$

The length from the origin to w is the minimum $2 \arctan \frac{|w|}{R}$. The Möbius transformation back from the diameter gives the distance of any two points z_1 and z_2 of the disc

$$d(z_1, z_2) = 2 \arctan \frac{1}{R} \left| \frac{z_1 - z_2}{\bar{z}_2 z_1 - 1} \right|$$

□

For $R = 1$ this is the well known distance formula along a geodesic.

4.2. Gaussian curvature of the Poincaré disc

We can expect that when Möbius moves send circles to circles with a different radius the hyperbolic structure within the circle is preserved. We just check this.

Proposition 8. *The Gaussian curvature is still $K = -1$ when the Poincaré disc has radius R.*

Proof. We consider a small disc around the origin.

For $z = x + iy$ in $\mathbb{R}^2$ apply the factor $\lambda(x,y) := \frac{2R}{R^2 - (x^2+y^2)}$ on the metric, then

$$d\hat{s} = \lambda ds = \lambda \sqrt{dx^2 + dy^2}$$

At the origin $\lambda_{xx} = \lambda_{yy} = \frac{4}{R}$ and $\lambda_{xy} = \lambda_{yx} = 0$.

We know from differential geometry that the first **fundamental form** with $E = \lambda_{xx}, \quad F = \lambda_{xy} = \lambda_{yx} = 0, \quad G = \lambda_{yy}$ characterizes a conformal (i.e. isothermic) surface due to $E = G$ and $F = 0$.

The BRIOSCHI formula for Gaussian curvature has for $F = 0$ the simplified form:

$$K = \frac{-1}{\sqrt{EG}} \left(\frac{\partial}{\partial x} \left(\frac{1}{\sqrt{E}} \frac{\partial \sqrt{G}}{\partial x} \right) + \frac{\partial}{\partial y} \left(\frac{1}{\sqrt{G}} \frac{\partial \sqrt{R}}{\partial y} \right) \right)$$

Using this and $E = G$ we get (Δ being the **Laplacian**):

$$K = \frac{-1}{\lambda^2} \left(\frac{\partial}{\partial x} \left(\frac{1}{\lambda} \frac{\partial \lambda}{\partial x} \right) + \frac{\partial}{\partial y} \left(\frac{1}{\lambda} \frac{\partial \lambda}{\partial y} \right) \right) = \frac{-1}{\lambda^2} \left(\frac{\partial^2}{\partial x^2} \log \lambda + \frac{\partial^2}{\partial y^2} \log \lambda \right) = \frac{-\Delta \log \lambda}{\lambda^2}$$

For $\lambda = \frac{2R}{R^2 - (x^2 + y^2)}$ follows $K = -1$ at the origin and everywhere as the curvature is constant. □

4.3. Inserting a lune preserves geodesics

What we want to do is to insert a cylinder into the pretzel, i.e. a lune into each of the infinitely many octagons of a tessellation. There is fortunately a less awkward method!

Proposition 9. *Using an octagon blown up by a lune as fundamental tile is the same as inserting a lune into each tile of a tessellation.*

Proof. When we open a lune of angle α the part of the unit disc beyond the cut is transformed to a part of a new disc of radius R bordered by an arc circle standing orthogonally on the other lip of the cut.

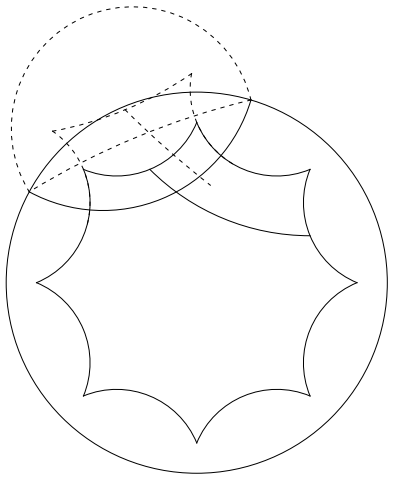

Figure 4.2.: Geodesics are preserved

The geodesical arcs of the tessellation, which were orthogonal to the unit disc, are transformed into new geodesical arcs, orthogonal to the border of the new disc of radius R by conformality.

Conformality also infers, that the tessellation of the new disc of radius R is made of regular octagons. The sum of the angles of a triangle defines the octagon uniquely up to a hyperbolic move. As the new octagon has the same angles, triangulating in octants satisfies that the image is the same regular octagon in the new disc. Triangulating leads to the analogous result for the displaced part of the octagon.

Due to the new disc radius $R < 1$ the Euclidean distance is scaled by the factor $\frac{1}{R}$ in the arctan of the distance formula, up to the coordinate change of the origin having been moved to the center of the new disc.

The Gaussian curvature is everywhere constant $= -1$. This respects also the statement of *theorema egregium*, that curvature does not change, when distorting a surface without stretching or shrinking. □

4.4. Finding a metric for grafting

We have seen that the bubbling up Poincaré discs all have Gaussian curvature $K = -1$. The lune being some sort of no man's land, the question arises of what happens there with the curvature. So we want to define a metric for any two Poincaré discs paired by a Möbius transformation.

We refer in the following to the methodology of R.S. Kulkarni and U. Pinkall in [19] *A Canonical Metric for Möbius Structures And Its Applications.*

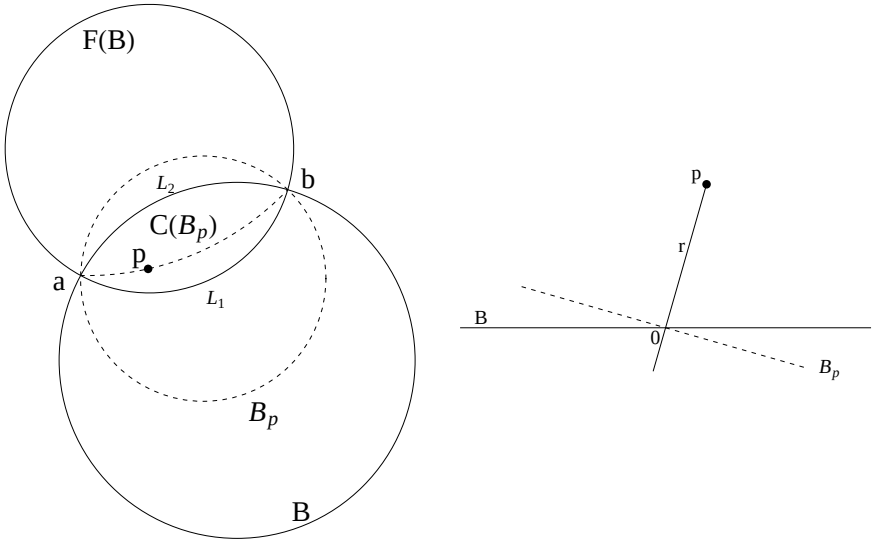

Figure 4.3.: Round balls

Let F be the Möbius transformation opening a lune of angle α. Let B be a round ball, i.e. an open disc (the unit ball around the octagon at the start).

Let L_1 and L_2 be the rims of the lune. L_1 stands for the geodesic before grafting, L_2 supported by B is the maximum grafting allowed (the rim cannot lie outside B). Let a and b be the points where $B, F(B), L_1, L_2$ intersect. Choose a point p inside the lune, defining a stratum i.e. an arc (a, p, b) and the ball B_p on which (a, p, b) stands

orthogonally. Every p defines an arc (a, p, b) between L_1 and L_2 corresponding to a grafting angle α.

The metric is to be defined on $M := B \cup F(B)$.

The part of B underneath L_1 can be considered as a bounded half space in a Poincaré disc, say H_B. All the same L_2 borders a half space $H_{F(B)}$ in $F(B)$. In both half spaces one can use the Poincaré disc metric for the ball of the corresponding radius.

Any point p on the lune defines a unique disc B_p orthogonal to the arc through a, p and b.

Letting p wander transversely from L_1 to L_2, the ball B_p moves from B to $F(B)$, sweeping along through all of M.

The convex hull of a subset of the unit disc $\mathbb{D}^2$ is here defined as the intersection of the complements $\mathbb{D}^2 \backslash B_p$, where B_p runs with p over all round balls which do not intersect the subset and are orthogonal to the unit circle.

The arc (a, p, b) touches the boundary ∂M only in a and b (so far $p \notin L_1, L_2$). So this arc is the convex hull of B_p, noted $C(B_p)$.

According to theorem 4.4 of [19] there is a unique maximal ball B_p such that $p \notin C(B_p)$. Consequently the arcs $C(B_p)$ form a stratification of the lune.

So M is the disjoint union of H_B, $H_{F(B)}$ and the family of arcs filling the lune:

$$M = H_B \cup \overset{\circ}{\bigcup_{p \in lune}} C(B_p) \cup H_{F(B)}$$

We can use a and b as pivots in order to work on the sphere $\mathbb{S}^2 \backslash \{0, \infty\} \cong \mathbb{C} \backslash \{0\}$ which is the topological cylinder $\mathbb{S}^1 \times \mathbb{R}$.

On the right of figure 4.3 a Möbius transformation sends a and b to 0 and ∞, so that the transformed of B_p is an open half space in $\mathbb{E}^2$. The same applies to B. We take B such that $x_1 > 0$ and B_p is another line through the origin, their angle being α due to conformality.

Due to conformality p lies on the perpendicular to B_p at a distance r of the origin.

Let z be the coordinate of the image of p. We identify the half space bounded by B_p which contains p with $\mathbb{C} \backslash \{0\}$.

Let $g_{B_p} := g_{\mathbb{C} \backslash \{0\}}$ be the metric of this half space and $\hat{g}_{B_p} := g_{\mathbb{C}/z \mapsto z + 2\pi i}$ be the metric on the cylinder.

Proposition 10.

$$g_{B_p} = |d \log z|^2 = \left| \frac{dz}{z} \right|^2 = \frac{|dz|^2}{|z|^2} = \frac{1}{r^2} dz^2$$

is a metric for the ball.

Proof. One can readily check that the axioms for metrics apply.

We claim that the mapping $\mathbb{C}/z \mapsto z + 2\pi i \to \mathbb{C} \backslash \{0\}$ is an isometry.

Let r be the distance of p from the origin in the mapping where the cusps a and b are sent to 0 and ∞.

For a tangent vector $X \in T_p\mathbb{C}\backslash\{0\}$ we have $g_{B_p}(X,X) = |(d_p \log)(X)|^2$.

Due to $d_p \log$ being the inverse function of $d_p \exp$, we get $g_{B_p}(X,X) = \hat{g}B_p\left(\hat{X},\hat{X}\right)$ for the vector $\hat{X} \in \mathbb{C}/z \mapsto z + 2\pi i$ pulled back from X. This is an isometry.

We use now the exponential function $\exp : \mathbb{C}/z \mapsto z + 2\pi i \to \mathbb{C}\backslash\{0\}$ to pull back g_{B_p} from the flat $\mathbb{C}\backslash\{0\}$, so as to define $\hat{g}_{B_p}$ on the cylinder $\mathbb{C}/z \mapsto z + 2\pi i$.

Consider $w \in \mathbb{C}/z \mapsto z + 2\pi i$. The differential map of the exponential function being the exponential function itself we get:

$$\hat{g}_{B_p} = \exp^* g = |(d\log)(de^w)|^2 = \left|\frac{d(de^w)}{de^w}\right| = \left|\frac{e^w}{e^w}dw\right|^2 = dw^2$$

So the pulled back $\hat{g}_{B_p}$ is an Euclidean metric, i.e. $\mathbb{C}/_{z\mapsto z+2\pi i}$ with this metric is flat. The isometry implies that g_{B_p} and $\hat{g}_{B_p}$ are flat metrics. So $g = \frac{1}{r^2}|dz|^2$ is a flat metric for all points $p \in C(B_p)$. □

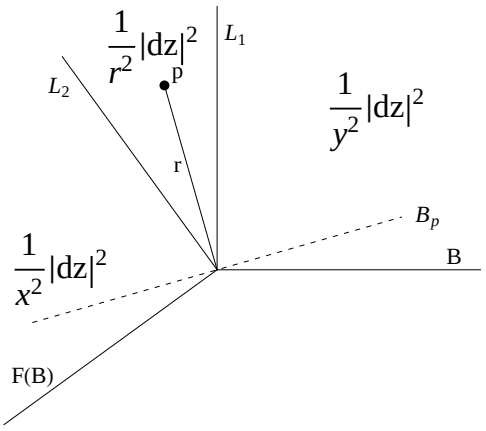

Figure 4.4.: Metric across a graft

The half space B bordered on the left by L_1 can be given the classical hyperbolic Poincaré metric $\frac{1}{Im(z)^2}|dz|^2$ of constant curvature $K = -1$, which is related to the disc B by the inverse Möbius transformation sending 0 and ∞ back to a and b. All the same the half space $F(B)$ bordered by L_2 gets this half space metric, which is then pulled back to the disc. So both discs B and $F(B)$ receive metrics of constant curvature -1. Only the radii differ, the curvature remains the same. Of course the radius has to be taken into account to fix the metric in all the discs.

The rim L_1 of the lune is as well a geodesic of the half plane as the line on the lune joining $p \in C(B)$ to the origin. So the transition in L_1 is smooth. The same consideration applies to the other rim of the lune L_2. So the metric function is smooth everywhere, although the curvature is flat on the lune but constant -1 elsewhere.

Thus sending the cusps a and b to 0 and ∞ gives a smooth metric function for all $p \in M$ which can be pulled back by the inverse Möbius transformation. This proves the

Proposition 11. *The metric function $g_{B_p} = \frac{1}{r^2}|dz|^2$ is flat within the lune and of constant curvature -1 outside. This metric function propagates to the whole grafted cover, i.e. to the images generated by a tessellating Möbius transformation.*

4.5. Finding a metric for pruning

Let us add a point∞ to $\mathbb{C}$ so as to obtain the Riemann Sphere $\mathbb{C}P^1$. There the Poincaré disc is bordered by a circle. The outside of the circle is another Poincaré disc, which can also be tessellated with the analogous tessellation, this comes up to exchanging 0 and ∞. When grafting the interior of the circle is blown up, pushing away the exterior which gets crushed. This counterpart of grafting is pruning. Instead of inserting a cylinder into the pretzel along a closed geodesic a cylinder is removed.

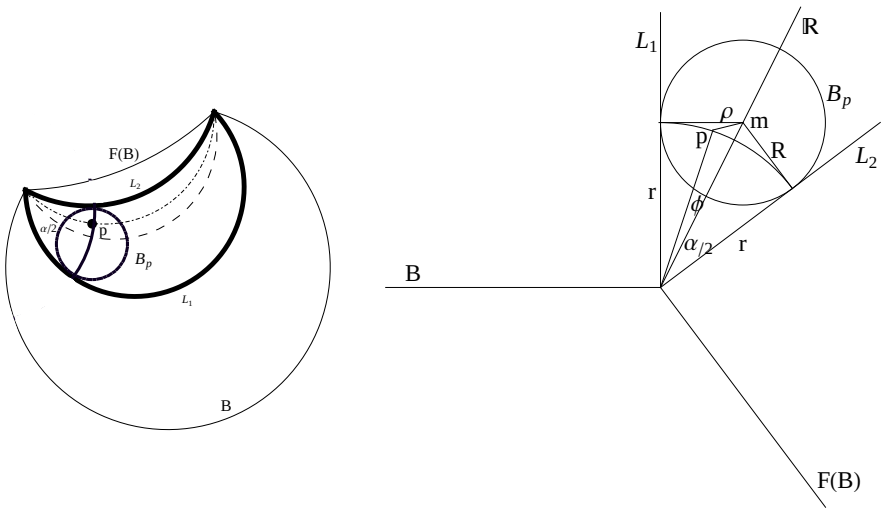

Figure 4.5.: Pruning lunes

We exchange 0 and ∞ and examine what happens. The upper part is unmoved. The cut L_1 is pushed up to L_2, the rest of the circle as well. B and $F(B)$ form a large lune containing the inner lune bordered by L_1 and L_2.

Any point p on a stratum of the small lune defines a unique circle orthogonal to all the arcs through the cusps (= Apollonian pencil). This defines again the unique circle B_p centered on the bisector of α and tangent to the lips of the small lune.

In picture 4.5 we send the cusps to 0 and ∞ (as for grafting the schematic picture at infinity does not reproduce the same stratum nor the same opening angle).

- Let φ be the angle fixed by p.
- Let m be the midpoint of the circle B_p, R its radius and ρ the distance from p to m.
- Let r be the distance from p to the origin.

The circle B_p with radius R gets as a Poincaré disc the hyperbolic metric (4.1):

$$g_{B_p} = \frac{4R^2}{\left(R^2 - \rho^2\right)^2} \left|dz\right|^2$$

Consider alternatively the metric

$$g_{D(1)} = \frac{4\left|dz\right|^2}{\left(1 - \left|z\right|^2\right)^2}$$

for the disc of unit radius.

With the mapping $z \mapsto z/R$ we get for the disc $D_{(R)}$ of radius R:

$$g_{D(R)} = \frac{4\left|\frac{dz}{R}\right|^2}{\left(1-\left|\frac{z}{R}\right|^2\right)^2} = \frac{4R^2}{\left(r^2-|z|^2\right)^2}$$

We chose the bisector as the real axis, so that $m \in \mathbb{R}^+$. We write $p = re^{i\varphi}$.

By easy trigonometry $R = r\tan\frac{\alpha}{2}$ and $m = \frac{r}{\cos\frac{\alpha}{2}}$ enable to compute:

$$\begin{aligned}
\rho^2 &= |p-m|^2 \\
&= \left|re^{i\varphi} - \frac{r}{\cos\frac{\alpha}{2}}\right| \\
&= \left(re^{i\varphi} - \frac{r}{\cos\frac{\alpha}{2}}\right)^2 + r^2\sin^2\varphi \\
&= \frac{r^2}{\cos^2\frac{\alpha}{2}}\left(\cos^2\frac{\alpha}{2} - 2\cos\varphi\cos\frac{\alpha}{2} + 1\right)
\end{aligned}$$

We put ρ^2 in the formula for the metric:

$$\begin{aligned}
g_{B_p} &= \left(\frac{2r\tan\frac{\alpha}{2}}{r^2\tan^2\frac{\alpha}{2} - \frac{r^2}{\cos^2\frac{\alpha}{2}}\left(\cos^2\frac{\alpha}{2} - 2\cos\varphi\cos\frac{\alpha}{2} + 1\right)}\right)^2 |dz|^2 \\
&= \left(\frac{1}{r}\frac{\sin\frac{\alpha}{2}\cos\frac{\alpha}{2}}{\sin^2\frac{\alpha}{2} - \cos^2\frac{\alpha}{2} + 2\cos\varphi\cos\frac{\alpha}{2} - 1}\right)^2 |dz|^2 \\
&= \left(\frac{2}{r}\frac{\sin\frac{\alpha}{2}\cos\frac{\alpha}{2}}{-2\cos^2\frac{\alpha}{2} + 2\cos\varphi\cos\frac{\alpha}{2}}\right)^2 |dz|^2 \\
&= \frac{1}{r^2}\frac{\sin^2\frac{\alpha}{2}}{\left(\cos\varphi - \cos\frac{\alpha}{2}\right)^2}|dz|^2
\end{aligned}$$

g_{B_p} is positive and finite so far $\varphi \neq \frac{\alpha}{2}$. The other metric axioms are also respected.

With the notation $\lambda(\alpha,\varphi) := \frac{\sin\frac{\alpha}{2}}{\cos\varphi - \cos\frac{\alpha}{2}}$ the metric becomes

$$g_{B_p} = \frac{1}{r^2}\lambda^2|dz|^2$$

Let $g = \begin{pmatrix} E & F \\ F & G \end{pmatrix} = \begin{pmatrix} g_{11} & g_{12} \\ g_{21} & g_{22} \end{pmatrix}$ be the first fundamental form for a metric and ds be the line element. Then

$$ds^2 = \begin{pmatrix} du & dv \end{pmatrix}\begin{pmatrix} E & F \\ F & G \end{pmatrix}\begin{pmatrix} du \\ dv \end{pmatrix} = E\,du^2 + 2F\,dudv + G\,dv^2$$

For a real function μ and a conformal metric $ds^2 = \mu^2\left(du^2+dv^2\right)$ the comparison with $E\,du^2 + 2F\,dudv + G\,dv^2$ implies $E = G = \mu^2$ and $F = 0$. But $F = 0$ simplifies the Brioschi formula for the Gaussian curvature:

$$K = \frac{-1}{2\sqrt{EG}}\left(\frac{\partial}{\partial u}\left(\frac{G_u}{\sqrt{EG}}\right) + \frac{\partial}{\partial v}\left(\frac{E_v}{\sqrt{EG}}\right)\right)$$

$E = G = \mu^2$ yields a further simplification

$$K = \frac{-1}{\mu^2}\left(\frac{\partial}{\partial u}\left(\frac{1}{\mu}\frac{\partial \mu}{\partial u}\right) + \frac{\partial}{\partial v}\left(\frac{1}{\mu}\frac{\partial \mu}{\partial v}\right)\right) = \frac{-1}{\mu^2}\left(\frac{\partial^2}{\partial u}\log\mu + \frac{\partial^2}{\partial v}\log\mu\right)$$

Let Δ be the Laplacian, then $K = \frac{-\Delta \log \mu}{\mu^2}$ (alternatively: $K = \frac{-\Delta u}{e^{2u}}$ for $\mu = e^u$).

Here : $\mu = \frac{\lambda}{r} \rightsquigarrow K = \frac{-r^2}{\lambda^2}\Delta \log \frac{\lambda}{r}$.

Choosing for p polar coordinates $\{r, \varphi\}$ the formula for the Laplacian becomes:

$$\Delta = \frac{\partial^2}{\partial r^2} + \frac{1}{r^2}\frac{\partial^2}{\partial \varphi^2} + \frac{1}{r}\frac{\partial}{\partial r}$$

Now we can compute:

$$\frac{\partial}{\partial r}\log\frac{\lambda}{r} = -\frac{1}{r} \rightsquigarrow \frac{\partial^2}{\partial r^2}\log\frac{\lambda}{r} = \frac{\partial}{\partial r}\left(-\frac{1}{r}\right) = \frac{1}{r^2}$$

$$\begin{aligned}\frac{\partial^2}{\partial \varphi^2}\log\frac{\lambda}{r} &= \frac{\partial}{\partial \varphi}\left(\frac{\sin\varphi}{-\cos\frac{\alpha}{2} + \cos\varphi}\right) \\ &= \frac{\cos\varphi}{-\cos\frac{\alpha}{2} + \cos\varphi} + \frac{\sin^2\varphi}{\left(-\cos\frac{\alpha}{2} + \cos\varphi\right)^2}\end{aligned}$$

Hence

$$\begin{aligned}\Delta \log\frac{\lambda}{r} &= \frac{1}{r^2} + \frac{1}{r^2}\left(\frac{\cos\varphi}{-\cos\frac{\alpha}{2} + \cos\varphi} + \frac{\sin^2\varphi}{\left(-\cos\frac{\alpha}{2} + \cos\varphi\right)^2}\right) - \frac{1}{r}\frac{1}{r} \\ &= \frac{1}{r^2}\left(\frac{\cos\varphi}{-\cos\frac{\alpha}{2} + \cos\varphi} + \frac{\sin^2\varphi}{\left(-\cos\frac{\alpha}{2} + \cos\varphi\right)^2}\right)\end{aligned}$$

Hence $K = -\frac{-r^2}{\lambda^2}\Delta \log\frac{\lambda}{r} \rightsquigarrow$

$$K = -\frac{r^2\left(-\cos\frac{\alpha}{2} + \cos\varphi\right)^2}{\sin^2\frac{\alpha}{2}}\frac{1}{r^2}\left(\frac{\cos\varphi}{-\cos\frac{\alpha}{2} + \cos\varphi} + \frac{\sin^2\varphi}{\left(-\cos\frac{\alpha}{2} + \cos\varphi\right)^2} + \frac{1}{r^2}\right)$$

For $\varphi \neq \pm\frac{\alpha}{2}$ this is:

$$\begin{aligned}K &= -\frac{1}{\sin^2\frac{\alpha}{2}}\left(\cos\varphi\left(-\cos\frac{\alpha}{2} + \cos\varphi\right) + \sin^2\varphi\right) \\ &= -\frac{1}{\sin^2\frac{\alpha}{2}}\left(1 - \cos\frac{\alpha}{2}\cos\varphi\right)\end{aligned}$$

Near to both rims of the lune, i.e. for $\varphi \to \pm\frac{\alpha}{2}$, we get $K \to -1$. For $\varphi = \pm\frac{\alpha}{2}$, we are allowed by continuity to set $K = -1$ as the curvature is everywhere -1 outside the lune.

We write this result as

Proposition 12. *The curvature $K(\varphi, \alpha)$ crosses smoothly the rims of the lune, although the metric*

$$g_{B_p} = \frac{1}{r^2} \frac{\sin^2 \frac{\alpha}{2}}{\left(\cos\varphi - \cos\frac{\alpha}{2}\right)^2} |dz|^2$$

becomes infinite.

For a given $\alpha > 0$ the gradient $\frac{\partial K}{\partial \varphi} = -\frac{\sin\varphi}{\tan\frac{\alpha}{2}\sin\frac{\alpha}{2}}$ vanishes for $\varphi = 0$. Then there is for all α a maximum $K_{max} = \frac{\cos\frac{\alpha}{2}-1}{\sin^2\frac{\alpha}{2}} > -1$. This K_{max} is a monotonous decreasing function of α with maximum of $-0,5$ for $\alpha \to 0$. This proves the

Proposition 13. *The range of local curvature is*

$$-1 \leq K \leq \frac{\cos\frac{\alpha}{2} - 1}{\sin^2\frac{\alpha}{2}} < -0,5$$

Gathering results

- Inside the lune the hyperbolic conformal metric $g_{B_p} = \frac{1}{r^2} \frac{\sin^2\frac{\alpha}{2}}{\left(\cos\varphi - \cos\frac{\alpha}{2}\right)^2} |dz|^2$ is a function of the angle φ for any point with polar coordinates (r, φ). The curvature is $-1 \leq K \leq \frac{\cos\frac{\alpha}{2}-1}{\sin^2\frac{\alpha}{2}} < -0,5$.
- Outside the lune the Poincaré disc metric has constant curvature $K = -1$.
- The curvature $-1 \leq K \leq \frac{\cos\frac{\alpha}{2}-1}{\sin^2\frac{\alpha}{2}} < -0,5$ of $B \cup F(B)$ remains smooth when crossing the lune.

Summary of this chapter

Using a Möbius transformation as geometric scissors we cut a pretzel along a closed geodesic and insert a stripe widening out the geodesic. The boundary of the universal cover becomes a fractal due to the lunes created in each tile by the insertion of the stripe.

This fractal cover was given a metric and the curvature was established.

When grafting on the Riemann sphere the blown up tessellation has constant negative curvature -1 but for the lunes which are Euclidean.

The metric changes smoothly when crossing a lune, whereas the curvature jumps abruptly from -1 to 0.

From the point of view of what happens in the exterior disc of the Riemann sphere, exchanging 0 and ∞ describes pruning as a crushing. Outside the lens the curvature is still constant $= -1$. Crossing into the lune the conformal metric has a singularity whereas the curvature changes smoothly in the range $-1 \leq K < -0,5$.

Chapter 5.

The harlequin model

The octagon model hides a secret jewel that enables us to visualize the inner life of the pretzel.

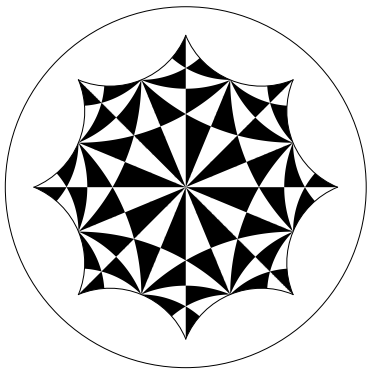

Figure 5.1.: Checked octagon

The Euler characteristic χ discloses the area of an orientable closed surface S as $-2\pi\chi(S)$. For genus $g > 1$ follows $\chi = 2 - 2g$, thus the area of the pretzel is 4π. For a triangle the area is the complement to π of the sum of angles. The triangle 2-3-8, say T, has area $\pi - \left(\frac{\pi}{2} + \frac{\pi}{3} + \frac{\pi}{8}\right)$. Consequently the pretzel has exactly 96 times the area of the triangle T. It is marvelous that these 96 triangles can actually be arranged to pave the octagon.

Take an octagon with angle $\frac{2\pi}{3}$ and cut it into 8 quadrilaterals, each made of two triangles T glued along their hypotenuses. These are 8 quadrilaterals. Glue then a half octagon along each edge of the central octagon. These are 32 new quadrilaterals. Complete with 8 quadrilaterals to get the vertices.

This is the decomposition of the octagon into 48 quadrilaterals, i.e. 96 times one and the same triangle 2-3-8.

This nearly anecdotic property delivers when tessellating a quite impressive feeling for the inner structure of the pretzel. Using undecorated pretzels failed to reveal what happens inside the octagon.

5.1. Tessellating with the checked tile

The octagon tessellates the disc, thus the triangle 2-3-8 also tessellates the disc. This seems to be an elegant way to construct the tiling with 2-3-8 triangles, but obviously

it is still easier to use the small octagon! Just enter *ShowXLTess[8,3]* and our program *diskgeometry* returns the same tessellation, as obtained with the larger octagon. The tessellation using the 16 triangles of the $\frac{2\pi}{3}$-octagon is the same as with the 96 triangles of the $\frac{\pi}{4}$-octagon.

Both octagons have the same universal cover. This makes clear why the smaller octagon dominates so much the visual impression. Still worse: it is extremely difficult to locate the larger octagon!

The good reason, why we prefer using the more complicated polygon is that we do not only want to show a tessellation but primarily to study the pretzel. The larger octagon is the so called standard fundamental polygon. Using such a 4g-gon (presently genus $g = 2$) has many advantages, for instance:

- All vertices are identified to one and the same,
- The edges can be marked off in pairs, with only one relation $a_1 b_1 A_1 B_1 \cdots a_g b_g A_g B_g = 1$,
- The edges are simple closed geodesics,
- The area is $4\pi\,(g-1)$.

When looking at the tiling the observer gets the feeling of floating in hyperbolic space over the hyperbolic plane. Staring at the horizon lets sense how it slopes away towards infinity.

The idea of this harlequin pavement was initiated by H.S.M. Coxeter see [9]. This tiling inspired M.C. Escher to his *Circle limit I*, where a hexagon is paved with black and white fishes. This paves the hyperbolic plane with triangles 2-4-6.

5.2. Harlequin earthquake and grafting

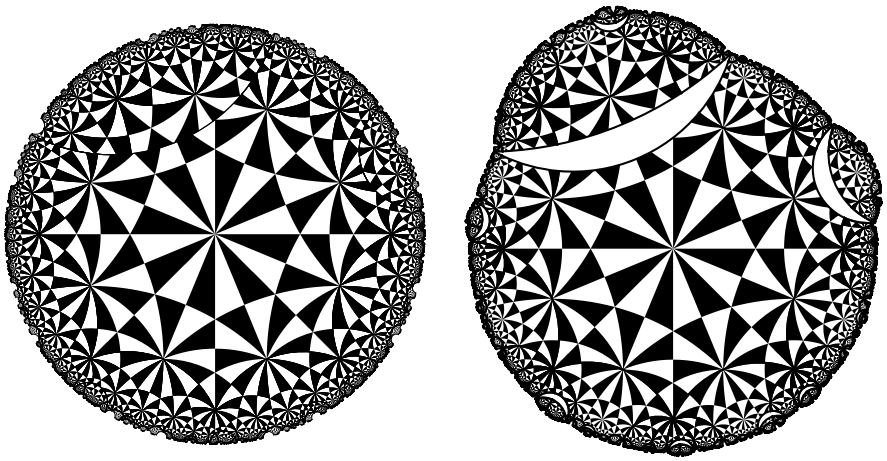

Figure 5.2.: Mishandling the harlequin

We must confess that the visualization of an earthquake on figure 5.2 is not impressive. The disarranged triangles along the clefts are an improvement of our previous picture but a sharp look is required.

Much more impressive is the visualization of grafting showed on the right and in the frontispiece.

The program Earthquake_96_tri for twisting and grafting is strictly the same but for putting in the appropriate matrix. One might be tempted to cut along the line joining the midpoints of two identified edges, but this is no simple closed geodesic. We used again the common perpendicular to two identified edges. This is a meticulous work, as there are cuts transversal to the triangles, but the result is worth the pain. The lunes are good visible and their effect on what is behind is instructive. The program builds on the algorithm for the plain octagon. Machine time is much longer due to the 48 triangles of the tile that have to be discretized for coloring (the white triangles are only lines marking the rims of the lunes).

We abstained from illustrating pruning as the result would be almost as messy as with the earthquake.

5.3. Weierstrass points

We anticipate on a property of non separating simple geodesics : they go through exactly two so called Weierstrass points. The common perpendiculars to the edges a_1/A_1 and b_1/B_1 live in the same handle of the pretzel. Each must go through two Weierstrass points. As there are only three points in the handle they must intersect in one of the three Weierstrass points.

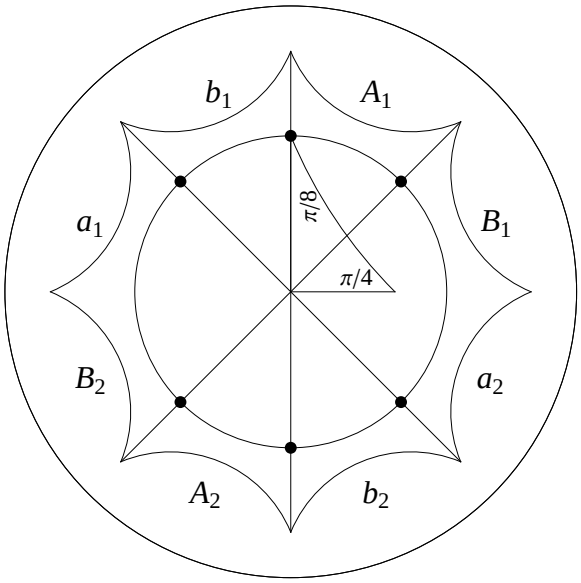

Figure 5.3.: Weierstrass points on the octagon

We have computed and checked in Weierstrass_octo that the above mentioned point is a vertex of the triangle 2-4-8. It is also a vertex of one of the harlequin triangles. The exact ordinate is

$$\sqrt{1-\frac{2}{1+\sqrt{2+\sqrt{2}}}}$$

It suffices to rotate about $\frac{\pi}{4}$ and $-\frac{\pi}{4}$ get the two other points of the handle. This means multiplying with $e^{i\frac{\pi}{4}} = \frac{1+i}{\sqrt{2}}$. Then the three points of the other handle follow by conjugating. All six points lie on a circle, the axis of the hyperelliptic involution.

5.4. Evaluation of the octagon model

We have praised the advantages of this standard model. One weakness is related to the position of the observer looking at the model.

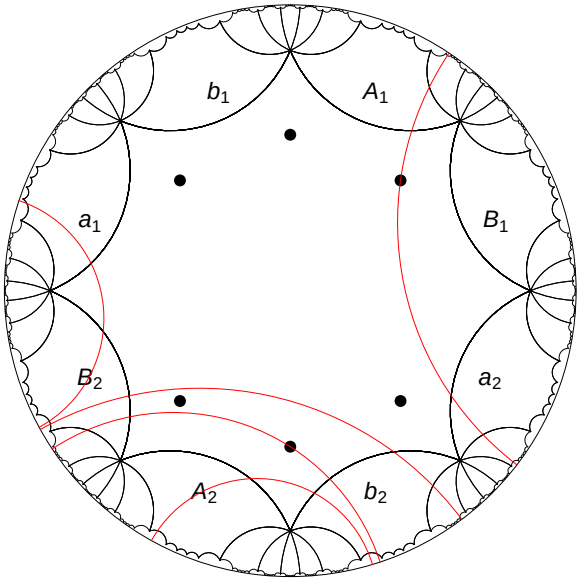

Figure 5.4.: Simple geodesic through two WP

Figure 5.4 shows a simple closed geodesic across the handles obtained from our program *Geo_Finder_octo*. The cyclic word is $a_1a_2b_2b_2b_2$. The program recognizes self intersections and returns their coordinates if there are any.

In this example it is really hard to convince oneself, that the hyperelliptic involution maps this geodesic to itself, although it must be so.

As Weierstrass points and hyperelliptic involution play an important role in our analysis of the simple closed geodesics, we shall privilege other models where the observer is placed in a more favorable position.

Another weakness of the model is that all sides of the tile have the same length. This could be cured using an irregular octagon, but the decomposition in pair of pants will enable us varying lengths with more advantages.

Chapter 6.

Models for the pretzel

We have used up to now the classical regular octagon for representing the pretzel. The many symmetries were helpful when computing the tessellation. However these symmetries allowed only one side length. Further we disliked that eight angles around a vertex slow down the calculation, the acting group not being free. Bad enough the rendering of pruning and earthquake were not enlightening.

6.1. Which polygons are suitable for the pretzel?

6.1.1. How to make pictures to tiles

Although it is well known that the fundamental polygon of the torus is either a square or a hexagon, a compact surface is usually associated with a regular 4g-gon.

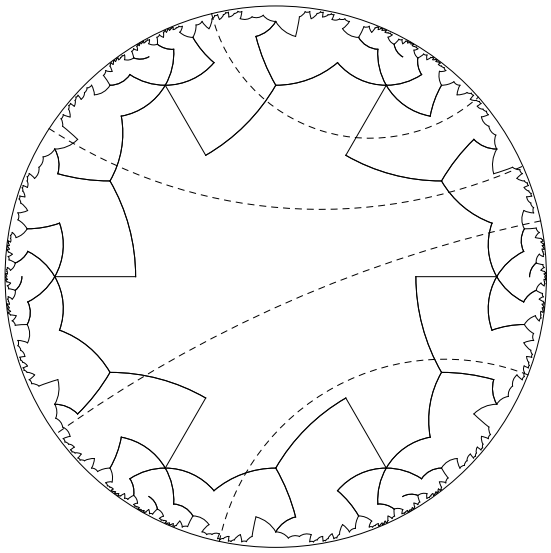

Figure 6.1.: A funny model

This must not be. Figure 6.1 shows cogwheels covering a pretzel with dotted lines representing a 4-leaved closed geodesic. It looks crazy, but it is a model!

From Euclidean geometry we know that the polygonal tile is not inevitably geodesical.

This is not specific to Euclidean geometry. The fishes of M.C. ESCHER, e.g. in his *Circle Limit I* or *Circle Limit I*, are hyperbolic. We do not how he did that, presumably H.M.S. COXETER gave him a hand. How it might ever be, we give in our program Hyperbolic_ghosts a recipe how to make a picture from a polygon, which recipe can be used in the three geometries.

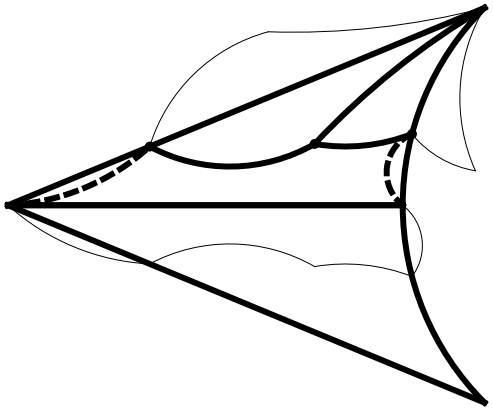

Figure 6.2.: Cut a ghost from a triangle

Take one of the eight triangles which are subtiles of the octagon. Fold it along its axis of symmetry, so as to obtain two superposed halves. Take any point inside the half triangle and join it to each of the three vertices. Any (non self intersecting) curves can be chosen, but it is allowed to also run through the underlying triangle, as the dots on figure 6.2 indicate. Finally mirror the three curves against the sides of the half triangle.

As mirroring preserves area, the developed picture has the same area as the triangle taken from the octagon. The vertices are preserved and the curves fit perfectly together. Of course the same procedure applies to any closed polygon.

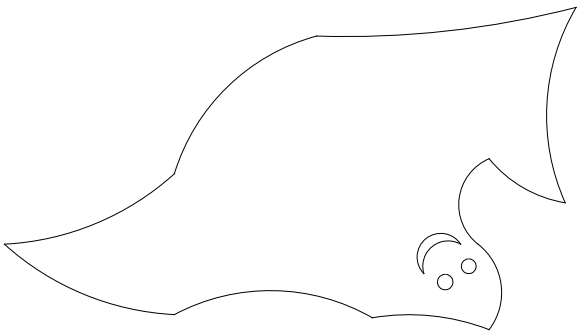

Figure 6.3.: Here is the ghost tile

On figure 6.3 we just added the mouth and the eyes.

It is intuitively clear and not difficult to prove, that this ghostful tile can be used with no change of the tessellating group, as figure 6.4 confirms.

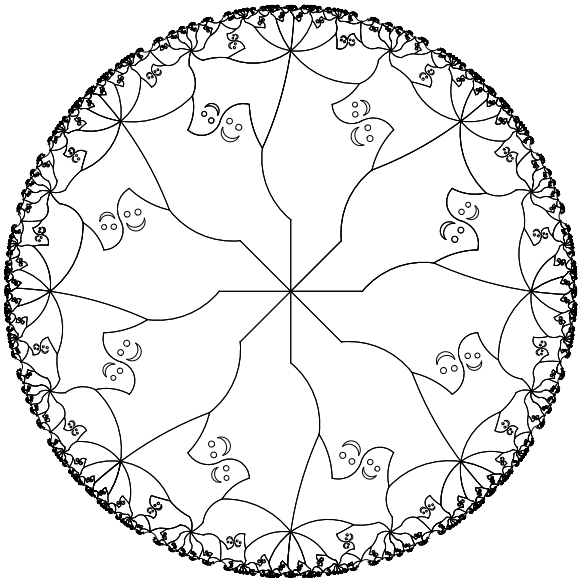

Figure 6.4.: Tessellating ghosts

6.1.2. The side and angle conditions

We shall now of course only use geodesic polygons, as we want to graft, prune and twist.

We have experienced that it is worth taking several models into consideration according to what properties are to be visualized.

Thus it is important to first identify whether a polygon is suitable for tessellation.

The conditions for a polygon to be a fundamental region of a tiling have been defined by Henri Poincaré and investigated by John Stillwell.

Theorem 5 (Stillwell - Side and Angle Conditions)**.** *If a compact polygon* Π *is a fundamental region for a group* Γ *of orientation-preserving isometries of* $\mathbb{S}^2$, $\mathbb{R}^2$, *or* $\mathbb{H}^2$ *(often referred to as side-pairing transformations) then*

i) for each side s *of* Π *there is exactly another side* $s' = gs$ *with* $g \in \Gamma$,
ii) each set of vertices identified when pairing sides corresponds to a set of corners of Π *with angle sum* $\frac{2\pi}{p}$ *for some* $p \in \mathbb{Z}$.

Theorem 6 (Poincaré 1882)**.** *A compact polygon* Π *satisfying the side and angle conditions is a fundamental region for the group* Γ *generated by the side pairing transformations of* Π.

To represent specifically a pretzel, a polygon must fulfill additional conditions.

First requirement: the area of the polygon must be 4π.

This states the global version of Gauß-Bonnet: $\int_M K dA = 2\pi\chi(M)$ for a variety M of Riemannian curvature K with area element dA and $\chi = 2 - 2g$ being the Euler characteristic of the genus g. [34, John Stillwell] gives an easy to follow proof not referring directly to Gauß-Bonnet, but using instead the area of the hyperbolic triangle computed from its angles.

The polygon area is then $A(\Pi) = -2\pi\chi(\Pi) = 4\pi(g-1)$, hence 4π for the pretzel with $g = 2$.

Remark. The area being 4π the fundamental tile will be extensive in all models. However side length and the number of loops around a vertex allow to influence the look of the tessellation.

An n-sided regular polygon Π with a unique angle α decomposes into n hyperbolic triangles. Each triangle Δ has area Π - angle sum of Δ. The angle sum of all triangles centered on the origin is $n\alpha+2\pi$, thus the area of the polygon is $A(\Pi) = (n-2)\pi - n\alpha$. Now for the pretzel

$$4\pi = A(\Pi) = (n-2)\pi - n\alpha \rightsquigarrow \alpha = \frac{n-6}{n}\pi$$

A further constraint is that the sum of angles around a vertex be 2π.

We know already that the 8-gon is suitable. What about the candidates among the regular polygons?

Let $\#V = \frac{n\alpha}{2\pi}$ be the number of vertices of Π and $\#\alpha$ be the number of angles around a vertex. We go through the candidates.

	α	$\#\alpha$	$\#V$
8-gon	$\pi/4$	8	1
10-gon	$2\pi/5$	5	2
12-gon	$\pi/2$	4	3
14-gon	$4\pi/7$	7/2	4
16-gon	$5\pi/8$	16/5	5
18-gon	$2\pi/3$	3	6

The usual 14-gon and the 16-gon fall out as $\#\alpha$ is not an integer. We only quote the 18-gon to show that the list does not end, but we do not intend to further test polygons with too many sides, involving many generators, thus long computing time.

What about the candidates 10-gon, 12-gon and the pseudo 12-gon which will appear to be a 14-gon? We have to check whether they fulfill a further constraint.

6.1.3. The free parameters of the Teichmüller space

RIEMANN stated 1859 that the isomorphisms classes of compact Riemann surfaces of genus $g \geq 2$ have real dimension $6(g-1)$. This was then proved by FRIECKE and KLEIN and extended by TEICHMÜLLER.

Hence we have to expect for the pretzel $6g - 6 = 6$ real parameters. We identify these 6 parameters in the octagon-model.

Since each vertex has two degrees of freedom there is a 16-dimensional space of octagons. Isometric octagons must have the same structure, so we must deduct the 3 parameters of the Möbius transformation producing the isometry. The 4 pairs of opposite edges being glued together must have equal length, so we deduct those 4. All 8 angles around a vertex are equal and sum up to 2π (or equivalently the area must be 4π), so we deduct 1. All vertices are identified to a single point on the pretzel positioned by 2 real coordinates. Finally we have deducted $3+4+1+2=10$ parameters from the 16 at the start. This indeed does leave 6 real parameters.

This result can be extended to surfaces of higher genus. These can be described as 4g-gon fundamental standard tiles with 8g vertices. 2g paired edges are to be deducted, 3 parameters for the Möbius isometries, 1 for the sum of the angles and 2 for the position of the identified single vertex. So we deducted $2g+3+1+2$ from $8g$, which leaves $6\,(g-1)$ degrees of freedom.

Using another polygon may not affect the dimension of Teichmüller space. This constraint has to be checked.

6.1.4. Checking the 10-, 12- and 14-gons

The usual 12-gon falls out. The 12 sides build a 24-dimensional space. We must deduct 6 parameters for pairing. We know $\#V=3$ from the table, so $2\times 3=6$ come away for the vertices. The Möbius transformation of the isometry takes 3 parameters. To get 6, only the number of different angles around the vertices is left. It would have to be 9, which is too much. However we shall see how this can be healed.

The 10-gon seems to also fall out. The 20 sides build a 20-dimensional space. 5 must be deducted for the pairing. $\#V=2$ infers $2\times 2=4$ for the vertices. The obligatory Möbius transformation takes 3. To get 6 we would need 2 different angle sizes around a vertex. Hence the regular decagon with all sides and angles equal falls out. However there exists a decagon with equal sides but 2 sizes of angles, which matches the condition. This is even a very good model, that we shall use later on, as it well shows the symmetry of the hyperelliptic involution, among other qualities.

There remains the 14-gon. The obvious regular 14-gon falls out. We would have to deduct from the 28-dimensions 7 pairings, $2\times 4=8$ for the vertices, 3 for the isometry. We would be left with 4 different angles. We need not to check whether this would be possible, because we have a good replacement.

We take a dodecagon but add a supplementary vertex in the middle of two identified sides with a flat angle. Then we have a 28-dimensional space. As $\#V=4$ we deduct $2\times 4=8$. We still have 3 for the isometry. Having two different angles we deduct 2. This leaves 9 pairing alternatives. As we shall see in the following this really works! This model happens to be very interesting for visualization. We can prescribe three length parameters, which creates a great diversity. We shall also decompose the tile into four colored hexagons, which reveals satisfactorily the effects of earthquakes and pruning.

We found this model not by accident but after having decomposed the pretzel into pairs of pants.

6.2. Decomposition in pairs of pants

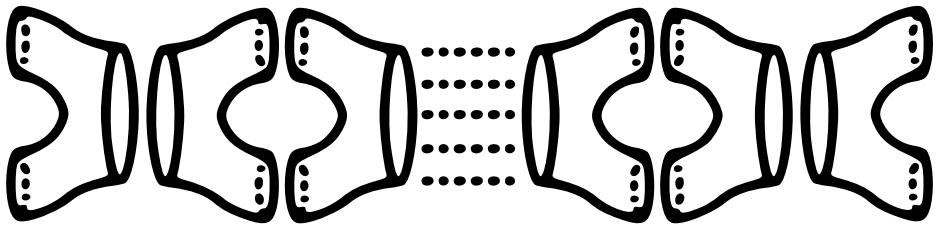

Figure 6.5.: Decomposition in pants

As figure 6.5 suggests any oriented compact surface of genus > 1 can be decomposed with 3(g - 1) cuts in 2(g -1) pairs of pants. There are several possibilities to position the cuts but the number of pairs of pants is a topological invariant depending only on the genus.

Topologically a pair of pants is a sphere minus 3 open holes.

The two pieces of fabric only need to be sewn along the three seams to get a pair of pants. Each piece, one for the front the other for the back, has 6 edges. Each hexagon can be again decomposed into two pentagons. Each seam will join two holes.

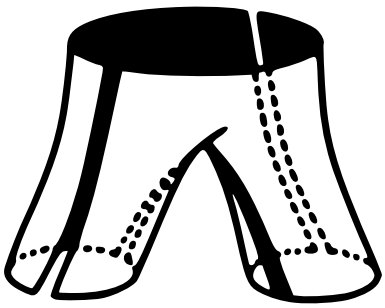

Figure 6.6.: Tailoring pants

As the pants inherit the hyperbolic structure of the pretzel, lengths can be measured. So that they match together, the seams must have the same length in each hexagon. The hexagons are right angled, the seams being orthogonal to the holes.

Hyperbolic geometry provides us with the hexagon suitable for our purpose.

6.3. Geometry of the hexagon

6.3.1. The right angled hexagon

Proposition 14. *There is exactly one hyperbolic right angled hexagon with prescribed alternated side lengths a, b, c.*

Proof. Let the lengths a and b be given.

Trace any support of B, here a vertical h-line. Trace any h-line of given length a orthogonal to the support of B. Then the support of C is the h-line orthogonal to the support of a in its endpoint.

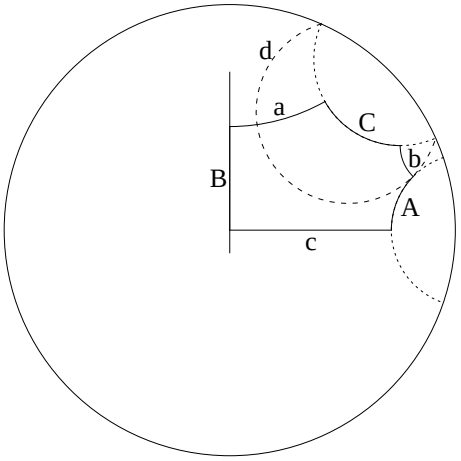

Figure 6.7.: Geometry of the right angled hexagon

This determines the Euclidean circle d equidistant to C through the given distance b.

Trace the h-line tangent to d, this is the support of A. The common perpendicular to the supports of A and C determines the edge of length b and the length of C.

The supports of A and B intersect when C is shorter than some C_0. Otherwise, i.e. for $C > C_0$, A and B are ultra parallel, so they have a common perpendicular, this is the support of c.

This construction is not yet satisfactory, because we have not used c as prescribed! So we have to examine how c and C are correlated.

When $C > C_0$ gets longer the support of A gets squeezed between the dotted d and the unit circle, so c moves upwards and gets longer, whereas B gets shorter.

Consider the hexagonal law of sines for all right angled hexagons

$$\frac{sinha}{sinhA} = \frac{sinhb}{sinhB} = \frac{sinhc}{sinhC} \rightsquigarrow \sinh c = \frac{sinhC}{sinhB} \sinh b$$

Now b is given, the hyperbolic sine is a strictly monotonous increasing function, C increases and B decreases, so c is a strictly monotonous function of C. For $C = C_0$, i.e. when the supports of A and B are parallel, $c = 0$. So c goes from 0 for $C = C_0$ to ∞ for $C \to \infty$. Every value of c occurs exactly once.

Thus we can prescribe any length c, there exists a unique corresponding C. Finding the construction was not our purpose, but we have proved the existence and unicity of a right angled hexagon with alternated side lengths a, b, c. □

Remark. The law of sines is not enough for computing A, B, C for given a, b, c. The formula $\cosh B \sinh b \sinh c = \cosh a + \cosh b \cosh c$ does the rest. See [2, Alan F. Beardon] for proofs.

6.3.2. Constructing the hexagon

Trace any three ultraparallel geodesics. Completing with the three common perpendiculars gives a right angled hexagon.

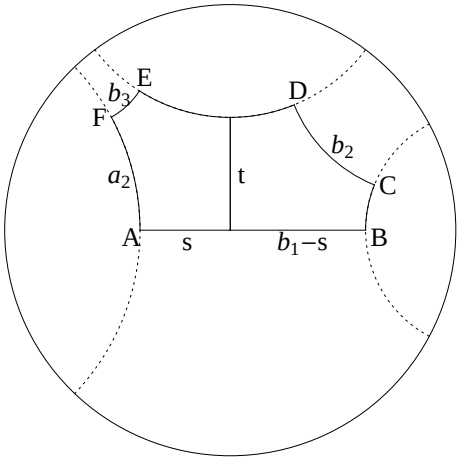

Figure 6.8.: Constructing a right angled hexagon

The common perpendicular to the edges AB and DE divides the hexagon into two right angled pentagons.

The pentagons are uniquely defined when the length b_1 of the hexagon is given. In the left pentagon trace the perpendiculars to the real and the imaginary axis supporting t and s. The common perpendicular defines the pentagon. Do the same on the right.

Generally this construction of the pentagon supposes that the supports of AF and ED are ultraparallel. However the hexagon being given the pentagons of course exist and uniquely.

By hypothesis the lengths b_1, b_2 and b_3 are given. The length a_2 in the hexagon as well as the lengths t and s in the pentagon are computed using well known formulas of the cosine laws.

Using b_1, t and s we obtain the support of BC, ED and AF, hence the common perpendiculars CD and EF.

A pair of pants being made of two hexagons we shift the hexagon along the real axis. The Möbius transformation $z \mapsto e^{i\theta}\frac{z-a}{\bar{z}-1}$ exchanges a point $a \in \mathbb{C}$ with the origin. Here $\theta = 0$ and $a = s$. Using the same formula we rotate the half pant through 180° around its midpoint to get the other half (move the midpoint to the origin, turn 180°, move the midpoint back). The other pair of pants of the pretzel is obtained by mirroring.

In our package *diskgeometry* the instruction *RightangledHexagon* gives directly the vertices of the hexagon with the given three opposite side lengths.

6.4. Tailoring the pretzel

Figure 6.9 shows how to glue 2 pairs of pants to get a pretzel.

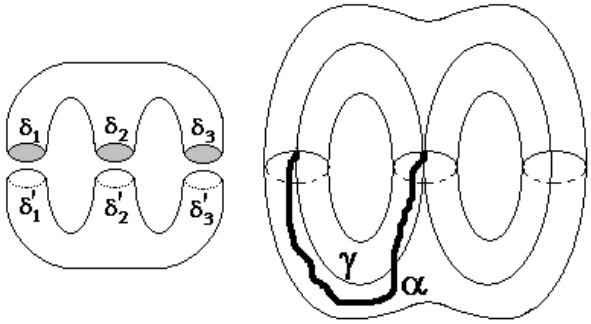

Figure 6.9.: Geodesic tailoring of a pretzel

Obviously the holes must have the perimeter on both sides. This gives us 3 of the 6 parameters we are looking for. We can further twist around each hole before gluing. These are the three missing parameters, provided the seams behave correctly. We check this.

According to well-known results (e.g. [1, Benedetti]) any loop α in the hyperbolic structure of a pant can be straightened to the geodesic loop γ with the same endpoints through a free homotopy. Further this geodesic must be orthogonal to the boundaries δ_i. Indeed we can double the pant by gluing it to a copy of itself. This does not alter the geodesic γ. Should γ not be orthogonal to the boundary, the union of γ and its copy would be no geodesic, which may not be.

These geodesical loops are our seams. Taking the same lengths for the 3 pairs of edges to be sewn together implies that the other 3 pairs of edges also have the same lengths (both hexagons are congruent). This means that the seams separate the boundary of the holes in equal parts of length $\frac{\delta}{2}$.

Before examining the effect of twisting the legs we first make a tessellation varying the 3 parameters of the boundary length.

6.5. Tessellation with the right angled hexagon

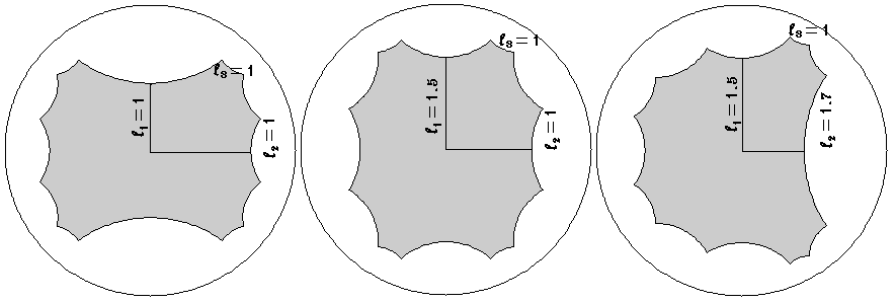

Figure 6.10.: Varying side length

There are three tiles in figure 6.10. On the left the edges have equal length $l_1 = l_2 = l_3 = 1$. In the middle $l_1 = 1,5$, both l_2 and l_3 have still unit length. On the right $l_2 = 1,7$, all three lengths are different. The lengths of the edges in between vary accordingly but out of our control.

To obtain the fundamental tile we take the top left hexagon, rotate it about π around the midpoint of the edge on the real axis and translate to the right. Then we conjugate this pair of hexagons (we may not change orientation when tessellating, but we may construct the polygon to our liking).

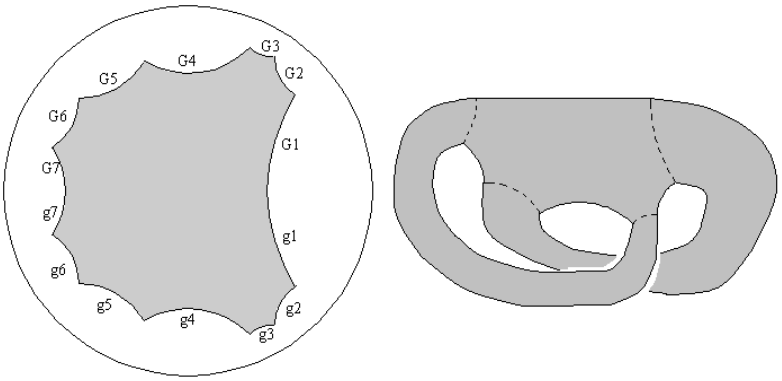

Figure 6.11.: Folding the dodecagon

With our notation $G_i = g_i^{-1}$ we see on picture 6.11 the tile with the generators, on the right the gluing when the upper side is folded down onto the lower one.

This polygon is obviously a dodecagon, but we have numbered 7 generators and their inverses. The folding shows why this hidden 7th generator is necessary.

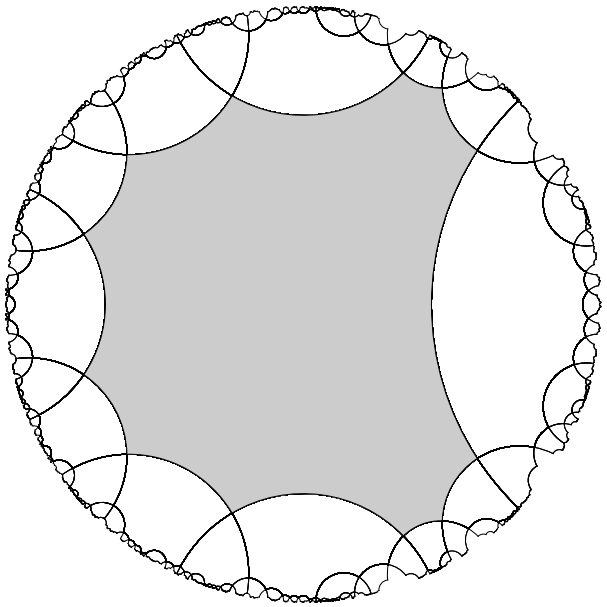

Figure 6.12.: Skew tessellation

The 12-gon becomes a 14-gon, a tetradecagon, with two new vertices on the real line, the vertical pair of edges are supported by the same line. As this 14-gon with a flat angle is a 12-gon for the observer, we shall speak of the dodecagon model.

The handles have not the same girth at both ends. The edge g_1 pairs itself with G_1 to a half handle joined to the half handle of g_5 paired with G_5. The same applies to the pair g_3/G_3 associated to g_7/G_7.

The points locate the 4 vertices which we had computed to be required.

With these 7 generators the tile tessellates to the universal cover of the pretzel in figure 6.12.

The shading uses our instruction *filledPoly*. This extension of the instruction Polygon discretizes the arcs of circle of the polygon by taking the midpoint n times.

6.6. Grafting & twisting ⇝ loxodromy

An Euclidean move is the composition of a rotation in one or the other direction and a translation. Likewise grafting (positive angle), pruning (negative angle) and twisting in a Möbius structure are the components of what we shall call a Möbius move.

Proposition 15. *Grafting, pruning and twisting compose to a Möbius move expressed through a matrix of* $PSL(2,\mathbb{C})$.

Proof. We show the construction, so that $\tan\frac{\alpha}{2}$ be the width of the lune.

When grafting or pruning the opening of the lune is measured by its angle α. To construct it we move the geodesic supporting the cut onto the real axis.

As figure 6.13 suggests the distance between the real axis and the equidistant curve is $\tan\frac{\alpha}{2}$. We know that the points -1 and 1 are invariant and the image of the origin is $\tan\frac{\alpha}{2}$. The Möbius transformation doing this is:

$$M(\alpha) = \begin{pmatrix} \cos\frac{\alpha}{2} & i\sin\frac{\alpha}{2} \\ i\sin\frac{\alpha}{2} & \cos\frac{\alpha}{2} \end{pmatrix}$$

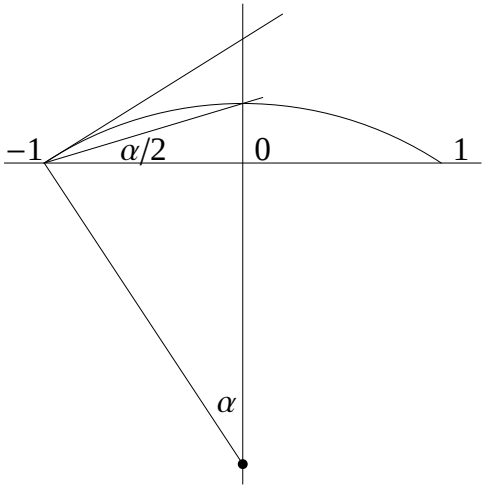

Figure 6.13.: Loxodromy

When the cut is not supported by the real axis, a Möbius transformation, say T, will be used to bring the geodesic to the real axis, then the cleaving $M(\alpha)$ is operated, finally the geodesic is moved back with T^{-1}. The use of this so called conjugation $T^{-1}MT$ is to revisit the generators g_i, so that they act on the new grafted or pruned fundamental tile. Computing the new generators may seem to be an easy exercise, but

in practice it is often tedious to retrace the action of α on the generators, specially when the geodesic has not a single leaf like in the present case.

No problem at all occurs with the insertion of a Dehn-twist. In this case $\tanh\frac{\varphi}{2}$ will be the distance of the slide along the cut. The matrix which leaves invariant i and $-i$ and moves the origin to $\tanh\frac{\varphi}{2}$ is computed in an analogous way to be :

$$M(\varphi) = \begin{pmatrix} \cosh\frac{\varphi}{2} & \sinh\frac{\varphi}{2} \\ \sinh\frac{\varphi}{2} & \cosh\frac{\varphi}{2} \end{pmatrix}$$

It suffices to use the product $M(\varphi)\, M(\alpha)$ to get a formula for all (suitable) α and $\varphi \in \mathbb{R}$.

Due to $M(\varphi), M(\alpha) \in PSL(2,\mathbb{C})$ follows $M(\varphi)\, M(\alpha) \in PSL(2,\mathbb{C})$. We now calculate it whereby we drop the factor $\frac{1}{2}$, which we will reintegrate at the end. For simplicity we do not change notations. Let $P := M(\varphi)\, M(\alpha)$.

$$\begin{aligned} P &= \begin{pmatrix} \cosh\varphi & \sinh\varphi \\ \sinh\varphi & \cosh\varphi \end{pmatrix} \begin{pmatrix} \cos\alpha & i\sin\alpha \\ i\sin\alpha & \cos\alpha \end{pmatrix} \\ &= \begin{pmatrix} \cos\alpha\cosh\varphi + i\sin\alpha\sinh\varphi & i\cosh\varphi\sin\alpha + \cos\alpha\sinh\varphi \\ i\cosh\varphi\sin\alpha + \cos\alpha\sinh\varphi & \cos\alpha\cosh\varphi + i\sin\alpha\sinh\varphi \end{pmatrix} \\ &= \begin{pmatrix} \cosh i\alpha\cosh\varphi + \sinh i\alpha\sinh\varphi & \cosh\varphi\sinh i\alpha + \cosh i\alpha\sinh\varphi \\ \cosh\varphi\sinh i\alpha + \cosh i\alpha\sinh\varphi & \cosh i\alpha\cosh\varphi + \sinh i\alpha\sinh\varphi \end{pmatrix} \\ &= \begin{pmatrix} \cosh(i\alpha+\varphi) & \sinh(i\alpha+\varphi) \\ \sinh(i\alpha+\varphi) & \cosh(i\alpha+\varphi) \end{pmatrix} \end{aligned}$$

We have used $\cosh ix = \cos x$ and $\sinh ix = i\sin x$.

Reintegrating the factor $1/2$ and setting $\rho = 1/2\,(i\alpha+\varphi)$:

$$M(\rho) = M(\varphi)\, M(\alpha) = \begin{pmatrix} \cosh\frac{i\alpha+\varphi}{2} & \sinh\frac{i\alpha+\varphi}{2} \\ \sinh\frac{i\alpha+\varphi}{2} & \cosh\frac{i\alpha+\varphi}{2} \end{pmatrix} \tag{6.1}$$

□

This matrix with determinant $= 1$ has imaginery trace so far $\alpha \neq 0$ and $\varphi \neq 0$. This is a **loxodromy**. The effect of the loxodromy will be to curl the limit set of fractals in the next chapter. More precisely:

On the Riemann sphere

i) α rotates about the axis of the poles,
ii) φ stretches along the meridians.

It is obvious that we can twist in both directions according to the sign of the angle φ. Less evident is that grafting and pruning also only differ in the sign of the angle α. Our programs for grafting and pruning are basically the same, we only choose the angle > 0 or < 0. On the Riemann sphere $\mathbb{C}P^1$ grafting blows up the tessellation beyond the unit disc. Pruning crushes down the tessellation into the outer unit disc. Both tessellations kiss each other along their common fractal limit set.

Unfortunately the term Dehn surgery has already a precise meaning. Otherwise we would have liked to call 'geodesic surgery' the common operation from which grafting, pruning and twisting arise. Thus we call it a Möbius move. The choice of one complex number, using the angles as real and imaginary part, $\rho = 1/2\,(i\alpha+\varphi)$, determines the matrix.

6.7. The limit set is quasi Fuchsian

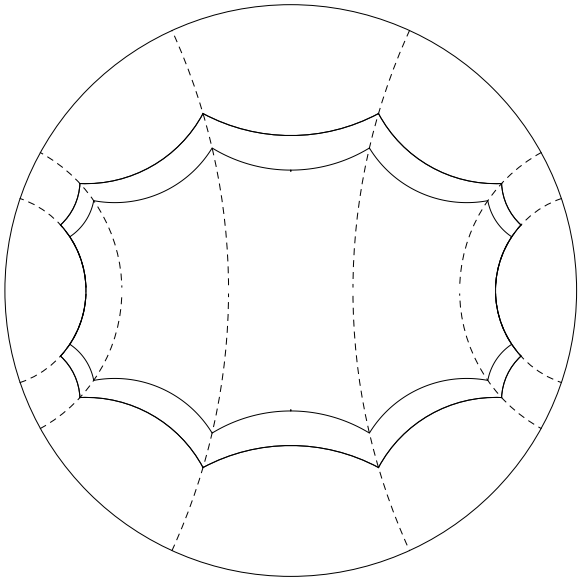

Figure 6.14.: Gliding vertices

The pictures we obtained when grafting or pruning (one being the counterpart of the other on the Riemann sphere) without twisting, show a limit set made of bubbles riding on bubbles instead of the neat circular boundary of the Poincaré disc. The tessellation has been blown up (down) and fractalized but not destroyed.

The reason why we can still glue the edges neatly is that the Möbius transformation just pushes the vertices of the tile orthogonally to the geodesic supporting the cut.

We see in figure 6.14 the crushing process (bursting would be analogous). The crushed tile lies inside the original tile. Every vertex of the original tile lies on a vertical geodesic. The Möbius transformation takes away from this geodesic a piece of constant h-length the perimeter of the cut-off cylinder.

Of course the vertices of the lower part do no lie on the same but on other geodesics as there is no horizontal symmetry for the tile, the 4 hexagons composing the tile not being regular. The loci of the vertices form an Apollonian bundle (coaxial system) centered on the point circles $(-1, 0)$ and $(1, 0)$. The real line is orthogonal to this bundle as well as the arc of circle bordering the cylinder. In terms of Möbius geometry the half neighbourhoods of both boundary points corresponding to one and the same point before inserting or removing the cylinder fit neatly again to a new neighborhood.

Chapter 7.

Tetradecagon and flying fractals

We now implement the 14-gon alias dodecagon model. The real axis supports a very convenient simple closed geodesic, along which we graft or prune about an angle α above the real line and β under it. We twist to the right about an angle φ, to the left about ψ. Last but not least there is a choice of 9 side pairings.

The model is good not only for varying side lengths. As the tile is made of 4 hexagons we color them differently (with gray tones as option). This is not as impressive as the 96 triangles of the octagon model but it shares the advantage of showing something of the interior life of the tile. This begins with retracing the action of each generator. Then the effect of pruning or twisting becomes observable.

7.1. Fundamental tile and pairings

Gluing 4 hexagons, where every second length can be chosen, implies that every 3rd prescribed (as well as every 3rd not prescribed) length lies within the tile in such a way that pairing matches.

Without loss of generality we can lay the 4 copies of the first prescribed length, say l_1, along the real axis, above and under the origin, to the right and to the left. Then the neighbouring unprescribed length will lie analogously along the imaginary line. This allows us to make the tile thinner or broader (higher or thinner if we lay l_1 along the imaginary axis). Of course the tile will always have area 4π due to the genus $= 2$.

The other lengths $4 \times l_2$ and $4 \times l_3$ will lie on the peripheral polygon. They alternate or not with the unprescribed lengths, as lengths alternate in the hexagons, not in their union.

Let us consider that the prescribed lengths stand for the holes of the pair of pants, i.e. both pairs are glued along their belt l_1. Each of the four l_2 can be paired with the three others, the same for l_3, so there are 3×3 pairing alternatives.

The fat edges are the prescribed lengths, the dotted ones are the seams, the pairing of which results automatically. This means that each dotted edge is always paired with its image against the imaginary line.

In figure 7.1 the generators are $h_{ij} = H_{ij}^{-1}$. The subscripts refer to the halves $j \in \{1, 2\}$ of the both handles $l \in \{1, 2\}$ to suggest how the gluing works.

With these schemes it is easy to fix the Möbius transformation moving each h_{ij} onto H_{ij}, using our instruction *Moeb3ptsC*.

It is not immediate to find out how the angles α which grafts (prunes) above the real line and β doing the same under the real line affect the generators. However as the

combinations all are unique the exercise requires more patience than wits. The angles φ and ψ twisting to the right and to the left modify the generators in the same way, i.e. one is free to modify the generators for grafting or twisting, the other operation has not to be taken care of.

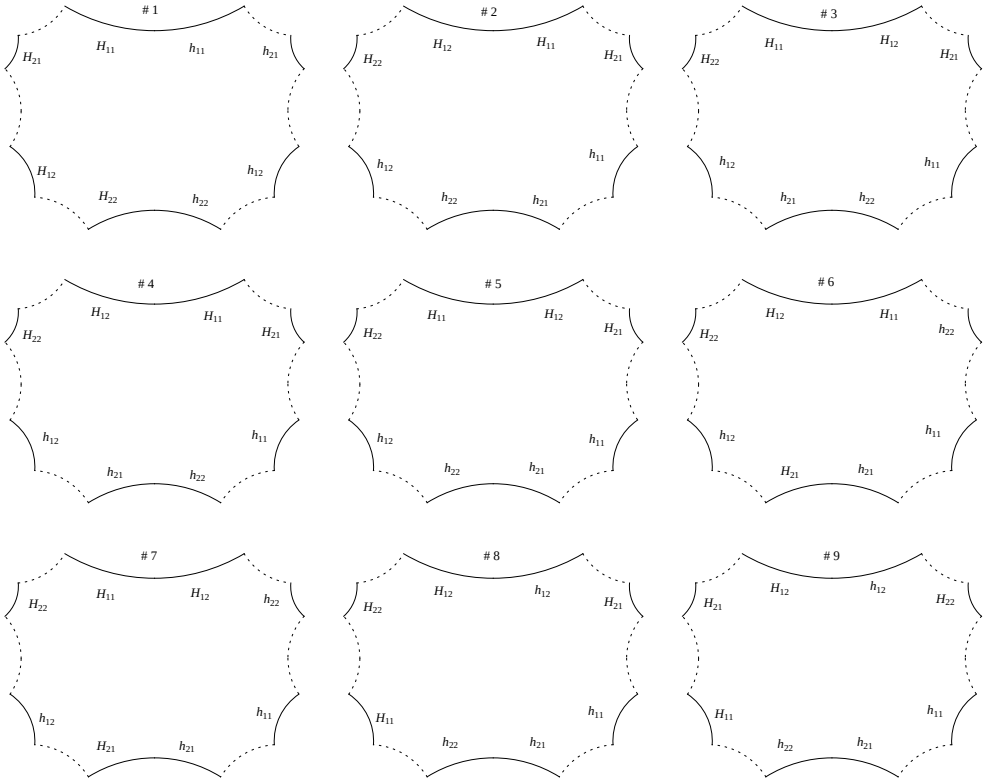

Figure 7.1.: The 9 pairings of the 14-gon

7.2. Feats of the program

The program is called Flying_fractals.

The high number of parameters is confusing at first, but rewarding *in fine*. This multiplicity discloses, that the operations along a geodesic proceed from a common mechanism originating in Möbius geometry.

The break condition is important because 14 generators involve a lot of combinations of words. Thus it requires much time to compute the limit set. Fortunately having only 4 tiles around a vertex limits the duplications due to the group not being free. Using `limitsetrad = .9` and `nbofletters = 2` allows a quick computation combined with a fair representation of the tiling.

One of the angles α or β (resp. φ or ψ) can be set $= 0$ in order to work on only one side of the geodesic. The many possibilities of varying disclose so many other baffling effects that we give up presenting examples. One should just play around with the parameters.

7.3. Fractals

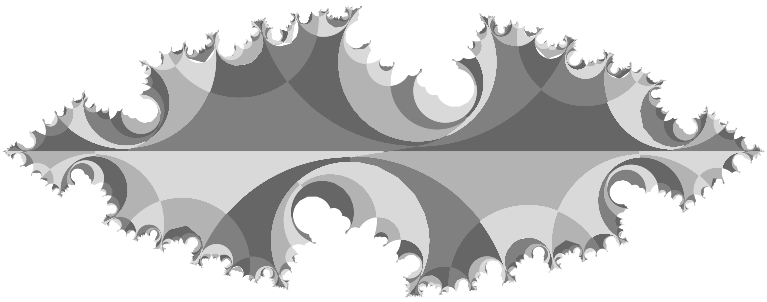

Figure 7.2.: Squeezing to a fractal

We make an exception and show a result which might not come across accidently.

Using a 1-leaf geodesic to cut along has the advantage to allow using large angles. However there are still limits. One limit is reached, when α and β are made larger and larger until the sides of the fundamental tile would intersect, there is no flesh more to be pruned away!

Choose for instance $l_2 = l_3 = 1.5$, $\alpha = \beta = 45°$. This is a limit only for pruning, there is still a lot of room for twisting. Of course the condition is only $l_2 = l_3$ and $\alpha = \beta$ are chosen accordingly.

The enigmatic header is just to remind the choices for l_1, l_2, l_3, a break condition at 95% of the unit radius and 3 letter-words, the paving 6 and finally the angles $\alpha, \beta, \varphi, \psi$.

It is worth allowing some longer computing time to render the delicate lace of the limit set in order to better see the fine curls the loxodromy produces. This winding around demands a higher discretization of the tile, this is the job of the parameter *fine*, that should be set `fine = 7`.

The user should choose the coloring option. It is easy to select another choice of colors by adapting the instruction *RGBColor* which defines `colorpant1` up to `colorpant4`.

Chapter 8.

Groping for the limits

The choice of the real line for cutting along followed our purpose to show how to graft, prune and twist. Closed geodesics which do not close within the fundamental tile will show us that grafting is still possible, but the grafted cylinder may not be too wide. This will bring us close to infinite geodesics as limit case of very long closed geodesics. First it is to show that even 1-leaf closed geodesics set limits to grafting.

8.1. Grafting angle along a 1-leaf geodesic

We have stated that the pruning angle is bounded. Using a too large angle, i.e. beyond the angle where the polygon sides kiss each other, the tile will be no more simply connected and the program crashes. Which polygon sides intersect depends on the choice of side lengths. When pinching the tiling in the middle for fractals, we had chosen the lengths so that the accident occurs where the effect is more impressive. Using our program Flying_fractals with side lengths (1,8, 1,2, 1,5) and $\varphi = \psi = 0$, the collision happens when $\alpha = \beta$ are > 45 °.

Grafting meets hitherto no problems, until $\alpha = \beta$ become $> 61°$. However if we set $\beta = 0$, then α can be increased up to 107°. Nothing could happen with the polygon sides, like when pruning, as they move away from each other. Hence this must have to do with the lunes. The accident occurring much later when $\beta = 0$, one side of the lune will have intersected the opposite side of some other lune. The third accident by $\alpha = 107°$ corresponds to a self intersection of the tessellation. Let us examine how the lunes collide.

8.1.1. Lunes cross infinitely many tiles

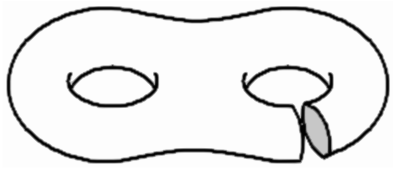

Figure 8.1.: Grafting into a pretzel

We took a closed geodesic, not belonging to the trivial homotopy class. We inserted or removed a small cylinder. The Fuchsian group of generators was replaced by a quasi-Fuchsian group of new updated generators, thus the tessellation with limit set the unit circle became a fractal of bubbles piled upon each other.

Figure 8.2 recalls that the geodesic common perpendicular to an edge, say a_1/A_1, is present in every tile on the way to $\mathbb{S}^1_\infty$. This common perpendicular propagates into the whole disc. Every tile carries a geodesic segment, which associates to the segment of the neighbouring tiles until infinity and there are infinitely many of these infinite geodesics.

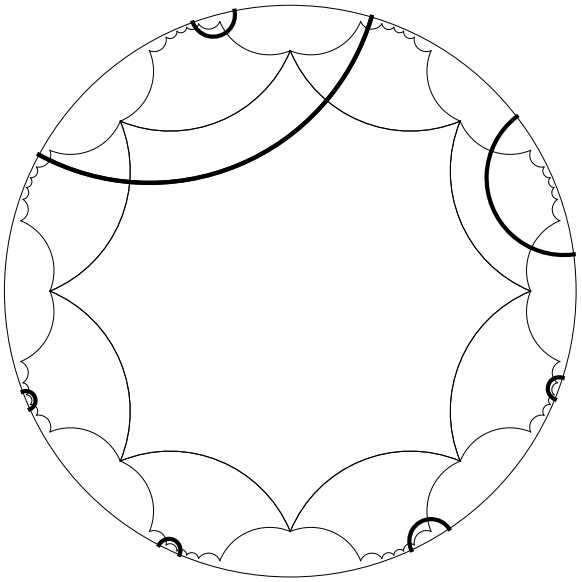

Figure 8.2.: Scattering across the tiles

When grafting the inserted cylinder is represented by a lune limited by the geodesic and the (not geodesic) equidistant curve according to the width of the cylinder.

When increasing the width of the graft, the disjoint lunes will move closer and closer to each other.

8.1.2. The injectivity radius

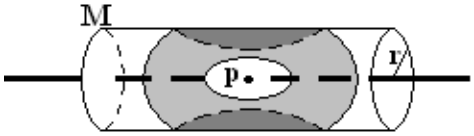

Figure 8.3.: The injectivity radius

Suppose we are in a point p of the tangential space to an euclidean tube M of radius r rolled around a straight axis. With the exponential map the radial tangential rays going out at p are mapped isometrically on geodesics on M.

The gray annulus on M will intersect itself when the outer circle gets radius $> \pi r$. A point q in the intersection would be hit once by the short radial geodesic from p and once again by the long opposite geodesic around M (the same effect as on the sphere where two points can be joined by the short or the long path on the great circle). Then the exponential function is no more injective for a too big ball of radius $> \pi r$.

Generally the injectivity radius $i(p)$ for $p \in T_pM$ is defined as:

$$i(p) := \sup\left\{r > 0 \mid exp|_{B_r(0) \subset T_pM} \text{ is injective}\right\}$$

Standing on the cylinder in p we can send, in both directions orthogonal to the axis, arcs of length $\leq \pi r$. Both arcs of length πr will meet in the antipode of p. Thus the meridian is the common limit for a simple connexion.

Defining a geodesic as the shortest junction between two points, any point is fixed uniquely by reference to its distance from p. The universal cover of the cylinder is made of horizontal strips of width πr. Gluing to each other the rims of the strips gives an isometry to the cylinder.

A tessellation results from the action of a discontinuous group on a space, $\mathbb{H}^2$ or $\mathbb{D}^2$ in the case of the pretzel. This implies injectivity. The action of the group copies the fundamental polygon. Every point of a tile obtained by the group action must belong to a different orbit in the group of isometries. In other words a fundamental polygon Π for a group G includes a representative from each G-orbit and each G-orbit is represented at most once in the interior of Π.

8.1.3. How wide may the graft be?

Proposition 16. *The injectivity radius $i(\alpha)$ is an upper bound for the size of a graft into a tessellation of $\mathbb{C}P1$.*

Proof. We use the octagon model.

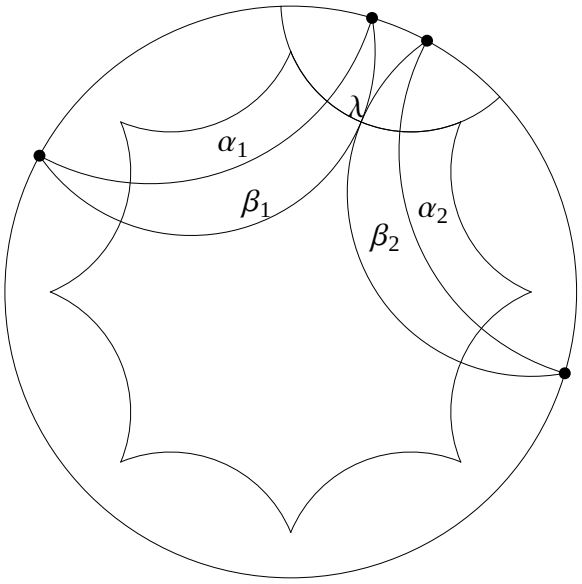

Figure 8.4.: Kissing limit

Let α_1 and α_2 be the common perpendiculars to the sides pair a_1/A_1 and to B_1 and a_2. β_1 and β_2 are equidistant curves. There are lunes on both sides of α_1 and α_2, otherwise the collision would take place much later. However we show only the sides of the lunes heading to each other, to make the picture less confuse. We also ignore

the octagon side symmetric to a_1/A_1 where obviously the same things happens. We choose two neighbouring sides, the other sides being farther away. The collision we expect will occur throughout the tiling, as we can move any tile to center it around the origin.

The h-distance between geodesic and equidistant curve is the same everywhere as we have lifts of one and the same graft.

Draw now λ the common perpendicular to α_1 and α_2. This is a closed geodesic starting and ending on an identified point of α supported by a circle with center P. We have a bundle of circles. β_1 and β_2 stand orthogonally on λ, so they will touch on λ when the graft is wide enough. They would meet there anyway, even if the lunes had not the same width.

The holonomy is a translation moving α to β, i.e. a vector field of constant length orthogonal to the geodesic α (with opposite orientation in each half lune). As long as β_1 and β_2 are disjoint we can widen out the lune.

Increasing the lune width beyond the radius of injectivity β_1 would intersect β_2, i.e. there would be points in the lune along α_1, which are closer to α_2 than to α_1 (the distance being measured by the vector field foliating the lune and the width of both lunes being the same). Hence the intersection of the lunes contains two images of the same point of the pretzel. Due to this intertwining we cannot push away β_1 and β_2 anymore. The perpendicular λ would start in one leaf of the universal cover and get back on another leaf, which would be contradictory to the tiles containing exactly an unique point of each orbit. □

Although grafting and pruning are counterpart of each other on the Riemann sphere, the limit is there where the first accident occurs.

8.2. Grafting along infinite geodesics

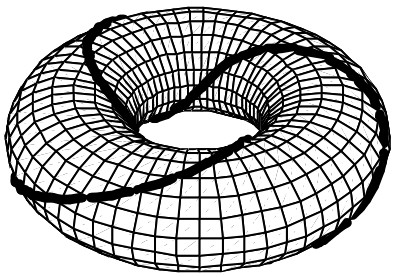

Figure 8.5.: Geodesic trefoil knot

We have grafted up to now along the geodesic orthogonal to an edge of the polygon.

An advantage of such a geodesic is that it is closed and lies entirely in the fundamental polygon. But there was another reason for this choice.

If the geodesic were not orthogonal to an edge we would obtain a closed curve with a pinch, a so-called geodesic monogon. Who attempts to travel geodesically around the axis of Beltrami's pseudosphere will not move in a circle orthogonal to the axis, but will describe such a monogon. The edges of the regular octagon picturing the pretzel also are monogons closing on the unique vertex with an angle of $\frac{\pi}{2}$ to themselves. A

monogon in the disc model is homotopic to a unique closed geodesic, however not in a homotopy with fixed base point but in a free homotopy.

There is no chance to graft into a monogon, because the graft would intersect itself in a neighbourhood of the endpoints identified in the pinch. The same applies to any broken curve of geodesic segments. Therefore we concentrated on geodesics and dropped geodesic segments.

Figure 8.5 shows a trefoil knot on the torus. The geodesic winds 3 times around the core and 2 times around the hole.

This geodesic only closes after crossing several tiles. We could have chosen to wind q times around the core and p times around the hole.

For figure 8.5 we only need 3 parameters a, b, c, fixing the 3 dimensions of the torus and apply the easy formula:

$$\left((a + b\cos qt)\cos pt, (a + b\cos qt), c\sin qt\right)$$

If we cut a disc from the torus and join two copies along the cut we get a pretzel. Thus the pretzel will also have such geodesics (plus others of course running from one half to he other half). This torus is not hyperbolic but there is a conformal homeomorphy. Specially a closed and simple (i.e. non self-intersecting) geodesic will be mapped to a closed simple geodesic.

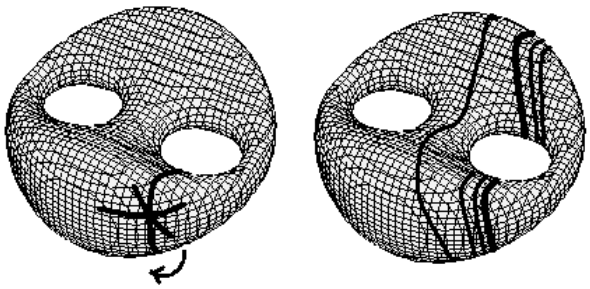

Figure 8.6.: Foliation through looping a vertex

A geodesic is either closed or infinite. To construct an infinite geodesic we let a winding parameter p or q go to infinity. In hyperbolic geometry we can choose any point on the pretzel, construct a 1-vertex triangulation and move the vertex infinitely often around the loop. This results in a foliation of the pretzel made of ideal triangles (i.e. the vertices are at infinity) spiralling around the loop.

For constructing an infinite geodesic we use the former geodesic, closed within the polygon, as limit. Choose any point on it and construct a one-vertex triangulation of the pretzel. Then move the vertex infinitely often around the loop. We so obtain a geodesic foliation of the pretzel made of ideal triangles spiralling around the loop, as shown on figure 8.6.

We can also use a pair of limiting geodesics and let an infinite geodesic spiral between them. With two geodesics the spirals may be on either side of the supports.

We now transport this picture into the Poincaré disc. We use again the geodesic α and its conjugates, identifying the edges a_1 and A_1. As second limit we choose the geodesic β identifying hereby the edges a_2 and A_2, see figure 8.7.

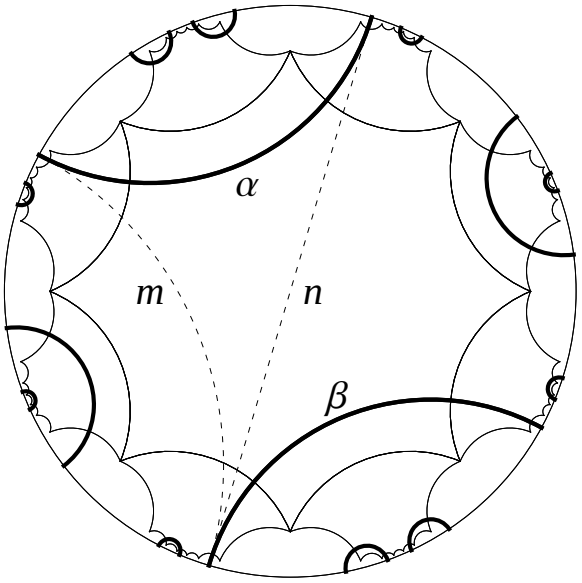

Figure 8.7.: Inserting between two geodesics

The geodesics m and n touch α_1 and β_1 at infinity, so they spiral around the images of α and β in the quotient space, i.e. on the pretzel.

Clearly we cannot add any graft on n, not even on one side, as it would cut α or β.

Not possible either would be a graft against m although one side ob m seems to offer free room. To see this we would have to zoom into a region near the circle at infinity.

As we used the common perpendicular, the cut lay somewhere in the octagon but always at the same place in every tile (every tile is a hyperbolic moved copy of the central tile). Now the case is different. The geodesic is wandering across the tiles. In a neighbourhood of the limit set lunes will intersect, how narrow they may be.

This may not be obvious from the representation in the disc, but when we look at the spirals on the pretzel there is no free space for not intersecting neighbourhoods. The spiraling loops lay dense in any neighbourhood of the endpoints of α or β.

Chapter 9.

Laminations and Cantor set

9.1. Many leaved geodesics pleat in a Cantor set

Consider a geodesic lamination λ on a surface S. A proof of J. BIRMAN and C. SERIES quoted by F. BONAHON states that the union of all simple geodesics of S has Hausdorff dimension 1. The union of all simple geodesic is also the union of all geodesic laminations. Thus an individual lamination has Hausdorff dimension 1. Let k be a differentiable arc transverse to the leaves of λ, then $k \cap \lambda$ has dimension 0, i.e. it is totally disconnected. This leads to Bonahons'

Proposition 17. (Bonahon)

i) If a geodesic lamination has no isolated leaves, then for every arc k transverse to λ, the intersection $k \cap \lambda$ is a Cantor set.
ii) If an arc k is transverse to the geodesic lamination λ and if the components of $k - \lambda$ are $d_1, d_2, \ldots, d_n$ ordered in non increasing size, then $|\log(length(d_n))| \propto n$.

These are propositions 7 and 8 in [4, F. Bonahon], on which we shall now comment.

We proved in chapter 1 that the classical Cantor set is characterized by the property

$$|\log(\text{length}(d_n))| \propto \log n$$

Writing n instead of $\log n$ on the right hand side is only a scaling. We shall concentrate on the second statement of the proposition.

First we need following

Lemma 1. *Consider in the half plane model a cusp between a geodesic and the imaginary axis. Let $\{d_n\}_{n\in\mathbb{N}}$ be a sequence of infinitesimal segments cut off from two horocycles with ordinates y_n and y_{n+1}. Let δ be the hyperbolic distance between y_n and y_{n+1}. Let $l(d_n)$ and $l(d_{n+1})$ be the hyperbolic lengths of d_n and d_{n+1}. Then*

$$\frac{l(d_{n+1})}{l(d_n)} \propto e^{-\delta}$$

where $a_n \propto b_n$ means that the ratio $\frac{a_n}{b_n}$ is bounded between two positive constants for n large enough.

Proof. We first prove the lemma.

We established in chapter 1 the metric (1.1) in the half plane model

$$\delta = l(y_n - y_{n+1}) = \left|\log \frac{y_n}{y_{n+1}}\right| \rightsquigarrow \frac{y_n}{y_{n+1}} = e^{-\delta}$$

as $y_{n+1} < y_n \ll 1$.

Applying this along the horocycles segments d_n and d_{n+1} it follows

$$\frac{l\,(d_{n+1})}{l\,(d_n)} = \frac{d_{n+1}}{d_n} : \frac{y_n}{y_{n+1}} = \frac{d_{n+1}}{d_n} e^{-\delta}$$

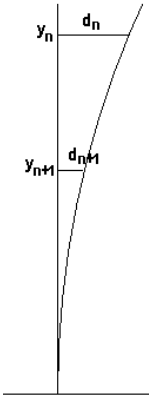

Figure 9.1.: Hyperbolic contraction

As also stated in chapter 1 there is in a cusp a Lipschitz direction field, so that the asymptotic leaves of a geodesic lamination are nearby parallel. Thus the infinitesimal Euclidean lengths d_n and d_{n+1} become approximately equal, i.e. $d_{n+1} \to d_n$ as we progress towards the end of the cusp. The ratio of lengths is not equal to $e^{-\delta}$ but the margin of approximation $\frac{d_{n+1}}{d_n} \to 1$ is a factor bounded by two positive constants. This proves the claim. □

Now we prove the proposition.

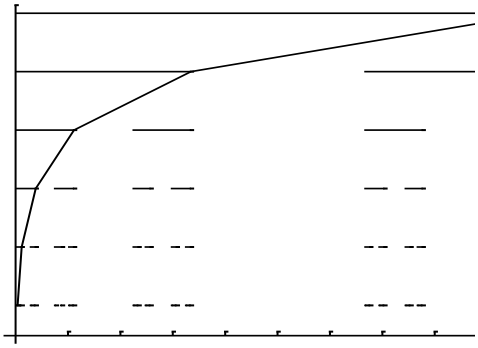

Figure 9.2.: Contraction in the Cantor set

Proof. In the classical Cantor set the remaining segments d_n are ordered in decreasing length. A sequence of d_n lies between the y-axis and a polygonal path.

Figure 9.2 only shows how the length of the not removed segments regresses in the classical Cantor set. Being Euclidean there are no horocycles, but it corresponds to the hyperbolic figure 9.3.

The decreasing order is not given on a hyperbolic surface, when a geodesic lamination is cut by a transversal. However, as we are only interested in segment length, we may reorder the sequence of horocycle cuts according to segment length.

To this effect we note that all but finitely many d_n are in the spikes of the completion of $\overline{S-\lambda}$ which we can go through one after the other.

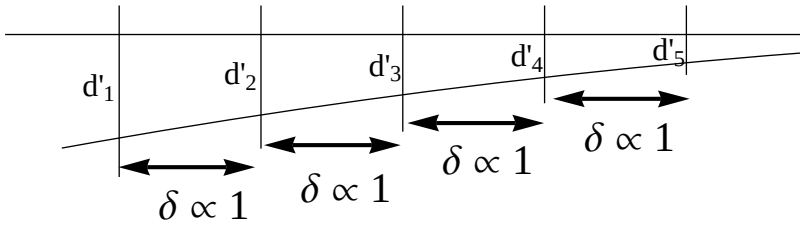

Figure 9.3.: Contraction in a spike

Select a spike and reorder the sequence $d_1, d_2, \ldots, d_n, \ldots$ into $d'_1, d'_2, \ldots, d'_n, \ldots$ in the order of the progression towards the end of the spike.

$k \cap \lambda$ being compact the hyperbolic distance δ between neighbouring horocycles is bounded between two positive constants. Thus we may write $\delta \propto 1$.

Let $l\left(d'_n\right)$ and $l\left(d'_{n+1}\right)$ be the hyperbolic lengths of d'_n and d'_{n+1}. Then it follows from lemma (1)

$$\frac{l\left(d_{n+1}\right)}{l\left(d_n\right)} \propto e^{-\delta}$$

where δ is the distance between d'_n and d'_{n+1}.

The lamination being compact δ is bounded between two constants, thus

$$l\left(d'_{n+1}\right) \propto e^{-\delta} l\left(d'_n\right) \rightsquigarrow \left|\log l\left(d'_n\right)\right| \propto n$$

Since $\overline{S-\lambda}$ has only finitely many spikes the estimate of the proposition follows. □

9.2. A graphic view of the Cantor set

We give in chapter 1 a δ-Dirac-measure for the middle third Cantor set transferable by isomorphy to all Cantor sets of Lebesque measure zero.

This lamination measure removes the gaps of the Cantor function, it is continuous. The stairs in the staircase represent the jump from one stage to the other.

Think of somebody walking on a transversal across the Cantor set generated by the pleating of a many leaved closed geodesic. In this representation the vertical jumps would arise when the walker crosses a leaf of the geodesic. Then nothing happens until a new leaf will be crossed. The steps correspond to the bends of the surface in hyperbolic space. As the geodesic makes more and more loops, the vertical jumps will steadily decrease in size (but they still all have equal size).

The Cantor set when crossing a lamination will not be the classical Cantor set. The set will depend on the lamination, which might have one or more leaves. The length of

the stairs will be different due to the scaling and the flat regions between the leaves not being ordered in decreasing size. However there will always exist a bijection between the Cantor set of the lamination and the classical set we use here.

An adaptation is necessary.

Should we define the stairs as a pleating about the constant angle α, the height of the jumps would get very small when the number of leaves increases, the visualization would get worst and worst. Anyway we have no jumps but bends in hyperbolic space.

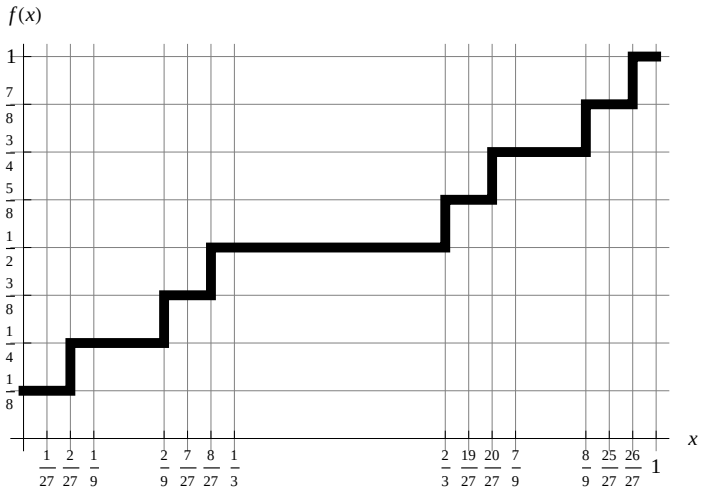

Figure 9.4.: Transverse measure of bending

We have constructed a turtle program using the same staircase principle but the jumps are replaced by a turn about the angle of pleating. The length of the segments of the polygon are in the same ratio as the distances between the geodesic leaves. Nothing happens when walking between the leaves. When crossing a leaf, a new segment of the polygon begins with a turn about the pleating angle.

The total length of the polygon is unchanged $= 1$, as we are only interested that the distances are in the correct ratio. The interval $[0, 1]$ has gone over to a spiralling convex polygonal curve.

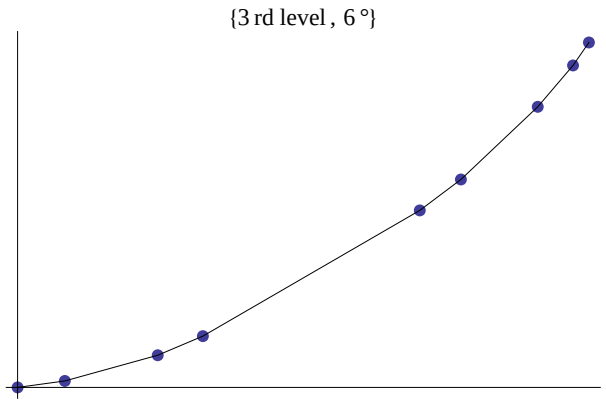

Figure 9.5.: Bending at level 3 of the Cantor set

Figure 9.5 is an example for $n = 3$ and a pleating angle $\frac{\pi}{30}$.

For $n = 6$ and the same angle $\frac{\pi}{30}$ the polygon will curl stronger.

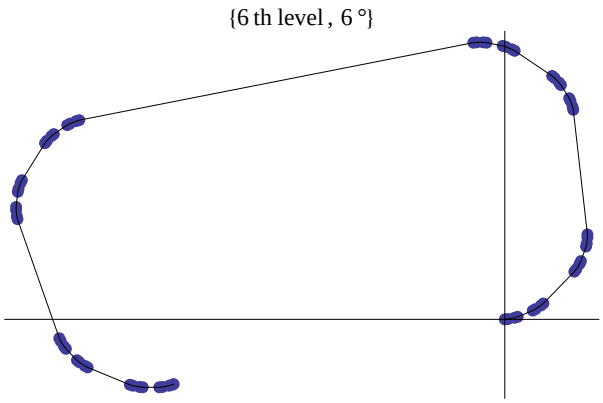

Figure 9.6.: Bending at level 6 of the Cantor set

Using $n = 7$ the polygon would intersect itself with $\frac{\pi}{30}$. This is easy to heal: the pleating angle must be decreased when n increases. In other words the size of the bends represented by the lunes on $\mathbb{C}P^1$ have an upper bound depending on the number of leaves of the geodesic. For any finite number of loops grafts can be inserted but they must be chosen smaller and smaller. Obviously the pleating angle along an infinite geodesic will be $= 0$, i.e. no pleating any more.

All graphics of this section are from the program Lamination_measure.

Chapter 10.

Closed curves on the torus

We compare in this chapter the homotopy classes of the flat and the 1-punctured torus. We use the results to put up an algorithm for finding many-leaved geodesics.

10.1. (m, n) curves

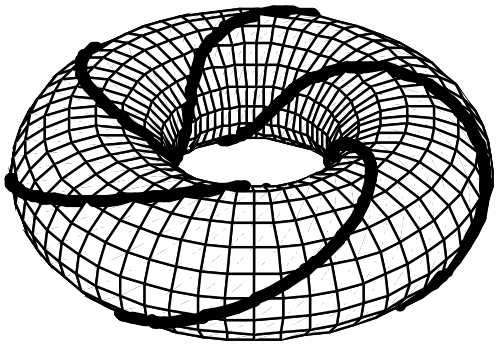

Figure 10.1.: (3,5) curve on the torus

Figure 10.1 uses the equation

$$((10 + 5\cos mt)\cos nt, (10 + 5\cos mt)\sin nt, 4\sin mt) \tag{10.1}$$

10 is the radius of the equator, 5 and 4 are the axes of the elliptic core. We have chosen $m = 3$ and $n = 5$ to get an $(3, 5)$ torus curve. More generally an (m, n) torus curve winds m times around the torus core and n times around the torus hole.

Increasing m or n by 1 is the same as inserting a 360°-Dehn-twist around a meridian or around the equator. As the windings are regularly spaced, they find exactly together again. It suffices to straighten the curve for getting the $(m + 1, n)$ or $(m, n + 1)$ curve. Inserting the Dehn-twist means: cut out a narrow cylinder, rotate one end about 360° and reinsert the cylinder into the torus. This operation creates no new intersections in the curve.

10.2. Homotopies

The pretzel is the topological sum of two tori. It can be obtained by removing an open disc from a torus, taking a copy and regluing along the rims.

Removing an open disc, we obtain a perforated torus. The 1-punctured torus is the perforated torus where only one point is missing. One missing point changes quite a lot. Indeed the 1-punctured torus can be turned inside out. It is hyperbolic instead of Euclidean. Its fundamental group is free.

The fundamental group of the usual torus is not free

$$\pi_1\left(T^2\right) = \pi_1\left(\mathbb{S}^1\right) \times \pi_1\left(\mathbb{S}^1\right) \cong \mathbb{Z} \times \mathbb{Z}$$

It is even abelian, therefore isomorphic to the first homology group $\pi_1\left(T^2\right) \cong H_1\left(T^2\right)$.

Proposition 18. *The fundamental group of the perforated torus is F_2, the free group of rank 2.*

Proof. Choose any two orthogonal $\mathbb{S}^1$, which do not cross the perforation. Enlarge the perforation until the rims touch the circles.

This deformation retract is a figure eight, i.e. a bouquet of 2 circles. The fundamental group is preserved. The generators in a bouquet of circles are free. □

However we are only interested in homotopies of closed curves and these happen to be analogous, whether the torus is perforated or not.

We quote a well-known

Theorem 7 (Poincaré)**.** *Each non-trivial homotopy class on the flat torus has a unique geodesic representative, conversely each closed geodesic path is homotopically non trivial.*

Sketch of the proof : lift a closed path with base point to the universal cover $\mathbb{H}^2$. The base point is mapped into two different tiles. Joining these points gives a unique geodesic on the universal cover, which is lifted back as unique representative of the homotopy class.

There are as well simple as self intersecting geodesics on the torus, but equation (10.1) delivers only simple geodesics :

Proposition 19. *All closed (m-n) geodesics from* (10.1) *are simple for all m and n.*

Proof. Every homotopy class is represented by an unique (m,n) geodesic, which is obtained from its $(m-1,n)$ or $(m,n-1)$ predecessor by inserting a Dehn-twist and spanning. As the Dehn-twist creates no new intersection and the $(1,1)$ geodesic is simple, the claim follows by induction. □

Poincaré's theorem is also valid for surfaces of genus ≥ 2. The proof is more delicate as it uses free homotopy, i.e. a homotopy where the endpoints are not required to be fixed (see [34, J. Stillwell] for the proof of the theorem).

Remark. What are simple curves good for?

Not all closed geodesics are simple. Geodesics obtained by straightening paths keep the intersections that are no trivial loops. According to the Jordan Curve Theorem a geodesic with essential intersections is not the boundary of a simply connected domain. This motivates why the definition of laminations refers to simple geodesics. The use of

laminations reminds in a certain sense of (also not intersecting) level lines. It would not make sense to graft along a self intersecting geodesic, as the grafts would intertwine in a neighbourhood of the crossing. Therefore we are looking for closed paths homotopic to a simple geodesic.

The condition for a path to be homotopic to a simple curve is still the same whether the torus is perforated or not. This was established by Poincaré in 1904.

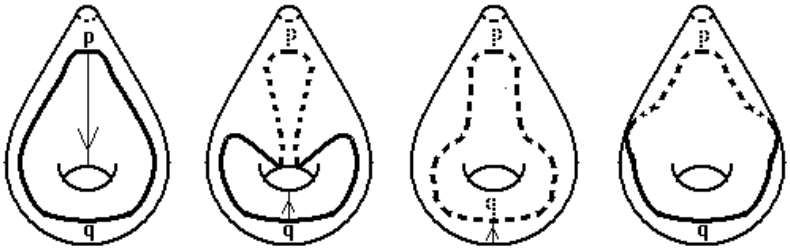

Figure 10.2.: The puncture does not prevent homotopy

Figure 10.2 illustrates why a perforation or puncture does not bar the way to homotopy.

Grab the closed path at the point p and let p glide through the hole so that p is behind. Then let q glide through the hole to the other side. The path lies now entirely behind. Keep on dragging at q until it reaches again its original position. The result is the same as had we let p jump over the perforation of the puncture at ∞.

Consequently we are allowed to study homotopies on the flat torus and use the results on the 1-punctured and on its double, the pretzel. Of course the pretzel will have a supplementary set of geodesics running from one handle to the other, the fundamental group of the torus being a subgroup of the fundamental group of the pretzel.

It is Poincaré again who initiated the model of the unit disc and the characterization of homotopy classes by limit points on the unit circle. This is the property we shall use to draw multiple-leaved geodesics on the pretzel. We begin doing this on the flat torus.

10.3. Constructing simple geodesics

The tessellation of the Euclidean plane for the torus is given by two generators a/A and b/B arranged along a tessellation of squares.

Figure 10.3 shows again the $(3, 5)$ geodesic. We have unrolled the torus (more exactly a homeomorphic flat parent) onto the Euclidean plane. The slope of the geodesic is $\frac{3}{5}$. The line joins the point marked with a 3 in the upper square to the identified point marked with 3 on the lower square. The line on the bottom indicates the jumps in the numeration and the edges being crossed. This induces the word $BABBABBA$.

Any path with the same base point 3 on these upper and lower tiles is homotopic to this geodesic. The path might be longer or have more crossings due to back steps. These are homotopic variations which disappear when straightening. Thus neither a nor b will appear in the geodesic word.

However we could have started from any other tile and drawn a line with the same slope. This is why the picture shows all these parallel lines crossing the tessellation. Thus the word $BABBABBA$ is just a member of the family of all words obtained by

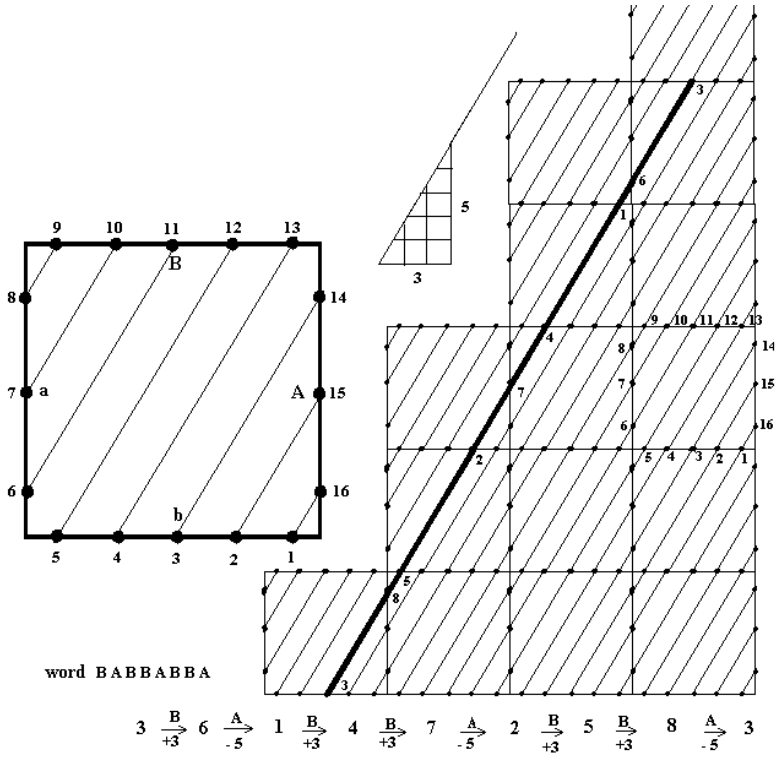

Figure 10.3.: (3,5) geodesic developped on $\mathbb{R}^2$

shifting the letters to the right or to the left :

1) $BABBABBA$
2) $ABBABBAB$
3) $BBABBABA$
4) $BABBABAB$
5) $ABBABABB$
6) $BBABABBA$
7) $BABABBAB$
8) $ABABBABB$

With a move of the plane we can choose any tile as fundamental tile with all the stripes. This tile is shown as a large square. 16 points are numerated but there are in fact only $3 + 5 = 8$ points on the torus due to the identification of the sides. When leaving our start point 3 on B, the line hits A in $14 = 6 \mod 8$. As points 14 and 8 are identified the next point is $9 = 1 \mod 8$. But 9 is 5, this leads to $12 = 4 \mod 8$, etc. Finally the starting point 3 is hit again after eight steps. Thus computing the word only requires to chase along the line within the fundamental tile and record the crossings modulo 8. This gives the word, from which we shift the letters 8 times to get all equally righted alternatives.

The algorithm works with any integers m and n, which have only to be prime to each other. Our reflexions on homotopy show that we can also use the algorithm for the 1-punctured torus, actually also for surfaces of genus ≥ 2. The algorithm will correctly

return the geodesics around one and the same handle. It will also return the geodesics crossing the handles.

A small technical problem is that we must indicate the number of times the line crosses each polygon side to get the proper word in return. As the corner points are on both sides, the algorithm does not work. However there is only a finite number of corners, hence a finite number of such geodesics.

10.4. The 1-punctured torus

10.4.1. Mapping the 1-punctured torus

One can easily imagine the 1-punctured torus as the usual torus minus one puncture at ∞.

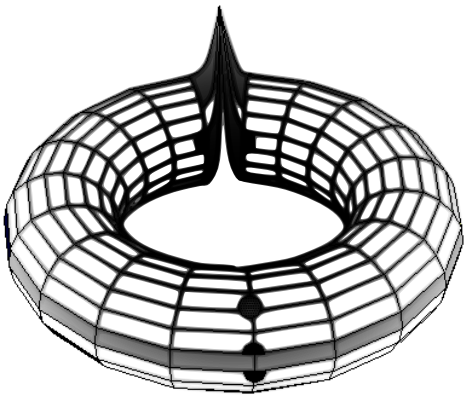

Figure 10.4.: 1-punctured torus

Why is the puncture at infinity? The fundamental region of the flat torus was obtained by using the intersection of the equator and a meridian and cutting along these. Take now this intersection away. If this missing point were not at infinity and the angle of the square were $\neq 0$, adjacent copies of the square would rotate around the missing vertex, until some tile is mapped on the fundamental domain. This is incompatible with the fundamental group being free. Thus the angle must be $= 0$ and the missing point at infinity. Figure 10.4 sketches the corresponding cutting.

Figure 10.5 shows the mapping in the Poincaré disc. The fat points in both figures are the Weierstrass points. Due to identifying the sides there are three of them : both midpoints of the sides and the origin.

These points are the fixed points of the elliptic involution. Pierce the torus with a needle through the 3 points (and through the point at infinity) and rotate it about 180° around this axis. The 3 points on the real line are invariant. This corresponds with the elliptic involution of the flat torus, which has 4 fixed points, the 4th being the missing point at ∞ on the 1-punctured torus.

Figure 10.5 also shows a 3-leaved geodesic. Obviously this geodesic runs trough two Weierstrass points. This is a consequence of the elliptic involution, as we shall prove. This is also a similar property of the pretzel, where it is called hyperelliptic involution.

This constraint of running through invariant points definitely influences the behavior of the geodesics. There is no obligatory involution on surfaces of genus ≥ 3. The pretzel which is the double of a perforated torus inherits properties of the torus. Surfaces of genus ≥ 3 are the topological sum of two 1-perforated tori and 2-perforated tori in between. This remark of course does not prove the absence of involution but makes at least plausible that surfaces of genus ≥ 3 must not behave the same way.

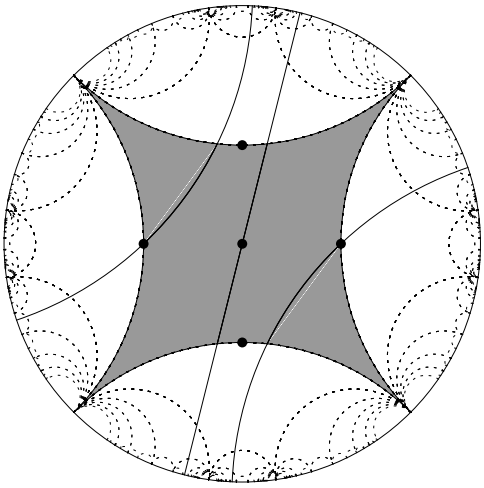

Figure 10.5.: Simple geodesic on 1-punctured torus

Due to the rapidly decreasing hyperbolic metric we shall prove that the leaves of a geodesic of irrational slope accumulate infinitely close to the three Weierstrass points.

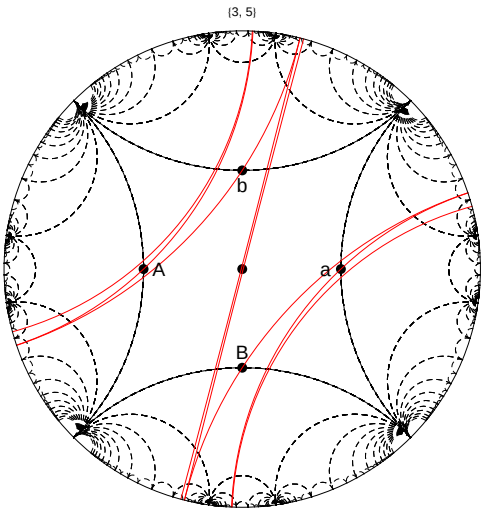

Figure 10.6.: (3,5) geodesic on the punctured torus

We now look at the (3,5) geodesic in figure 10.6. This is the next one when increasing the number of loops of the (2,3) geodesic by 1, m and n have to be prime to each other. Thus there is neither a (3,3) nor a (2,4) geodesic.

Our program Geo_Finder_torus visualizes simple geodesics on the 1-punctured torus. There is a more complete version Simple_geos_torus used for figure 10.6 with addi-

tional features for testing any word, returning whether the geodesic is simple or where are the intersections and which alternative words exist. The program Farey_torus visualizes simple closed geodesics and can handle quickly pretty long words.

We shall now comment on this program, but let us first notice how close the leaves come to each other. The geodesic does not run through the origin but only through the both Weierstrass points on the sides. Two leaves look nearly like diameters. They are not, they only run very close to the origin.

This observation illustrates why there is nearly no room between the leaves for grafting and still less for pruning. The allowed bending angle is already close to zero.

10.4.2. Farey tessellation and 1-punctured torus

There is a wonderful connection between the 1-punctured torus and the tessellation based on the modular group $SL(2,\mathbb{Z})$. This is a subgroup of the Möbius group, whose entries are integers. It happens to be the mapping class group of the torus (and of the pretzel).

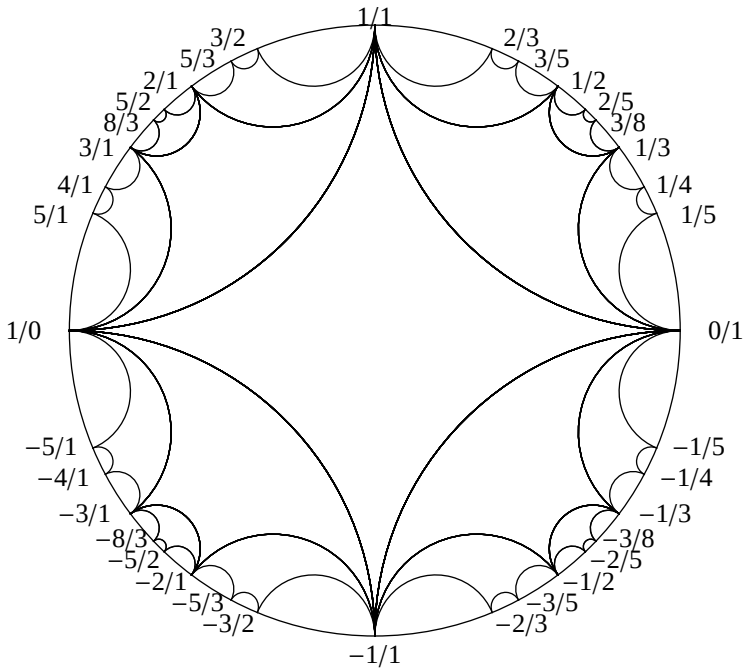

Figure 10.7.: Farey tiling of the torus

Figure 10.7 was drawn with the instruction InfTess[4, 1] of the package *diskgeometry*.

This tessellation does not only cover the 1-punctured torus but also the 3-punctured sphere. Opposite sides are identified in the case of the torus, whereas the sphere identifies adjacent edges. Cutting along a diagonal gives the tessellation by ideal triangles we showed in chapter 1. We also showed in this chapter the Farey tessellation in the half plane model, where the fractions lie on the real line.

The ideal vertices of the tessellation hit the unit circle exactly in the rational numbers, which are computed according to the naive rule of adding denominator and numerator of the Farey fractions, the dream of all children learning mathematics.

We already gave some insight of the use of Farey fractions. They are an easy tool for creating families looping around more and more p times in one direction and q times in the other.

We choose any number, approximate it by a fraction, so far it is not already a rational number and get a sequence of fractions, i.e. intermediary stages, around the selected p/q. This leads to a converging family of rational laminations.

With the program Geo_Finder_torus a sequence of (m, n) geodesics is produced for approximating an irrational slope, thus an infinite geodesic.

A number < 1 is entered and the precision of the approximation is chosen. The program returns a sequence of approximating fractions, which can be visualized.

A magnifying instruction allows to enlarge a region of the picture, e.g. around the origin, where the leaves run or do not run through, when the number of loops is increased.

On a hyperbolic surface simple closed geodesics of different homotopy classes usually intersect each other. Thus two points determine a unique geodesic only in the same class. Otherwise a finite number of Weierstrass points would not allow geodesics to always run through two points.

10.4.3. Intersecting geodesics

Proposition 20. *On compact surfaces of genus > 0 geodesics can only share two points, when their homotopy classes differ by more than only one Dehn-twist.*

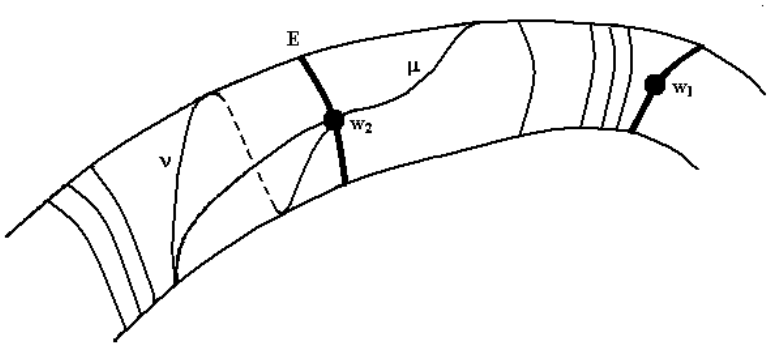

Figure 10.8.: Looping geodesic

Proof. Consider the geodesic μ making p loops in the cylinder section $[w_1, w_2]$ between the Weierstrass points w_1 and w_2 in one direction and q loops in the other direction, with $p + q =$ the number of loops of the homotopy class. Cut along the closed 1-loop geodesic E supporting the Weierstrass point w_2 and insert a full Dehn-twist in the section $[w_2, w_1]$. After tightening we obtain the new geodesic ν representative of the homotopy class of $(p + 1, q)$ loops.

Would ν run through w_2 on E, as pictured here, there would be a bifurcation in w_2! μ and ν would merge in the section $[w_1, w_2]$ with p loops. Two closed geodesics which

coincide between two distinct points cannot bifurcate, as a geodesic is the shortest and straightest path.

Exchanging the roles of the sections $[w_1, w_2]$ and $[w_2, w_1]$ extends the proof.

The Dehn-twist could also sit astride both sections. Then the number of full loops would be the same between w_1 and w_2. There would be in each section two homotopic geodesics joining w_1 and w_2, which cannot be. □

Consequently a (m, n) and a $(m+1, n)$ or $(m, n+1)$ geodesics cannot run through the same both Weierstrass points. There are 3 Weierstrass points on the torus, thus 3 choices. On the pretzel there are 6 Weierstrass points, hence more choices. This comforts the observation, that the leaves of a geodesic must not rush so quickly near to each other. However the question is still open, why the leaves run close to Weierstrass points through which they do not run.

10.4.4. Infinite geodesics accumulate on Weierstrass points

We give now a summary of the results [4, F. BONAHON] in the case of the 1-punctured torus.

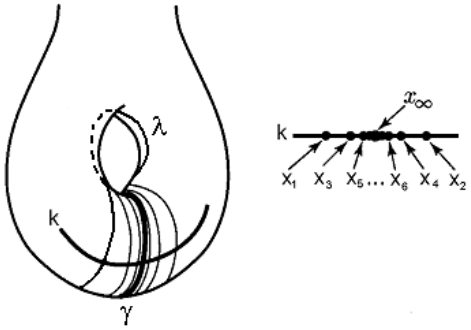

Figure 10.9.: Simple geo accumulating

Proof. Consider on a punctured torus T a sequence of simple closed geodesics looping n times across the edge k and once around the hole. The idea of the proof is that the distance between the leaves decreases exponentially inferring an accumulation against the bordering geodesic γ.

Each member of the family is a lamination λ_n. For $n \to \infty$ the lamination λ_∞ is the union of the simple closed geodesic γ and an infinite leaf going from one side of γ to the other, spiraling in opposite directions against γ. Note that the infinite leaf must be mapped to itself by the elliptic involution, i.e. when the torus is turned about 180° around the axis of the Weierstrass points.

To prove this Bonahon uses the concept of transverse Hölder distribution.

A distribution is a continuous linear form on the space of C^∞ functions $\varphi : T \to \mathbb{R}$ with compact support.

Bonahon remarks and proves that a homotopy of arcs transverse to λ admits no differentiable structure. This can be overcome as it suffices to choose the homotopy to be Hölder continuous.

A function φ between metric spaces is called Hölder continuous if there is a $\nu \leq 1$ and a positive constant C such that:

$$d\left(\varphi\left(x\right),\varphi\left(y\right)\right) \leq Cd\left(x,y\right)^{\nu}$$

for all x, y, whereby d is the distance function. When $\nu = 1$ the function is said to be Lipschitz continuous.

The metric used for the set of all closed subsets of a compact surface, here the punctured torus T, defines the Hausdorff distance $d_H\left(C,C'\right)$ between two closed subsets C and C' quite naturally as the smallest ϵ such that C is contained in the ϵ-neighbourhood of C' and reciprocally.

This allows to define a Hölder distribution on a compact metric space, here T, as a continuous linear functional on the space of all Hölder continuous functions $\varphi : T \to \mathbb{R}$ with compact support.

A transverse Hölder distribution α for a lamination λ is a Hölder distribution defined on each arc k transverse to λ, invariant under every homotopy of arcs transverse to k. The Hölder distribution induced by α on k has its support in $k \cap \lambda$, namely $\alpha\left(\varphi\right) = 0$ for every Hölder continuous function φ with support in $k - \lambda$.

From this follows $k \cap \lambda = \{x_\infty, x_1, x_2, \ldots, x_n, \ldots\}$, where x_∞ is the intersection of the transversal arc k and the lamination λ, against which the x_i accumulate.

For every Hölder continuous function $\varphi : k \to \mathbb{R}$ a Hölder distribution α is defined on k by choosing two parameters $a, b \in \mathbb{R}$ such that:

$$\alpha\left(\varphi\right) = a\varphi\left(x_\infty\right) + b\sum_{n=1}^{\infty}\left(\varphi\left(x_n\right) - \varphi\left(x_\infty\right)\right)$$

To see that the infinite sum converges, index the x_n so that the distance $d\left(x_n, x_\infty\right)$ monotonically tends to 0. Then

$$d\left(x_n, x_\infty\right) \propto \left(e^{-L}\right)^n$$

where L is the length of γ.

Why is this so? We established in chapter 9 the formula:

$$\left|\log l\left(d'_n\right)\right| \propto n$$

where the d'_n were the complement of $k \cap \lambda$, i.e. the ordered segments cut out by the lamination λ on a transversal k. So $l\left(d'_n\right)$ is the same as $d\left(x_n, x_\infty\right)$.

It follows

$$\left|\log l\left(d'_n\right)\right| \propto n \rightsquigarrow d\left(x_n, x_\infty\right) < e^{-Cn}$$

for some constant C, which we can choose to be the length L of the geodesic. This was the claim.

Using now the Hölder property $d\left(\varphi\left(x\right),\varphi\left(y\right)\right) \leq Cd\left(x,y\right)^{\nu}$ we get:

$$\left|\varphi\left(x_n\right) - \varphi\left(x_\infty\right)\right| \propto \left(e^{-\nu L}\right)^n$$

The infinite sum in $\alpha\left(\varphi\right)$ is absolutely bounded by a convergent geometric series, thus it converges too.

The distance between the geodesics decreases exponentially in the Cantor set.

Consider a sequence of geodesics with increasing number of leaves. They come exponentially closer to each other, thus also closer to the Weierstrass points, two out of three are alternately supported by each geodesic. □

The proof does not use that the geodesic only runs only once around the hole, which only makes presentation easier. It only uses the properties of the 1-punctured torus being a hyperbolic surface. It therefore also applies to the pretzel with its six Weierstrass points, but of course it does not apply to surfaces of genus > 2 which usually have no involution, hence no Weierstrass points.

Chapter 11.

Visualizing the torus

The 1-punctured torus is ideal for playing around. The tile is easy to handle. The free group avoids redundancy when setting up the tree of words. The properties are close to those of the pretzel but less complicated. The torus has only three Weierstrass points, so that the leaves of a simple non-separating geodesic rush swiftly against each other, thus leaving very little room for grafting and pruning.

11.1. Fractals

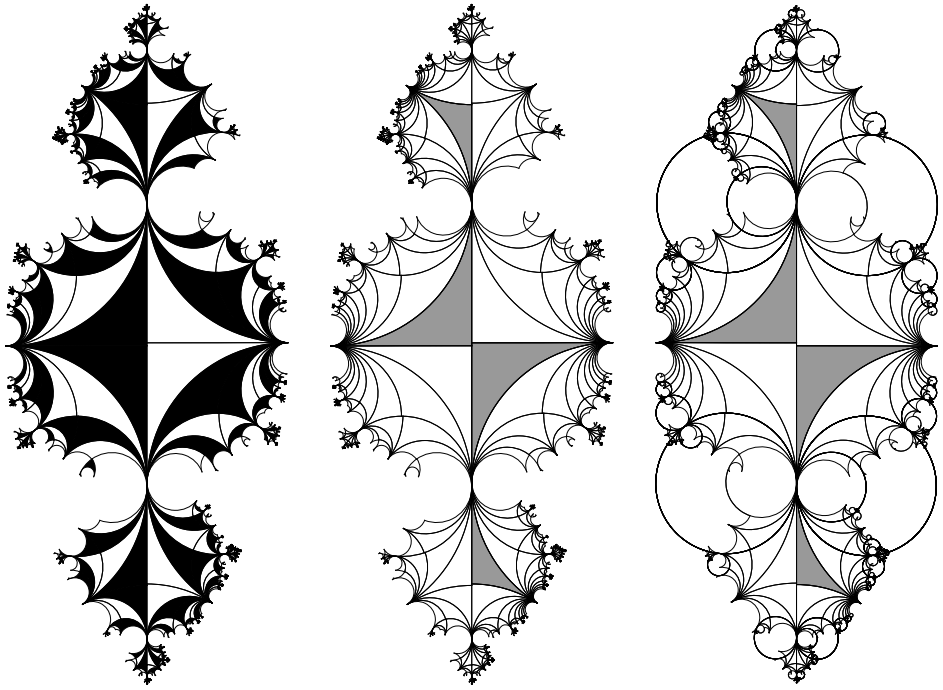

Figure 11.1.: Strangled torus

The poor torus on the left of figure 11.1 has been ruthlessly strangled until its sides kiss each other and, as were it not enough a twist has pushed the both halves in opposite directions until they are only connected in the origin. In this harlequin rendering half of the tile is black, the other white.

The rendering in the middle is exactly the same but for showing the fundamental tile in gray. The grafting angle $\alpha = 45°$ makes the lateral edges kiss. The twisting angle $\varphi = 50°$ is the limit for the fundamental tile being still connected.

The picture on the right shows what happens when the twisting angle $\varphi = 51°$ disconnects the tile in the origin. Nothing spectacular indeed but for alien circles. Beads of circles appear which do not look chaotic like when computing goes haywire. Still increasing φ infers no new accident, although the vertical parts of the tile drift against ∞.

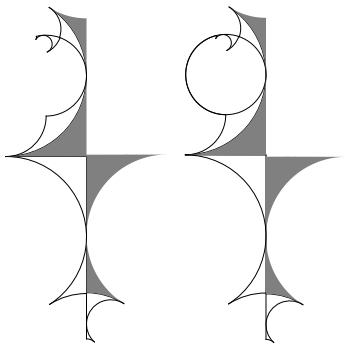

Figure 11.2.: Anatomy of the crash

Figure 11.2 shows the fundamental tile when the twisting angle jumps from 50° to 51°. By 50° everything is still OK. By 51° the circle closes itself. A meticulous look convinces that this may not happen, although everything looks plausible.

The treatment has been inflicted with the program Torus_fractal designed for Möbius moves , i.e. compositions of grafting/pruning with twisting. The rendering in harlequin is intended for aesthetics, the one in gray visualizes the torture inflicted to the fundamental tile. This program could be useful for educational purposes as the torus model is less intricate than the pretzel.

11.2. Multiple leaved geodesics

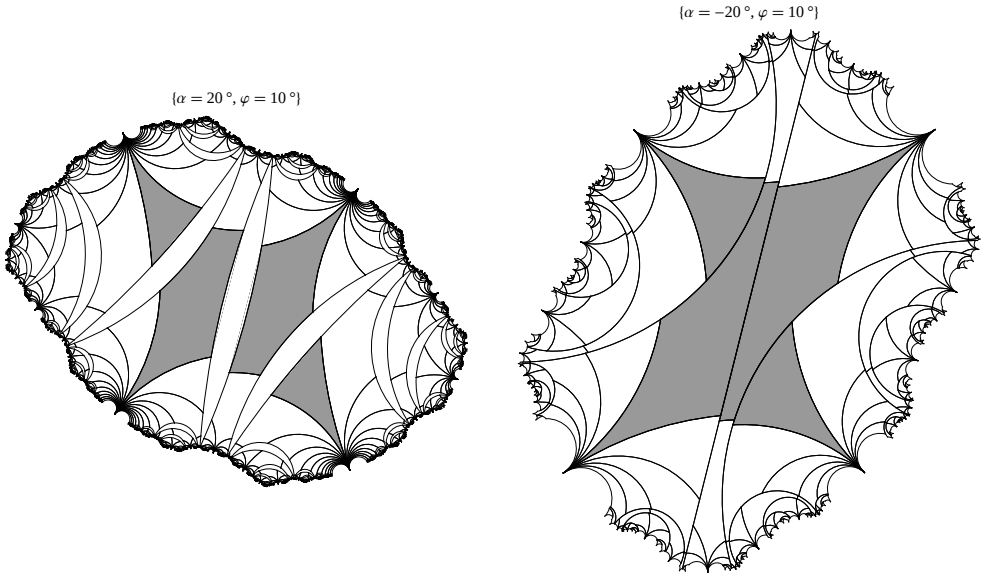

Figure 11.3.: Torus surgery

The program Torus_surgery is dedicated to Möbius moves on the torus, but it uses a 3-leaved geodesic.

Due to the rapid convergence leaves of (m, n) geodesics higher than $(2, 3)$ only allow a very small angle. We have shown in chapter 10 the geodesic $(3, 5)$, which is the next step after $(2, 3)$. The program Torus_surgery grafts, prunes and twists in figure 11.3 along the $(1, 2)$ geodesic.

The elliptic involution is a great help when constructing the tile. It suffices to work on one half and multiply everything with -1 to get the other half.

The construction we apply is the same, whatever polygon is involved, i.e. also for the pretzel. Thus some comments.

11.3. Programming recipes

The relatively easy to handle torus is a good paradigm of how to program a tessellation after a Möbius move.

Step 1: Generate a list of words.

It is a good idea to enlist the words right at the start. It might seem wiser to integrate this computation into the drawing instruction at the end. It is not, because once the generators have been calculated, you would have an impracticable list of figures. It is better to have a list of letters picturing the content of the tree. This makes computing time not significantly higher.

As already stated we use an algorithm building up a tree of reduced words. It is not related to the tile, it only needs to be tuned in according to the number of generators. The break condition sees to it that words are not computed for which the origin would be distant by more than '`limitsetrad`'' from its image. For instance $limitsetrad = 0.995$ disregards the tiles closer than $0,5\%$ to the unit circle. This is of course the distance in the original tessellation before grafting (pruning).

When the fundamental group is not free, i.e. for the pretzel, the algorithm will of course return redundant words. It would cost more time eliminating than tolerating these. To limit this useless calculation a second break condition will be added: compute only words up to some number of letters, in order not to loop too much around. Waste cannot be totally avoided. The torus is the sympathetic case of a free group with no redundancy, so that the second break condition is not required.

Step 2: Replace the fundamental tile.

The basic idea is to first of all revisit the fundamental tile, i.e. construct a new fundamental tile blown up or shrunk down by the angle α. The twisting angle φ has not to be taken care of. As φ only induces an automorphism of the Poincaré disc, it has just to be included in the transformation matrix.

The old tile is carved in domains, whose union is the old tile, bordered by the leaves of the geodesic. The transformation returns the ready to use blown up new tile or the deflated tile, which must be freed from its overlaps.

Even if the interaction of the moves along the different leaves might seem trivial, it requires some patience to solve the riddle. The matrices have all similar effects, so that a wrong choice infers only a slight hardly visible imperfection in the picture.

Here for the 1-punctured torus *Mdiam* is the Möbius matrix moving by $\frac{\alpha}{2}$ along the diametral cut, whereas *Mlat* moves by $\frac{\alpha}{2}$ along the lateral cut. The diameter, i.e. the axis of symmetry, remains unmoved as intended.

The product $Mlat \cdot Mdiam^2$ returns the move of the grey pentagon and *Mlat* the move of the gray triangle.

When pruning it is not enough to take a negative angle. Some stuff must be cut away too, because it overlaps! Therefore one has to know where the supporting geodesic leaf has been moved. Here it has been moved by the product $Mlat \cdot Mdiam$. When knowing this, cutting away is tedious but of course not difficult.

Step 3: Revisit the generators

The generators must be adapted to the new tile. Grafting, pruning or twisting follow the same formula. An easy hoax is to compute the Möbius transformation bringing an adjacent tile seamless along the fundamental tile. This means giving up to understand which laws the generators must obey. It is more rewarding to decrypt the process. Note that the solution is not unique, it depends on how one looks at the moves.

For the torus our solution is:

- $newb = Mlat \cdot oldb \cdot Mdiam^{-2} \cdot Mlat^{-1}$
- $newa = Mlat \cdot Mdiam^2 \cdot olda \cdot Mlat$

Then everything has been done. The instructions for tessellating apply without change on the new tile with the new generators.

11.4. Two more programs

Like for the other models there is a program Geo_Finder_torus, for finding closed simple geodesics in a Farey sequence approximating an infinite geodesic. It is structured to accept long words.

The program Simple_geos_torus does the same for shorter words, but it can also analyze any word in order to satisfy where the geodesic has self intersections and compute the effect of permuting letters. It gives the empiric confirmation that our algorithm for finding simple closed geodesics really returns all (m, n) -geodesics.

Chapter 12.

Weierstrass points and geodesics

We have defined the Weierstrass points as the fixed points of the involution of a Riemann surface. We have located them on the 1-punctured torus with its elliptic involution. This will now help us to find them on the pretzel with its hyperelliptic involution. The theory sustaining the hyperelliptic involution and the existence of Weierstrass points on the pretzel has been mainly developed by [17, Haas and Susskind]. We would like to give an idea of the proofs.

12.1. From the torus to the pretzel

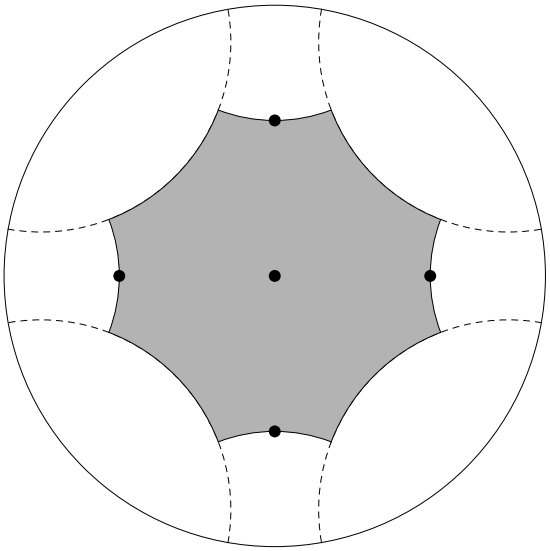

Figure 12.1.: 1-holed torus

Figure 12.1 shows a 1-holed-torus $T^2\backslash\mathbb{D}^2$ in the Poincaré disc. The 4th Weierstrass point of a not perforated flat torus is missing, because the needle of the involution pierces through the removed perforation. Like in the case of the Euclidean flat torus it is easy to localize the three remaining Weierstrass points as the origin and both midpoints of the identified edges of the torus. The perforation is a closed geodesic orthogonal to the sides of the torus, from which it inherits the side identifications.

In our program Weierstrass_pts it is possible to choose the distance between the Weierstrass points and the origin.

In figure 12.2 a vertical translation upwards has moved the 1- holed torus, say T_1, so that the rim of a perforation is sent to the real axis with its (Euclidean) midpoint sent to the origin. Then a double of T_1, say T_2, can be added in the lower half according to figure 12.3.

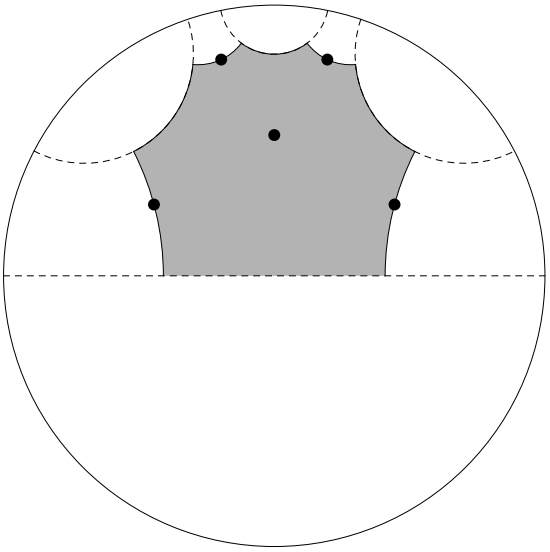

Figure 12.2.: Moved up 1-holed torus

The 3 Weierstrass points have been doubled to 6 points.

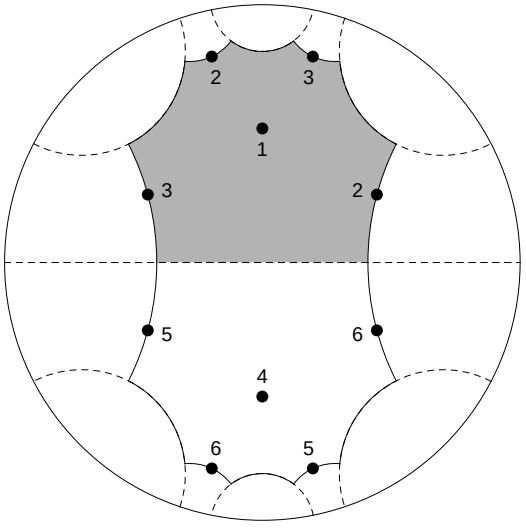

Figure 12.3.: The Weierstrass points of the pretzel

We look now at the hyperelliptic involution J and the 6 Weierstrass points of the pretzel M.

Let δ be the cut separating T_1 from T_2. Then $M = T_1 \cup T_2 \cup \delta$ is a pretzel, whose 6 Weierstrass points are just the respective Weierstrass points of T_1 and T_2.

Each torus T_1 and T_2 has an elliptic involution, say J_1 and J_2.

Following [17, Haas/Susskind] and [27, McShane] the hyperelliptic involution J is J_1, when restricted to T_1, and J_2, when restricted to T_2. The construction using pairs of pants makes this clear. Gluing defines a map on the whole of $M = T_1 \cup T_2 \cup \delta$ which itself induces a map $[v] \mapsto -[v]$ on the homology $J*$.

More formally, let v be a representative of the homology class $[v] \in H_1(M, \mathbb{Z})$, then the involution J infers a group homomorphism $J* : H_1(M, \mathbb{Z}) \to H_1(M, \mathbb{Z})$ with $J*([v]) = -[v]$.

The fundamental domain we obtain is the union of two pairs of right angled hexagons, i.e. two pairs of pants. The holes of the pants are the holes of the tori. They have equal length. The edges, i.e. the seams of the pants, also have equal length. Note that the vertical edges and the horizontal cuts merge when gluing, as they meet at right angles. So the fundamental domain is an irregular right angled dodecagon. This is the tessellation we already used.

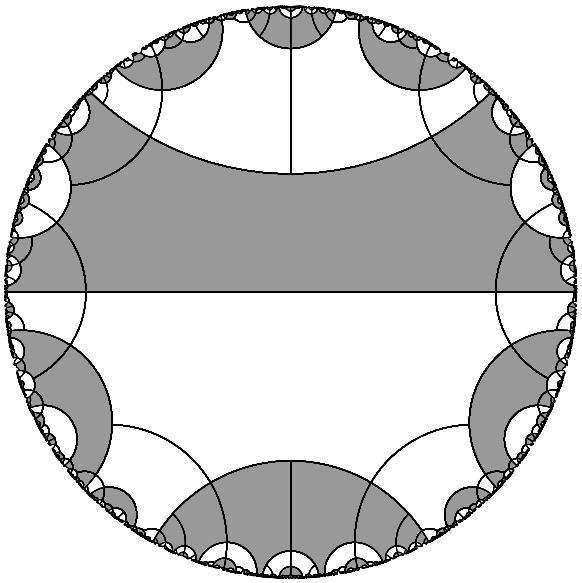

Figure 12.4.: Pretzel as doubled pair of pants

The tessellation of figure 12.4 was obtained from a doubled right angled hexagon with 3 different side lengths. The gray and the white tiles correspond each to the half of a pretzel. Up to side length this is the tiling obtained from the tiles we have constructed. The program Double_Pants can also render half pants in colors.

The pretzel as double of the perforated torus will have geodesics inherited from the torus, but also specific geodesics. On the 1-punctured torus each closed non-separating geodesic passes through exactly 2 Weierstrass points (see [26, Greg McShane].

12.2. Hyperelliptic involution

Referring to Haas and Susskind [27, G. McShane] states following properties:

Theorem 8 (Greg Mc Shane)**.** *Summary*

i) The hyperelliptic involution J has 6 fixed Weierstrass points on the pretzel.
ii) Every separating simple geodesic does not meet any Weierstrass point.
iii) Every non-separating simple geodesic passes through exactly 2 Weierstrass points.
iv) Each unoriented closed simple geodesic is mapped to itself by J.

The latter point is developed in HAAS and SUSSKIND:

Theorem 9 (Haas and Susskind)**.** *Let J be the hyperelliptic involution of a genus 2 Riemann surface M.*

i) Every simple closed geodesic α on M is mapped onto itself by J.
ii) Is α separating, then J preserves its orientation.
iii) Is α not separating then J reverses its orientation.

Figure 12.5 shows a pretzel cut into two 'pairs of pants' along a separating geodesic. Gluing two other pairs of pants, but along the legs instead of the belt, we obtain a torus minus two discs, which we can insert into the pretzel in order to add a new hole. Obviously we can get the standard form of a torus of any genus when inserting $(g-2)$

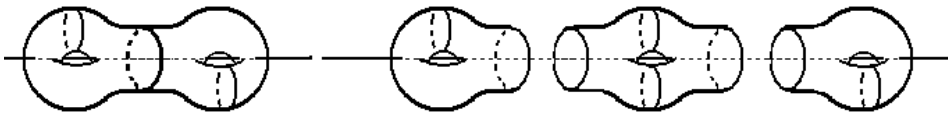

Figure 12.5.: Hyperelliptic involution

such 2-perforated tori.

Thus the pretzel is different from such surfaces of genus > 2. It is the unique case where no 2-perforated torus is inserted. It is the topological sum of two 1-perforated tori or up to homeomorphy the double of a 1-perforated torus, say T.

Let α be the separating geodesic along which the legs of the pants are glued together. The elliptic involution will have two fixed points on the geodesic α, the 3rd one on $T \setminus \{\alpha\}$. To understand this we refer to HAAS and SUSSKIND.

[17, HAAS and SUSSKIND] defines the hyperelliptic involution of a genus g Riemann surface as an order two conformal automorphism of the surface that fixes $2g+2$ points. Such an automorphism, so far it exists, is unique and the surface is said to be hyperelliptic. Every surface of genus 2 is hyperelliptic. Surfaces of higher genus have no involution: 'The automorphism group of the generic surface of genus ≥ 3 is trivial' [27, McShane].

12.3. Sketch of Haas and Susskind's proof

Proof. See [17, HAAS and SUSSKIND] for the complete proof sketched hereafter.

As a preliminary the authors consider a domain S in the Poincaré disc from which two smaller discs are removed. According to Poincaré there exist precisely 3 simple closed geodesics α, β, γ each homotopic to one of the bordering circles. This delimits what is usually called a pair of pants with geodesic boundary.

Let $l(c)$ be the length of a curve c in the hyperbolic metric, then

Lemma 2. *If $l(\alpha) = l(\beta)$ there is a conformal involution $j : S \to S$ that interchanges α and β and keeps γ invariant.*

After proving the lemma the authors remark that the involution j extends to a Möbius transformation with a single fixed point on S. Indeed would the involution have more than a single fixed point, it would have a fixed line, thus > 3 fixed points, and a Möbius transformation with more than three fixed points is the identity.The geodesic γ being mapped onto itself by j, if g is a primitive transformation covering γ in the generating Fuchsian group Γ there must be a transformation h in Γ extended by the normalisator of Γ such that $h^2 = g$. Consequently the involution is induced by the square root of a primitive boundary transformation and will be independent of choice of the simple closed geodesic we will now define.

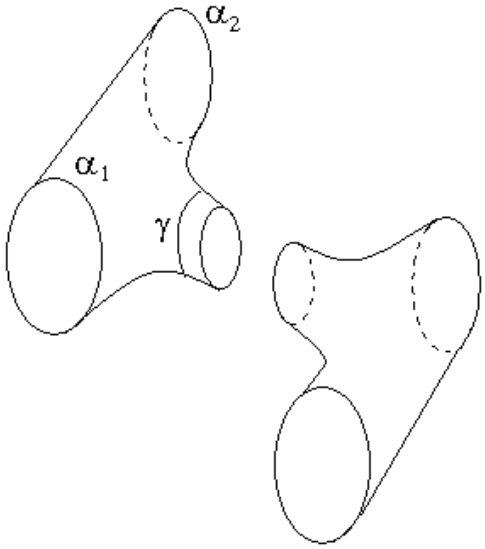

Figure 12.6.: Proof of Haas & Susskind

Consider a 1-perforated torus T and cut it open along any simple closed not separating geodesic α. The lemma infers the existence of an involution interchanging α_1 and α_2 which are the two copies of α. This induces an involution j of T regluing α_1 and α_2. Thus α is mapped onto itself with orientation reversed. As a consequence of the lemma j has a single fixed point on $T \setminus \{\alpha\}$. Since the involution maps α to itself with orientation reversed, j must also have two fixed points on α. Thus the involution j has three fixed points the so called Weierstrass points.

Consider the pair of pants S immersed in T and bordered by γ, the unique closed geodesic homotopic to the hole. γ is separating. Now glue to S its double $\widetilde{S}$ along γ to get a pretzel. The separating geodesic γ is made of the two copies γ_1 and γ_2. Since the hyperelliptic involution maps γ onto itself with orientation preserved γ cannot have fixed points. □

12.4. Gathering results

Proposition 21. *There are no separating geodesics on the 1-punctured torus.*

Proof. Suppose there was a simple separating geodesic. Cut along it to separate the torus, say T, into two components T_1 and T_2, the cusp being in T_2. Double T_1 to get a compact oriented surface $S = 2\,T_1$. Then this double S is certainly not a torus, as $T_1 \cup T_2$ was a torus. S must be a surface of higher genus with area $A(S) = 2A(T_1) \geq 4\pi \rightsquigarrow A(T_1) \geq 2\pi$. But $A(T) = A(T_1 \cup T_2) = 2\pi$, thus $A(T_1) \geq 2\pi$ is contradictory to $A(T_1) < A(T_1 \cup T_2) = 2\pi$.

□

As there are no separating simple geodesics, all geodesics run through two Weierstrass points due to the elliptic involution, and come nearer and nearer to the 3rd Weierstrass point. As hyperbolic distance decreases exponentially the leaves of a geodesic generate a Cantor set on a transversal.

Due to the hyperelliptic involution something similar happens on the pretzel with the difference that there are six Weierstrass points and separating geodesics never running through a Weierstrass point.

We formulate the results as:

Proposition 22. *Using Farey-fractions approximate a geodesic of irrational slope with simple closed geodesics.*

Choose $\epsilon > 0$.

i) On the 1-punctured torus almost all leaves run through the ϵ-neighbourhoods of the three Weierstrass points, the origin and both Euclidean midpoints of the identified sides.

ii) On the pretzel almost all leaves run through the ϵ-neighbourhoods of three Weierstrass points (out of six), so far the geodesic does not separate.

12.5. Visualization

We propose three programs for visualizing these results.

With Geo_Finder_torus, which we already presented, a Farey sequence is built up for any rational number <1. The program can use long decimal numbers. However convergence is so rapid that the increasing number of loops is not visually revealed in the standard view, therefore the possibility of magnifying an extract.

The program Geo_Finder_deca uses the decagon model. The entry is a set of edges the geodesic has to cross. When the geodesic is not simple, which is usually the case for a random choice of set, the program shows the geodesic and computes the intersections to sustain visualization. The advantage of this program is that the decagon model is shown in the symmetry of the involution. The drawback is that the construction of the tile is intricate and it is difficult to locate visually where the sides of the polygon are on the pretzel.

The program Geo_Finder_octo works in the same way. The point of view of the octagon model does allow to recognize conveniently the symmetry of the involution. However one handle is above the real line, the other underneath, so that it is very easy to see where the edges of the polygon are on the pretzel.

Chapter 13.

Simple geodesics on the pretzel

The feeling when hunting for simple closed geodesics may be the same Erastothenes had before he invented his sieve for prime numbers. Almost every path you try is a failure. When gathering up the little success you achieved, you do not know whether there might exist more interesting cases. One thing we must live with, is that long words stumble on machine precision because of too many multiplications of matrices.

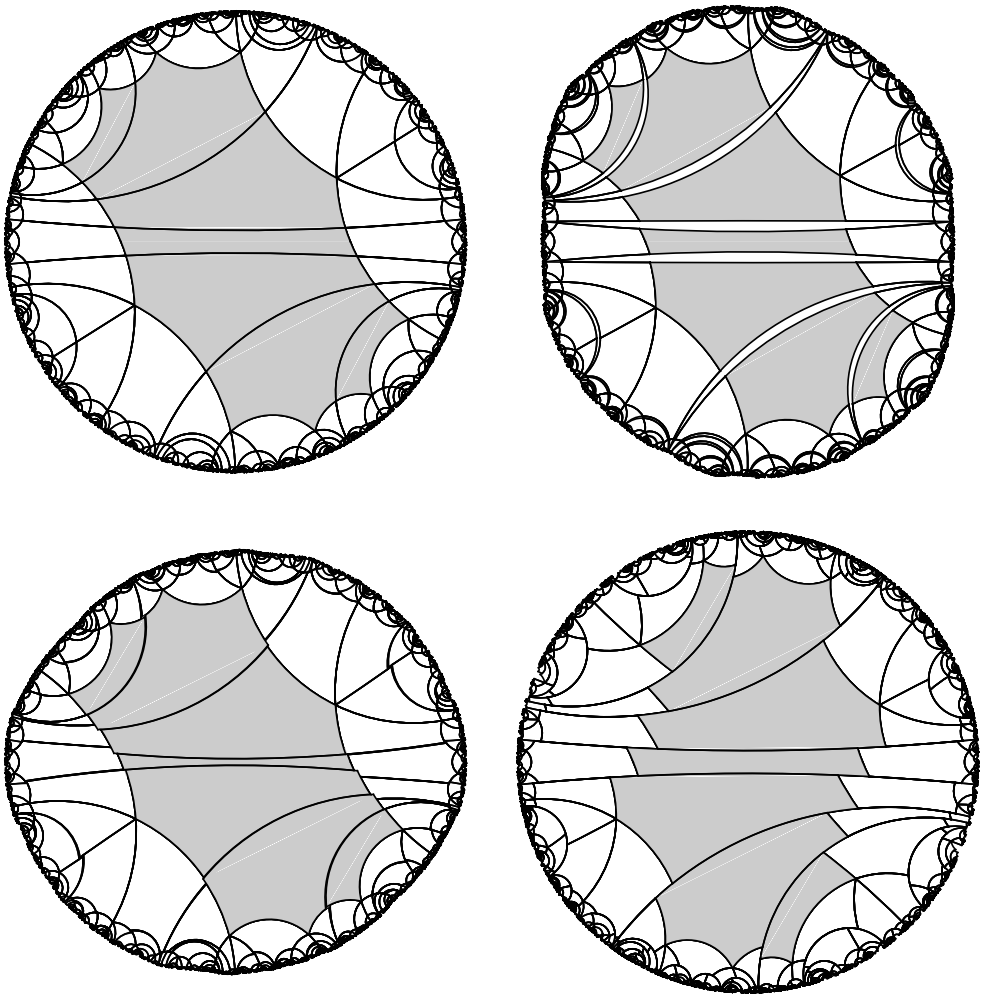

Figure 13.1.: 6-leaved geodesic

Another boring fact is that simple closed not separating geodesics dash with tremendous speed against their limit. Then the program cannot deal with arcs of circles of

very large diameter and intersections close to the unit disc. This makes a lot of trouble specially with longer paths.

Figure 13.1 shows a geodesic we have selected for its leaves being far apart.

However these difficulties do not prevent from trying to visualize how grafting and pruning work. Words longer than can be shown contain no hidden mysteries. They will only have many slits densely packed against the limit. Grafting works fairly well as the slits are so to say pumped up, but pruning often leads to a crash, as there is not enough stuff to be taken away when the angle increases.

These limitations to short words and small angles do no much harm. The interesting cases are those of short paths because we have only 5 generators (plus their inverses). Longer words only repeat within this small alphabet, they only have more nearly colliding loops based on the pattern of short words.

13.1. The decagon model

13.1.1. Constructing the tile

We use now a very comfortable model elaborated by Dr. Ekkehard-H. Tjaden of TU Berlin which takes advantage of the beautiful roundness of $\mathbb{S}^3$ to emphasize the symmetries.

Take two circles in $\mathbb{S}^3$, each from one copy of $\mathbb{R}^2$ so they live in $\mathbb{R}^4 \cong \mathbb{R}^2 \times \mathbb{R}^2$, put 6 equidistant points on the one circle and 4 points on the other.

Pairing two neighbouring points of the one circle with two neighbouring points of the other produces a K_{4-6} graph whose edges can be taken as facettes of a surface in $\mathbb{S}^3$.

There are $6+4 = 10$ vertices, $6 \cdot 4 = 24$ edges and 12 faces. Thus the Euler characteristic is -2, i.e. the surface has genus 2. Note that the original construction works for every genus.

Stereographic projection from $\mathbb{S}^3$ into $\mathbb{R}^3$ shows a pretzel from which we take the universal cover in the Poincaré disc.

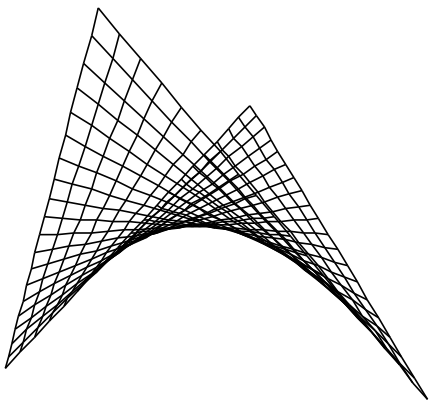

Figure 13.2.: Hyperbolic paraboloid

The facette is an equal sided quadrilateral with opposite angles $\pi/3$ and $\pi/2$ cut out of a hyperbolic paraboloid. We assemble in figure 13.3 the 12 quadrilaterals to the fundamental tile of the pretzel. Opposite edges are identified. Thus there are 2 vertices each in 5 copies. The midpoints of the identified edges plus the origin are the 6 Weierstrass points.

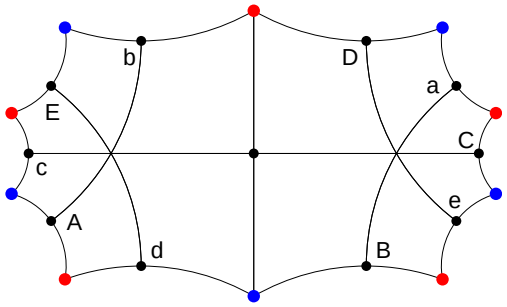

Figure 13.3.: The decagon tile as union of quadrilaterals

It is far from evident how the identification of the edges and Weierstrass points works. This is the weak point of this model.

One gets a fair idea by joining the tips of the thumb, the index and the middle finger of his right hand with those of his left hand. For a good understanding of the model load Comp_Surf_Ekki written by Dr. Ekkehard-H. Tjaden, where you can rotate the graphics sketched in figure 13.5.

The technique has been developed originally by Bernd Oberknapp and Konrad Polthier in a numerical algorithm for picturing the Lawson minimal surface (see *An Algorithm for Discrete Constant Mean Curvature Surfaces*in [30]). Their tile is made of 16 quadrilaterals with $\frac{\pi}{3}$ angles. We use instead only 12 quadrilaterals. To the blank eye our pretzel looks exactly the same as their Lawson minimal surface.

Figure 13.4 gives a more exact view of the pretzel seen from the front, from the side and from above. It looks like a torus with a half torus bridge. The both points used for the cutting are at the left and at the right extremity.

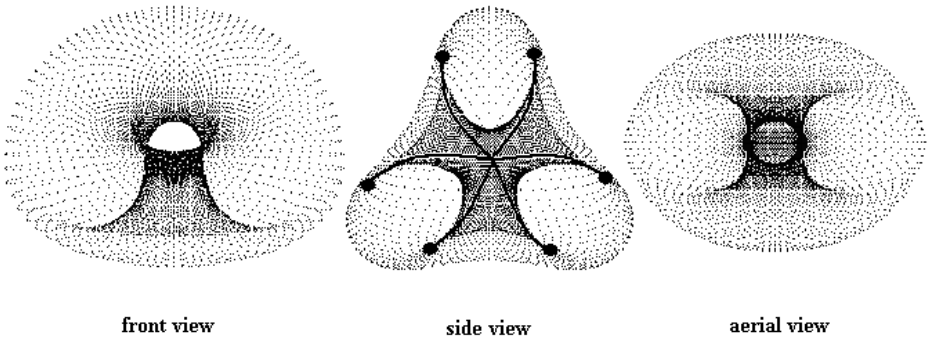

Figure 13.4.: The decagon pretzel

Figure 13.5 locates the 12 hyperbolic paraboloids. The pretzel is the union of them. We see on the left every second quadrilateral and the complement on the right.

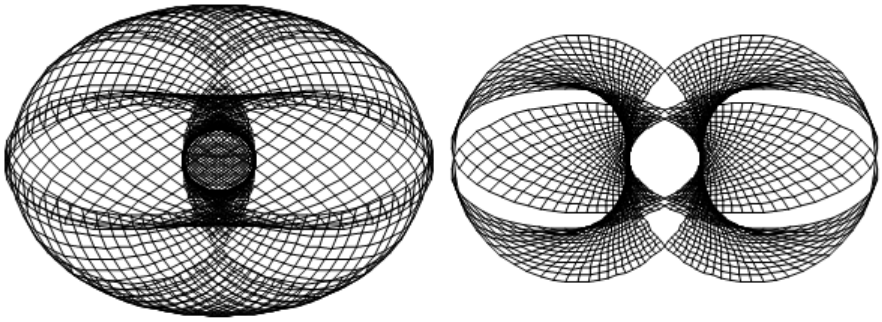

Figure 13.5.: Separating along the quadrilaterals

13.1.2. Using the symmetry of the hyperelliptic involution

The hyperelliptic involution is axed on the circle joining the 6 coplanar Weierstrass points. Simple closed geodesics will run symmetrically across the tile. When we take such a geodesic under scrutiny in the Poincaré disc we just need to rotate its axis of symmetry onto the real line and compute what happens in the upper half of the disc. We get the lower half for nothing, indeed by a π-rotation, i.e. by reversing the signs of all points.

The hyperelliptic involution produces a symmetry along a diameter, which is optimal for visualization. Only one half of the fundamental tile must be constructed. Last but not least the identifications of opposite sides are welcome.

13.2. Geodesic paths

A path, say {c,a,c,D}, is a sequence of letters, a cycle extracted from a biinfinite list. We understand these letters as the edges across which a geodesic runs. Note that {c,a,c,d} would be a different path. Although D and d are identified as one and the same edge, it depends from which direction one approaches.

The path repeats along the geodesic, so {c,a,c,D,c,a,c,D} is the same geodesic as {c,a,c,D} belonging to the same biinfinite support. Thus it is not possible to hit, say 4 times, the edge a in different places, because {a,a,a,a} is the same as {a}. However {a,a,a,a,D} containing the intruder D will actually hit 4 times the edge a (and once the edge D).

We understand the letters also as the generators covering the geodesic. This assimilation does no harm and simplifies notation. The generators are matrices which get multiplied, so c.a.c.D applied to a point gives its image on the geodesic.

The path {c,a,c,D} being the same as {...c,a,c,D,c,a,c,D,c,...} it must also be the same as {...,a,c,D,c,a,c,D,a,...} and the other cyclic shifts. It must also be the same as the inverse path {d,C,A,C} and its shifts when walking on the geodesic in the opposite direction.

Imagine Dr. Stickler of Indra's Pearls starting from anywhere in the fundamental tile with a piece of thread in his hand to mark his way. He stalks outwards and follows a not necessarily straight but cyclic path, until he becomes so small that he seems to us to have nearly reached the boundary of the unit disc. Where the cycle begins is arbitrary when walking from infinity to infinity. It only makes sense to consider all

shifted cycles. The walking direction will also be reversed in all cycles. Looking at the both points on the unit circle from where Dr. Stickler seems to have started to where he seems to aim at, it suffices to span the thread to get the geodesical path he should have followed to minimize his long walk (according to Poincaré's result, that homotopic paths have a unique geodesical representative). It does not matter from which point Dr. Stickler started in the fundamental tile because the image of this point lies in a tile close (for the Euclidean eye) to the boundary of the disc, so small a tile that it merges with the end point of the geodesic.

Consequently the fixed points of the 8 words c.a.c.D, a.cD.c, ..., A.C.d.C., C.A.C.d. are the endpoints of the leaves of the geodesic.

Before there is a proof that {c,a,c,D} generates a geodesic, it is not asserted that it will run twice across c and once across a resp. D. The path could be a cyclically repeated zickzack. But when considering the both endpoints of the path on the unit circle the geodesic joining them is the tightening of the path. Practically it seldom happens, that a path deviates so much that its tightening would cut different edges. Looking at the path nearly always indicates which edges are crossed over and how often.

Remark. As long as the leaves cross the fundamental tile they belong to one and the same geodesic. Of course every word can be shifted and inversed in the previous manner. The so obtained branches will run somewhere across the disc but not all across the fundamental tile. We have to imagine the covering of the pretzel as would a thin transparent film get unrolled from the pretzel onto the hyperbolic plane. A geodesic will run successively through the layers but all leaves are on the pretzel. When grafting (or pruning) a wedge gets inserted (removed) not only from one layer but from all layers. The branches outside the fundamental tile are no leaves of one and the same geodesic, so far they are not conjugated to leaves on the tile. We found many such isolated arcs - intersecting or not - which just happen to be related by shifting without belonging to one and the same geodesic.

Grafting or pruning is cutting along a geodesic in order to insert, resp. prune away, a small ring. This makes no sense when the geodesic is not simple. Nothing can be inserted where the geodesic intersects itself, because the cut along the geodesic runs into a grafted area which does not belong to the pretzel. Therefore the only candidates are simple geodesics. The profound reason for this was given in [32, Poincaré]: each free homotopy class of closed loops contains a simple (i.e. non intersecting) representative if and only if the unique smooth geodesic representative C is simple. Further C is simple if and only if for each lift of C on the Poincaré disc the supporting curves in the infinite family of conjugates are pairwise disjoint. This motivates why we hunt for simple closed geodesics along which grafting and pruning are possible. The last step will be to examine what happens when a finite simple closed geodesic with many loops comes near to an infinite geodesic.

13.3. The algorithm of Birman/Series

Having experienced great difficulties in practically finding simple closed geodesic, the question arose, whether these geodesics found by tapping around were representative of the set of simple closed geodesics (often called the Birman Series set).

As a liminary remark, note that there are simple closed geodesics which do not cross the interior of edges but run through vertices. They cannot be described with words. As there is only a finite number of them this does not limit too much the visualization.

A brutal searching method consists in computing all possible words of up to n letters. With 10 letters, i.e. 5 plus 5 inverses, $10n$ words are to be computed. There is unfortunately no way leading from a word of i letters to a word of $i+1$ letters. We set our target to find words up to six letters, i.e. we would have had to test more than 1 000 000 words!

Fortunately, due the symmetries of the polygon, is suffices to examine the words beginning with a, b, or c. If the first letter is not a, b, or c, but d, e, A, B, C, D, or E then just give the polygon a turn. Unfortunately, except for this very first letter, all 10 possibilities must be tested for each letter beyond, so 300 000 candidates were left.

We luckily found a really fine sorting tool in *An Algorithm For Simple Curves On Surfaces* published by [3, Joan S. Birman and Caroline Series]. This algorithm sorts the endpoints of a multiple leaved geodesic, so as to asset, whether the endpoints intertwine or not. One wonderful feature of this algorithm is that it is strictly combinatorial, it just combines letters with no need to compute the generating matrices. So there are no limitations coming from machine precision or speed.

The bad news are that this algorithm was made for surfaces with not empty boundary. The reason is that when working with a free group the conjugacy classes are unique, whereas they are generally not when the boundary is empty.

Our pretzel does have an empty boundary. Nevertheless the algorithm was still a bless to us as it tells something about whether the endpoints of the multiple geodesic intertwine. Passing the algorithm is a not sufficient but at least often a useful hint to take geodesics under scrutiny. A geodesic can pass the test but not be simple or the other way around (examples will be given hereunder). Anyway such accidents seldom arise with short words. So we had a sieve for sorting out candidates, an effective sieve as only 2 616 candidates were left.

It quite often happens that the leaves are disjoint but do not form a simple geodesic. These are only not intersecting geodesics, obtained from each other by permuting the path cyclically, but nothing more. Not all the leaves will run on the fundamental tile, there is no symmetry given by the hyperelliptic involution, they do not go trough any Weierstrass point. Before we sort again such and other bad candidates let us sketch the idea of the algorithm.

13.3.1. The idea of the Birman Series algorithm

Let us use again the example of the path {c,a,c,d}.

The first step is to shift along the cycle and its inverse. With a slight abuse of language we shall say 'words' for these paths.

$$
\begin{aligned}
w_1 &= \{c, a, c, D\} \\
w_2 &= \{a, c, D, c\} \\
w_3 &= \{c, D, c, a\} \\
w_4 &= \{D, c, a, c\} \\
W_1 &= \{d, C, A, C\} \\
W_2 &= \{C, A, C, d\} \\
W_3 &= \{A, C, d, C\} \\
W_4 &= \{C, A, C, d\}
\end{aligned}
$$

In a second step, order the words according to the alphabetical rule 'low case before high case': a,b,c,d,e,A,B,C,D,E but taken as a cyclical alphabet.

The first word is w_2 as it begins with a.

Then we have to choose between w_1 and w_3, both beginning with the letter c.

In the c-alphabet the second letter D precedes the letter c. so $w_3 \prec w_1$.

In the c-alphabet w_3 is followed by W_1, etc.

Finally we get the chain:

$$w_2 \prec w_3 \prec w_1 \prec W_1 \prec W_3 \prec W_2 \prec W_4 \prec w_4$$

In the third and last step multiply the words of the chain. It is immediate that the product simplifies here to the identity. This was the condition for {c,a,c,D} to pass the Birman Series test. It is a candidate for a simple closed geodesic.

It nearly never occurs with short words that a self intersecting geodesic passes the Birman Series test. Such a seldom counterexample is the word $\{b, C, b, E, c, E\}$:

$$\begin{aligned}
w_1 &= \{b, C, b, E, c, E\} \\
w_2 &= \{C, b, E, c, E, b\} \\
w_3 &= \{b, E, c, E, b, C\} \\
w_4 &= \{E, c, E, b, C, b\} \\
w_5 &= \{c, E, b, C, b, E\} \\
w_6 &= \{E, b, C, b, E, c\} \\
W_1 &= \{e, C, e, B, c, B\} \\
W_2 &= \{B, e, C, e, B, c\} \\
W_3 &= \{c, B, e, C, e, B\} \\
W_4 &= \{B, c, B, e, C, e\} \\
W_5 &= \{e, B, c, B, e, C\} \\
W_6 &= \{C, e, B, c, B, e\}
\end{aligned}$$

It follows:

$$w_1 \prec w_3 \prec W_3 \prec w_5 \prec W_5 \prec W_1 \prec W_4 \prec W_2 \prec w_2 \prec W_6 \prec w_6 \prec W_4$$

This multiplies to the identity but is no simple closed geodesic. This weird geodesic respects the symmetry of the hyperelliptic involution. Two leaves run through only the Weierstrass point on the c-edge (not two Weierstrass points as a simple closed non separating geodesic would meet) but it has 4 self intersections, two of them exactly in the Weierstrass point on the c-edge.

Inversely the path {b,E,b} does not pass the Birman Series test, although the geodesic is simple.

13.3.2. The inelegant job

After having sorted the candidates left by the Birman Series test it is necessary to sort out the few intersecting geodesics having passed the test. By default of a clever tool we used brachial force and programmed a procedure for computing the intersections of a set of geodesics. By we way we also sorted out the pseudo not intersecting geodesics with not all leaves on the pretzel. Doing that, we also checked whether the candidates meet or not Weierstrass points.

13.3.3. The final run

Our target was to investigate all words up to six letters. From more than 300 000 candidates at the start only 2 616 passed the Birman Series test. The rest was made of separating and off the tile leaves and some cases failing on machine precision.

# letters	1	2	3	4	5	6	Σ
simple not separating	3	24	38	194	118	949	1.326
separating	0	0	20	1	53	321	395
off the tile	0	3	17	111	94	523	748
bad cases	0	0	0	9	44	94	147
Σ	3	27	75	315	309	1.887	2.616

We were left with 1 326 'good' words of 1 to 6 letters and a rubbish of 147 bad cases stumbling on machine precision, or with leaves almost intersecting on the unit disc. In a couple of cases our algorithm for building up the tile failed (because the cuts are not above each other). Having 5 generators (and their inverses) this is a wide spectrum of the set of simple geodesics up to 6 letters. Longer words would only have more cuts with the edges of the fundamental polygon. Except for more densely packed loops, they would not look really different.

Gathering the results we wrote a program, Geo_Finder_deca , for examining and visualizing any path. It submits a path to the Birman Series algorithm, tests if all leaves are on the pretzel and if they run through a Weierstrass point. One can choose one of the selected simple geodesics and visualize them, or enter any path and see why it was not selected (so far machine precision was not the reason for not selecting).

13.4. Presentation of the Georama program

The program Big_Quake_Georama is made for grafting and pruning and twisting along simple closed geodesics.

We have tested the geodesics, thus grafting will work properly so far the angle is not so large that the leaves intersect. We got no problem with $\alpha = 3°$. Very often much larger angles will do, i.e. the lunes are distant enough so that they do not intersect.

Pruning quite often does not work due to intersecting lunes. Grafting takes nothing away, it pumps up a bubbly lune. When pruning, stuff is cut away, but there is little stuff around the axis of symmetry. So the angle has to be very tiny and the optical effect is as though nothing would happen. As we would not want to loose interesting graftings, we did not sort away the bad prunings.

When a positive angle α is entered the program grafts. It prunes when $\alpha < 0$. It of course returns the hyperbolic tessellation for $\alpha = 0$.

Once the angle has been selected, the program asks how many letters the word will have. When entering '0' the program makes itself a random choice.

Then a word has to be selected in the list of the appropriate number of letters. Entering '0' there is again a random choice.

The program returns always which choice is running, so that one knows what random chose. Fixing only the angle α you get a diaporama, until you find something you would like to examine more closely on the Geo_Finder_deca.

A last choice is how fine the fractal border should be.

Due to the symmetry of the tile we only had to tessellate the upper half of the disc and multiply by -1. We have calculated all shortened words up to 6 letters. Then we have calculated the distance from the origin to the image of the origin for all tiles. The rough tessellation selects the tiles where the image of the origin is within a radius $< 0,99$ (the radius of the unit circle being 1). The program needs 5 seconds to run this. The fractal border is very poor but one sees the geodesic. For the finest tessellation the distance to the origin is < 0.9995, the runtime is 20 seconds. The fractal border is visually well approximated. The two other choices are in between as indicated.

13.5. The idea behind the program

When grafting or pruning we leave hyperbolic geometry, we have to deal with arcs of circles instead of geodesics. Thus we loose the comfort of hyperbolic tools: among many other annoyances one needs 3 points to define an arc where only 2 define a geodesic.

The generators are deeply modified due to the insertion of suppression of lunes. Of course the revisited generators of the expanded or shrunk tessellation are related to the edges of the fundamental polygon of the hyperbolic tessellation. However it requires a lot of concentration to retrace what happens with a generator when it is altered by the Möbius transformation. The fundamental tile gets thicker when grafted along the leaves of the cut. The adjacent tiles have to move appropriately away but they also become inflated. The combination of all these moves is far from being unique.

It first seemed to us very difficult to tell the program how to handle with each individual tessellation. Fortunately brute force solves the problem. After computing some cases by hand we observed that only a small number of patterns occur. Only the order of the transformations is difficult to determine. So we just let the program go through all permutations until it finds a convenient one. This scheme always works and this very quickly.

What seemed to be difficult proved to be easy. Oppositely even a child would easily find the intersection of the fundamental tile with the leaves of the geodesic. The computer does not. It is quite a bore to find a way for cutting up the fundamental tile along all the types of leaves which may arise. This difficulty was overcome and we also succeeded in filling the fundamental tile with color, in order to visualize the deformation which is difficult to see when pruning.

Our program could deal with words of any length n. The first leaf 1 and the last leaf n require a specific treatment as only one side is affected. All leaves from 2 up to $n-1$ are equally treated on both sides. Practically this universality if of no use. There is so little room between the leaves of a geodesic that many words of six letters accept such a small angle that the grafting is visually uninteresting and the pruning all the more.

The program cuts the fundamental tile into polygons bordered by the leaves of the geodesic. The lunes are pushed between the domain when grafting, which works easily. When pruning the domains are crushed through each other, so that the overlappings are to be wiped out. This is a rather nasty extension of the grafting program.

13.6. Presentation of the Geodesic Finder

The program Geo_Finder_deca is dedicated to the examination of any geodesic. Part of it is the Birman Series test. Just enter any path of any length. If the return is 'True' this could be a simple geodesic. It is probably not a simple geodesic when 'False' is returned.

Then the program computes self intersections, if any, and shows the geodesic. In the last test the program returns whether the geodesic runs through a Weierstrass point (only computing the coordinates of was had already been visualized).

Here again a random choice is possible, but you can enter a path of your choice, the risk being that it is too long for machine precision or leads to nearby intersections on the unit circle. The first test is the Birman test. This test always works as it is purely combinatorial. Here again a random choice is possible, but you can enter a path of your choice.

13.7. The scarceness of simple geodesics

It is quite fascinating when drawing the leaves of a simple closed not separating geodesic in our decagon model that they run through exactly two Weierstrass points. If the number of leaves is augmented by more loops across some edge, the leaves will rearrange automatically giving room to the new leaf but there is still a leaf going through the same Weierstrass point. There is some sort of mysterious strength compelling the geodesic to run through exactly two Weierstrass points.

13.8. Many-leaved laminations

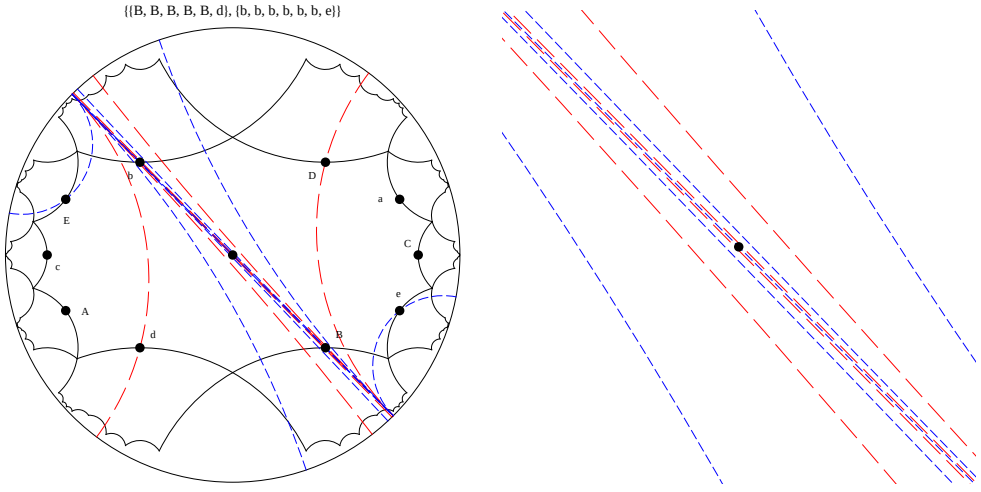

Figure 13.6.: Lamination through two geodesics

Our surgery operations were all performed along a unique geodesics. The program Duelling_geos offers a lamination made of a sequence of paired closed simple geodesics. The small figure 13.6 is just a hint at the use of the program.

Two geodesics are paired, adding the same letter in a sequence:

⋆ {B,d} paired with {b,b,e}
⋆ {B,B,d} paired with {b,b,b,e}
⋆ {B,B,B,d} paired with {b,b,b,b,e}
⋆ {B,B,B,B,d} paired with {b,b,b,b,b,e}
⋆ {B,B,B,B,B,d} paired with {b,b,b,b,b,b,e}

We have stopped the sequence, because the error in longer matrix multiplications creates problems. Obviously the sequence could be extended.

In figure 13.6 there is a zoom centered on the origin to better see that the geodesics do not intersect. This is only an example, there are many such sequences. The one deviating letter compels the geodesic to loop and loop without end. The other geodesic must use another Weierstrass point. Both geodesics run alternately through the origin. They of course must stay close to it, therefore the zoom into the very dense array.

The sequence of figure 13.7 shows how the leaves alternate through and close to their respective Weierstrass points. The number of leaves increases in single steps. The geodesic going through the origin in step i must leave the origin in step $i+1$, but the other geodesic that did not go through the origin in i does in $i+1$. It is a marvelous choreography, where an increasing number of leaves of a pair of geodesics dance denser and denser against each other through two Weierstrass points out of only three, exchanging places, but nether intersecting.

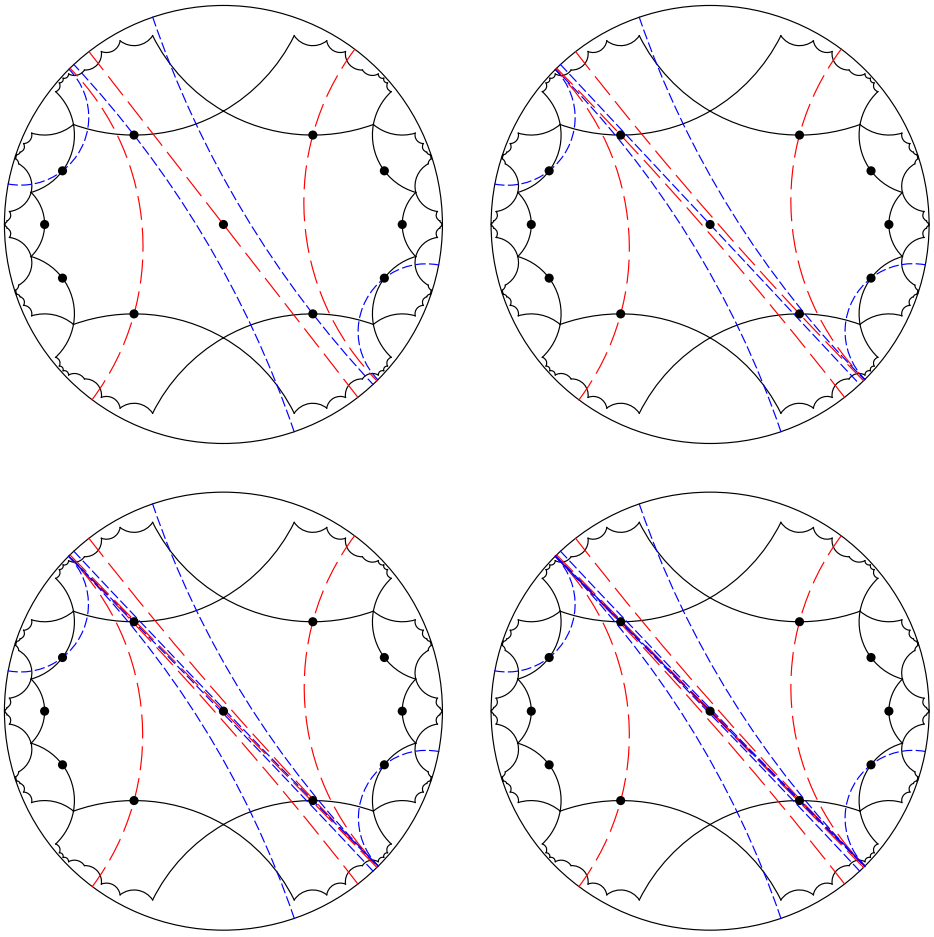

Figure 13.7.: Duelling Arrray

The array was obtained with the program Duelling_geos an extended version of the program Lam_2geos_deca.

Chapter 14.

A software for hyperbolic and Möbius geometry

Here we introduce the Mathematica® package *diskgeometry*, which provides a wide range of tools for who wants to visualize geometry in the Poincaré disc.

A geodesic in the Poincaré disc is an arc of an Euclidean circle. An arc is uniquely defined by three points. Using Mathematica® 4.0 the first problem we met was the instruction *Circle* defining an arc by the extreme opening angles with regard to the positive real axis. We have therefore written our own instruction defining the arc by three points given as complex numbers. This was the germ around which we constructed step after step the extensive program *diskgeometry* for hyperbolic and Möbius geometry. We rounded up the tools beyond what we actually needed for this paper. For a better oversight we wrote two further packages *geodesichunt* and *geodesichuntQuake* for those instructions, which we required but are not of general programming interest.

After some years of use and of add-ons *diskgeometry* covers not only the necessary tools but also many comfortable shortcuts. It is for instance oft convenient to define a geodesic by its endpoints on the unit circle, or it is nice to fill in a hyperbolic polygon with color, or you need the Möbius matrix mapping 3 points on 3 other ones, etc. The package, although primarily devoted to hyperbolic and Möbius geometry, also gives a basic kit for Euclidean geometry using complex numbers, e.g. find the intersection of two circles.

Practice showed that each of our programs makes largest use of *diskgeometry*. This is certainly a drawback for somebody who would like to trace back what we have programmed. On the other hand our programs became definitely shorter and thus much easier to overlook.

Appendix A lists up the instructions of *disgeometry* as an orientation about what the program can.

Appendix B gives the notebook *manual diskgeometry* with examples showing how the main instructions work.

Appendix C *Pinacotheca* gathers typical pictures and a short – what the program does in detail is reported in the program itself – summary of programs. We made our selection from the viewpoint of visualization or in relation with the contents of this paper. Three stars *** give a hint to those programs, which to our mind deserve special interest. As nobody will recall the program names, a search should start in *Pinacotheca*, the picture leads to the program name reported in the index, where the page of the topic in the main paper is indicated.

Appendix A.

diskgeometry

AngleC AngleC[p,q,r] returns in Degrees the angle of the geodesics through p,r and q,r.

Arc Arc[p,q,r] is extension of Threeptcirc[p,q,r]. It draws the arc of circle or the line segment with endpoints p=(_,_) and q=(_,_) and r(_,_) in between.

ArcC ArcC[p,q,r] is the same as Arc[p,q,r] but p, q, r are complex numbers instead of vectors.

ArcgeoC ArcgeoC[z,w,color] returns the graphic instruction for the geodesic through the points z and w in the Poincaré disk. Color uses the list of PolygonC, default value is no coloring.

atomizeArc atomizeArc[z,w,r,n] takes an arc (z,w,r) (r between z and w), geodesical or not, cuts it into 2^n points (default value is n = 3) and returns the list of these points, i.e. a discretisation of the arc.

Center3pts Center3pts[p,q,r] returns the center of the circle through the vectors p =(_,_), q=(_,_) and r(_,_).

Center3ptsC Center3ptsC[p,q,r] returns the center of the circle through the points p,q,r as complex number.

Choice Choice[x] is an internal instruction for choosing a color for a graphic instruction.

CleanList CleanList[x] eliminates most duplicates from a list of arcs.

Cut2Arcs Cut2Arcs[p1,p2,p3,q1,q2,q3] returns the intersection (empty, 1 point, 2 points) of the arcs (p1,p2,p3) and (q1,q2,q3).

Cut2circlesC Cut2circlesC[c1,R1,c2,R2] returns the crosspoints of the circles with center c1, c2, and radi R1, R2.

Cut2linesC Cut2linesC[z,w,u,v] returns the crosspoint of Euclidean straight lines through z,w and u,v.

Cut2geoC Cut2geoC[{a1,b1,m1},{a2,b2,m2}] returns the crosspoint of 2 geodesics (arc or line). Hereby ai and bi are the endpoints on the unit circle and mi is the middle. ai bi and mi are complex numbers. For internal use, common instruction is CutGeosC.

CutGeosC CutGeosC[z,w,u,v]returns the crosspoint of 2 geodesics trough z,w and u,v.

CutLineCircC CutLineCircC[z_,w_,c_,R_] returns the intersection inside the unit disk of the straight line through z and w with the circle of center p and radius R. When the straight line is no geodesic both intersections are given eventuelly.

CutSegmArc CutSegmArc[p1,p2,q1,q2,q3] returns the intersection (empty, 1 point, 2 points) of the segment (p1,p2) and the arc (q1,q2,q3).

DiperpC DiperpC[a1,b1,a2,b2] graphic instruction for the common perpendicular to the arcs through a1, b1 and a2, b2 in the disk.

drawHexagon drawHexagon[b1,b2,b3] draws the Hexagon[b1,b2,b3].

drawPentagon drawPentagon[a,b] draws Pentagon[a,b].

EdgetoArcC EdgetoArcC[{z1,z2,z3}] returns the graphic instruction for tracing the arc through 3 points. This avoids to apply ArcC to the 3 pts separately.

EdgetocR EdgetocR[{p1,p2,p3}] returns the midpoint and the radius of the arc (p1,p2,p3).

EndpointsC EndpointsC[a,b] returns both endpoints of the geodesic through a and b in the disk.

EuclMidPt EuclMidPt[r,s,p1,p2,p3] returns the Euclidean midpoint of any points r and s of the support of the arc (p1,p2,p3).

filledPoly filledPoly[poly,discr] returns the Polygon instruction for polygons bounded by arcs. It discretises a list of arcs at level discr-power of 2 (default value discr = 3).

FixptsC FixptsC[matrix] returns both fixpoints of a matrix of SL(2,C). Error message when Det is more than 10^-9 away from 1.

GeodesicC GeodesicC[z,w] returns center and radius of the geodesic through the points a and b in the Poincaré disk or the endpoints of the line when a and b are on a radial geodesic.

GraphPerpC GraphPerpC[z,w,p] returns the graphic instruction for the perpendicular through the points z and w in the Poincaré disk from p on or outside the geodesic.

GraphPolyC GraphPolyC[x,color] returns the graphic instruction for a closed polygon given by the list x of its vertices. color = 0,1,...9 is optional, default value is black.

HalfRegPoly HalfRegPoly[n,phi,psi] returns the halfregular polygon with n edges and alternating angles phi and psi.

hCenterC hCenterC[c,R] returns the hyperbolic center of the circle of Euclidean center c and Euclidean radius R.

hCircleC hCircleC[c,Rh] returns the graphic instruction for the circle of hyperbolic center c and hyperbolic radius Rh.

hDistC hDistC[z,w] returns the hyperbolic distance between the points z and w in the Poincaré disk.

InfTess InfTess[n,m] returns the edges of the tessellation with the ideal polyon of n edges turning m times around its vertices.

LineC LineC[z,w,color] returns the graphic instruction for the Euclidian line joining z and w in R^2. color = 0,1,...9 is optional, default value is black.

HoroRotateC HoroRotateC[poly,p,phi] returns the rotation with angle phi along horocycles touching the unit circle in p.

MakePolyC Makes out of the list x of points (vertices) with x1 = xn the list of edges, i.e. arcs defined by startpoint, end point and the midpoint.

MatonEdgeC MatonEdgeC[M,list] moves the points of the list with the matrix M of SL(2,$\mathbb{C}$).

MatonPtC MatonPtC[M,z] moves the point z with the matrix M of SL(2,$\mathbb{C}$).

Moeb3ptsC Moeb3ptsC[z1,z2,z3,w1,w2,w3] returns the Moebius matrix of SL(2,$\mathbb{C}$) moving 3 points z1,z2,z3 to the 3 points w1,w2,w3.

Midpoint Midpoint[v,w] is the same as midpointC, when v and w are given as vectors.

MidpointC MidpointC[p,q] returns midpoint of geodesic segment through points p and q in the disk.

MilieuC MilieuC[p,q] returns the fictive midpoint of the geodesic when p and q are endpoints,so as to obtain the 3rd point for ArcC.

MirrorC MirrorC[z,p,q] inverses in the geodesic supporting segment [p,q].

MorePts MorePts[y] inserts the Euclidean midpoints between the points listed in y.

MTess MTess[n,m] returns the edges of the tessellation with the polyon of n edges turning m times around the vertices. This medium tessellation covers the first crown of tiles around the central tile.

OtherEndpointC Being given an endpoint and another point of a geodesic OtherEndpointC[endpt,noendpt] returns the pair of endpoints.

PerpC PerpC[z,w,p] returns the endpoints of the geodesic through p orthogonal to the geodesic through z and w. p is any point on or outside the geodesic.

PointC PointC[z,color,g] returns the graphic instruction for a point in R^2 . color = 0,1,...9 is optional, default value is black. PointSize g is optional too, default value g = .02.

PolygonC PolygonC[x,color,lev] is the graphic instruction for a filled hyperbolic polygon discretised at level lev. color = 0,1,...9 is optional, default value is black. lev is optional too, default value is lev = 3.

PtonArc PtonArc[q,p1,p2,p3] returns True when the point q lies on the arc joining p1 and p2 through p3.

PtonSegm PtonSegm[q,p1,p2] returns True when the point q lies on the segment joining p1 and p2.

PtstocR PtstocR[p1,p2,p3] returns the midpoint and the radius of the arc (p1,p2,p3).

Radius3pts Radius3pts[p,q,r] returns the radius of the circle through the vectors p =(_,_), q=(_,_) and r(_,_).

Radius3ptsC Radius3ptsC[p,q,r] returns the radius of the circle through the points p,q,r.

RegPoly RegPoly[n,phi] returns the regular polygon with n edges and angle phi.

RightangledHexagon RightangledHexagon[b1,b2,b3] gives the vertices of the hexagon with edges-lengths b1,b2,b3. Always defined.

RightangledPentagon RightangledPentagon[a,b] returns the vertices of the pentagon with edge of Euclidean length a on imaginary axis, b on real axis. Not defined for all pairs a,b.

RotateC RotateC[poly,alpha,n:1,centr:0] returns the rotation of the list of points (poly) with the angle alpha, n-times (default value 1), around the point centr (default value the origin).

RotateMTess RotateMTess[n,m,phi,p] returns the edges of the medium tessellation MTess[n,m] rotated with the angle phi around the point p.

RotateSTess RotateSTess $[n, m, phi, p]$ returns the edges of the small tessellation STess[n,m] rotated with the angle phi around the point p.

RotateXLTess RotateXLTess[n,m,phi,p] returns the edges of the large tessellation XLTess[n,m] rotated with the angle phi around the point p.

scalC scalC[p1,p2] returns the dot product of the vectors coresponding to the points p1 and p2. If positive the angle α is $\alpha < \pi/2$ or $\alpha > 3\pi/2$, if negative $\pi/2 < \alpha < 3\pi/2$.

ShowInfPolyC ShowInfPolyC[x,n] visualises the list x of ideal polygons with n vertices on the unit disc.

ShowInfTess ShowInfTess[n,m] displays the tessellation using the ideal regular polygon with n edges and m turns around its vertices.

ShowMe ShowMe[graphics] displays a list of graphic instructions in the unit disk.

ShowPolyC ShowPolyC[x] visualises the polygon given by its list x of vertices.

ShowRotateMTess ShowRotateMTess[n,m,phi,p] visualises the medium tessellation MTess[n,m] rotated with the angle phi around the point p.

ShowRotateSTess ShowRotateSTess[n,m,phi,p] visualises the small tiling STess[n,m] rotated about the angle phi around the point p.

ShowRotateXLTess ShowRotateXLTess$[n, m, phi, p]$ visualises the large tessellation XLTess$[n, m]$ rotated with the angle phi around the point p.

ShowMTess Graphic instruction visualising the medium tessellation MTess[n,m] with the central tile and the first crown of tiles around it.

ShowSTess Graphic instruction visualising the small tessellation STess[n,m] with the central tile and its adjoining tiles.

ShowXLTess Graphic instruction visualising the large tessellation XLTess[n,m] with two crowns of tiles.

ShowTranslateMTess Visualises the medium tessellation MTess[n,m] translated along the vector (p,q).

ShowTranslateSTess Visualises the small tessellation STess[n,m] translated along the vector (p,q).

ShowTranslateXLTess Visualises the large tessellation XLTess[n,m] translated along the vector (p,q).

STess STess[n,m] returns the edges of the tessellation with the polyon of n edges turning m times around the vertices. This small tessellation limits to the central tile and its adjoining tiles.

Threeptcirc Threeptcirc[p,q,r] draws the circle through the points p =(_,_), q=(_,_) and r(_,_).

ThreeptcircC ThreeptcircC[p,q,r] is the same as Threeptcirc[p,q,r] but p, q, r are complex numbers instead of vectors.

ThreePtgeoC Obsolete instruction. ThreePtgeoC[c,R] returns endpoints and midpoint of geodesic with center c and radius R in the disk.

TranslateLeftC TranslateLeftC[poly,p1,p2] translates the list of vertices poly with the vector (p1,p2) to the left when p1 < p2 lie on the real axis. The effect is equivalent to -TranslateRightC.

TranslateRightC TranslateRightC[poly,p1,p2] translates the list of vertices poly with the vector (p1,p2) to the right when p1 < p2 lie on the real axis. The effect is equivalent to -TranslateLeftC.

TranslateMTess TranslateMTess[n,m,p,q] returns the translated edges of the medium tessellation MTess[n,m] along the vector (p,q).

TranslateSTess TranslateSTess[n,m,p,q] returns the translated edges of the small tessellation STess[n,m] along the vector (p,q).

TranslateXLTess TranslateXLTess[n,m,p,q] returns the translated edges of the large tessellation XLTess[n,m] along the vector (p,q).

TriangleC TriangleC[alpha,beta,gamma] returns the 3 vertices of the triangle defined by its 3 angles.

TriIsoInf TriIsoInf[phi] returns the 3 vertices of the 2/3 ideal triangle defined by its angle phi != 0.

TriOneInf TriOneInf[phi,psi] returns the 3 vertices of the 1/3 ideal triangle defined by its angles phi,psi != 0.

TriRect TriRect[phi] returns the 3 vertices of the 1/3 ideal rightangled triangle defined by its angle phi != 0 and Pi/2.

VertextoArc VertextoArc[vlist] returns the graphic instruction for the arcs joining the points of vlist.

XLTess XLTess[n,m] returns the edges of the tessellation with the polyon of n edges turning m times around the vertices. This large tessellation covers two crowns of tiles around the central tile.

WedgeC WedgeC[p1,p2,p3] returns the angle α between the extremities p1 and p2 of the arc (p1,p2,p3).

Appendix B.

Manual diskgeometry

In the next instruction Own is to be corrected according to the path leading to the package diskgeometry.

<< Own`diskgeometry`
Off[General::"spell1"]

The Package diskgeometry` uses the disk model of Poincaré for the hyperbolic plane. Particular consideration has been given to the of endpoints of geodesics. Error messages provide a motivated warning when inputs are against hyperbolic rules, e.g. when the sum of angles of a triangle would be $\geq \pi$.
The instructions all contain at least one letter in high case, so that no conflicts may arise when using low cases for programming. Instructions are wrapped in a module in order to make all variables local. Postponing the letter C suggests that the instruction works on complex numbers and avoids conflicts with names the user might like to choose. A few obsolete instructions were kept in this package so as not to rewrite existing programs.

A few instructions apply to vectors in R^2: Arc, Centrer3pts, Midpoint, Radius3pts, Threeptcircle. They have no ending in C and use vectors instead of complex numbers. They are almost superfluous but can sometimes be of help, as the graphic instructions of Mathematica® always use vectors. The word *point* always means the attached complex number in C.

ThreeptcircC[p,q,r] returns the graphic instruction for the circle through the vectors p,q,r. **Center3ptsC[p,q,r]** returns the center of this circle and **Radius3ptsC[p,q,r]** its radius. Of course one can extract these data from the graphic instruction as well.

ArcgeoC[z,w,color] returns the graphic instruction for the unique geodesic through the points z and w with a coloring option. **GeodesicC[z,w]** is only a shortcut returning center and radius instead of having to extract them from ArcgeoC.

PointC[*z*, color, *g*] returns the graphic instruction with coloring option for the point in R^2. The point size *g* is optional too, default value $g = .02$.

LineC[z,w,color] returns accordingly the instruction for the Euclidean line joining z and w.

ArcC[z,w,r] returns the graphic instruction for the arc of circle joining z to w over any r in between. Note that r is in the 3rd position. Which of z or w is in the first or the second position is irrelevant. ArcC does not define an hyperbolic line as such, just an arc of circle through 3 points. **EdgetoArcC[{z,w,r}]** is basically the same asArcC[z,w,r] but it accepts a bracket whithout having to extract the elements from their list.

ShowMe[obj] is just a shortcut displaying inside the Poincaré disk the hyperbolic objects given by a list obj = {g1,g2,...} of graphic instructions.

MidpointC[p,q] returns the midpoint of the hyperbolic arc joining the points p and q. It will be be used it frequently as 3rd point r in ArcC[p,q,r]. When drawing a geodesic defined over one or both endpoints on the unit circle, there is no midpoint! So we use **MilieuC[p,q]** instead, which returns the Euclidean midpoint of a geodesic arc. Both instructions could have been merged, but this might have been confusing.

MorePts[list] inserts the Euclidean midpoints between the points on a geodesic listed in list. Using the instruction Nest splits up the geodesic for discretising.

As an example we use now **ArcC** to draw an arc of circle through 3 points, which is neither a geodesic nor an hyperbolic arc of circle but only the equidistant curve for the geodesic with endpoints z and w. **ArcC** could be used as well for any 3 points in R00*b*2. With **MorePts** we fix the feet of perpendiculars to the geodesic. The geodesical segments within the lune have the same hyperbolic length.

```
z = e^(i3Pi/2); w = e^(iPi/5); r = .7e^(iPi/2);
finer = Nest[MorePts, {z, w}, 5]//N;
comb = Map[GraphPerpC[z, w, #]&, finer];
obj = {ArcgeoC[z, w],
ArcC[z, w, r],
comb,
PointC[z, 0, .03], PointC[w, 0, .03],
PointC[r, 0, .03]};
ShowMe[obj]
```

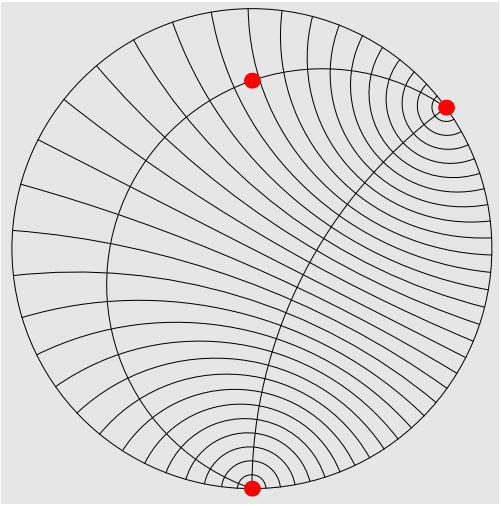

An immediate application of MidpointC is **hCenterC[c,R]**, which returns the hyperbolic center of a circle. A warning is issued when the circle cuts or touches the unit circle. Similarly **hCircleC[c,Rh]** returns the graphic instruction for the circle of hyperbolic center c and hyperbolic radius Rh. It is immediate to recover the Euclidean center and radius from the graphic instruction. Here are circles concentric to a given circle.

```
a = .4; psi = Pi/3; c = ae^(ipsi); R = 1 - a - .1;
hypcent = hCenterC[c, R];
k = Table[{Hue[i/10], hCircleC[hypcent, iR]},
{i, 15}];
ShowMe[{k, PointC[hypcent]}]
```

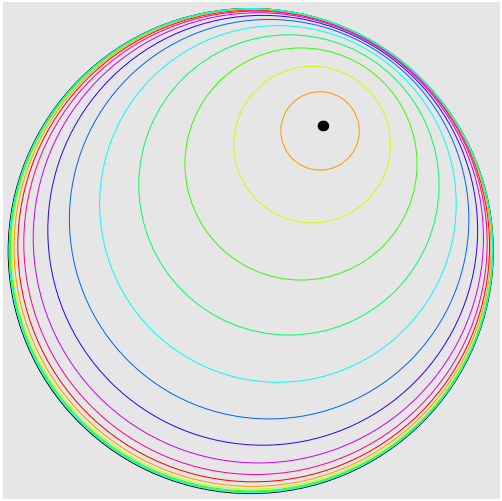

To show some structure of the inner life of a circle we picture a polygon inscribed in a disk. The look is not far from the Euclidean.

```
greentri = TriangleC[Pi/6, −Pi/6, Pi/6];
rotgreentri =
Table[RotateC[greentri, Pi/6, i], {i, 12}]//Chop;
graphrotgreentri =
Table[PolygonC[rotgreentri[[i]], 2], {i, 1, 12, 2}];
redtri = TriangleC[Pi/6, Pi/6, Pi/6];
rotredtri =
Table[RotateC[redtri, Pi/6, i], {i, 12}]//Chop;
graphrotredtri = Table[PolygonC[rotredtri[[i]], 0],
{i, 1, 12, 2}];
rond = hCircleC[0, hDistC[0, rotgreentri[[1, 3]]]];
ShowMe[{Disk@@rond, graphrotgreentri, graphrotredtri,
PointC[0]}]
```

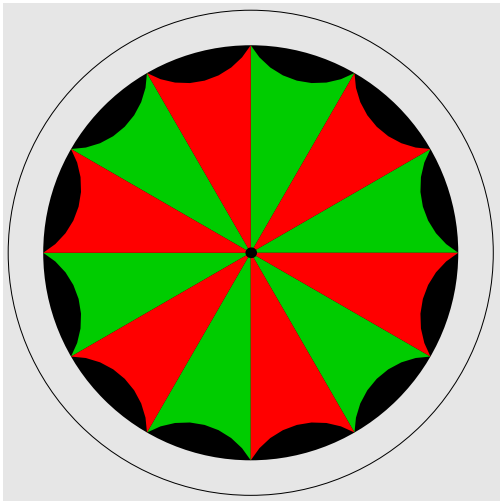

To show how the hyperbolic metric moves the midpoint and distorts the radii, we now translate by the vector (0,d) along the real axis. The programm is the same but for the added translation.

```
d = .5;
greentri = TriangleC[Pi/6, −Pi/6, Pi/6];
```

```
rotgreentri =
Table[TranslateRightC[RotateC[greentri, Pi/6, i],
0, d], {i, 12}]//Chop;
graphrotgreentri =
Table[PolygonC[rotgreentri[[i]], 2], {i, 1, 12, 2}];
redtri = TriangleC[Pi/6, Pi/6, Pi/6];
rotredtri =
Table[TranslateRightC[RotateC[redtri, Pi/6, i],
0, d], {i, 12}]//Chop;
graphrotredtri = Table[PolygonC[rotredtri[[i]], 0],
{i, 1, 12, 2}];
rond = hCircleC[rotgreentri[[1, 4]],
hDistC[rotgreentri[[1, 3]], rotgreentri[[1, 4]]]];
ShowMe[{Disk@@rond, graphrotgreentri, graphrotredtri,
PointC[d]}]
```

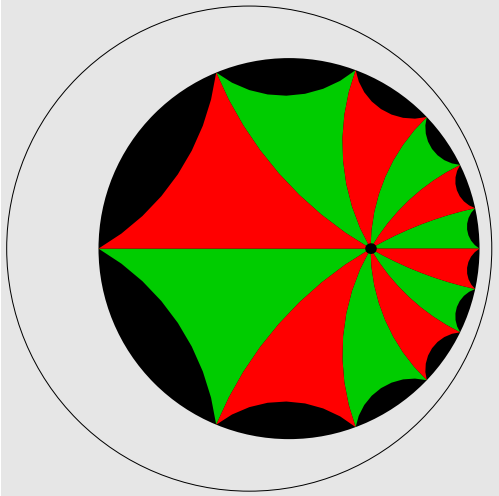

GeodesicC[a,b] returns center and radius of the geodesic through the points a and b in the Poincaré disk or the endpoints of the line when a and b are on a radial geodesic.
EndpointsC[a, b] returns both endpoints of the geodesic through a and b in the disk.
OtherEndpointC returns the second endpoint of a geodesic when entering an endpoint and any other point.
MakePolyC[poly] returns the edges of a closed polygon. **GraphPolyC[poly,color]** is the corresponding graphic instruction. GraphPolyC can use the color option like PointC, LineC, ArcgeoC and PolygonC.

MirrorC[z,p,q] inverses a point or a list of points i.e. mirrors against a geodesic.

```
p = .5e^(i5Pi/4); q = .8e^(iPi/2);
penta = RightangledPentagon[.5, .6];
imagepenta = MirrorC[penta, p, q];
obj = {
GraphPolyC[penta, 0],
GraphPolyC[imagepenta, 0],
ArcgeoC[p, q, 2],
PointC[p, 2],
PointC[q, 2]};
ShowMe[obj];
```

PerpC[z,w,p] returns the pair of endpoints of the perpendicular through p orthogonal to the geodesic through z and w. p is any point on or outside the geodesic.

GraphPerpC[z,w,p] is the graphic instruction. Choosing p as the midpoint of (z,w) returns the **mediatrix** (for which therefore no specific instruction is needed).

```
z = -.7e^(iPi/2); w = .3e^(iPi/5); q = .5e^(iPi/3);
p = MidpointC[z, w];
obj = {
GraphPerpC[z, w, p],
ArcgeoC[z, w, 0],
GraphPerpC[z, w, q],
PointC[z, 0],
PointC[w, 0],
PointC[p],
PointC[q],
Text["z", {.05, -.7}],
Text["w", {.3, .15}],
Text["p", {.12, -.37}],
Text["q", {.3, .48}]
};
ShowMe[obj]
```

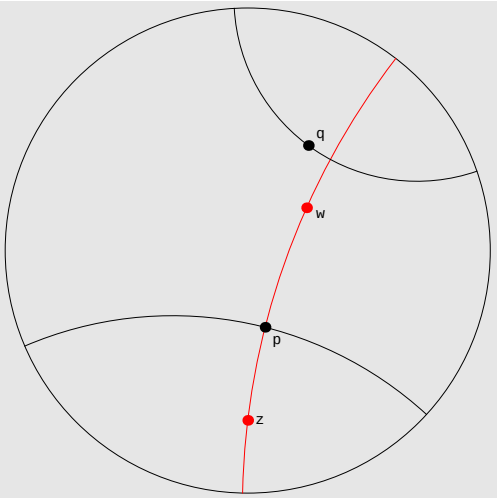

DiperpC[p,q,r,s] is the graphic instruction for drawing the common perpendicular to the geodesics through p,q and r,s. There is a warning when the geodesics are not ultraparallel. It is immediate to find the endpoints of the perpendicular by computing with Cut2circlesC or CutLineCircC the intersection of the support of the geodesic with the unit circle .

```
p = .4e^(i3Pi/4); q = .6e^(iPi); r = .75e^(iPi/4); s = .3e^(-iPi/5);
obj = {
DiperpC[p, q, r, s],
ArcgeoC[p, q, 0],
ArcgeoC[r, s, 0],
PointC[p, 0],
PointC[q, 0],
PointC[r, 0],
PointC[s, 0]};
ShowMe[obj];
With[{x = DiperpC[p, q, r, s]},
Cut2circlesC[x[[1, 1]] + Ix[[1, 2]], x[[2]], 0, 1]];
Print["endpoints of perpendicular = ", %]
```

endpoints of perpendicular = $\{-0.693304 + 0.720645i, 0.999361 - 0.0357397i\}$

TriangleC[alpha,beta,gamma] returns the vertices of the triangle with angles alpha, beta, gamma. In the case of an ideal or semi ideal triangle 1, 2, or 3 of these angles are = 0. The instruction still works but there is also a direct access over **TriIsoInf[phi]** for a 2/3 ideal triangle, **TriOneInf[phi,psi]** for a 1/3 ideal triangle and **TriRect[phi]** for a 1/3 ideal rightangled triangle.
Using the TriangleC instruction we display the ten optional colors for ArcgeoC, GraphPolyC, LineC, PointC and PolygonC.

```
rho = Pi/3; phi = Pi/5; psi = Pi/6;
obj = {
PolygonC[TriangleC[0, phi, Pi/2], 0],
PolygonC[RotateC[TriangleC[0, phi, psi], phi],
1],
PolygonC[RotateC[TriangleC[0, phi, 0], 2phi], 2],
PolygonC[RotateC[TriangleC[rho, phi, psi], 3phi],
3],
PolygonC[RotateC[TriangleC[0, phi, Pi/2], 4phi],
4],
PolygonC[RotateC[TriangleC[0, phi, psi], 5phi],
5],
PolygonC[RotateC[TriangleC[0, phi, 0], 6phi], 6],
PolygonC[RotateC[TriangleC[0, phi, Pi/2], 7phi],
7],
PolygonC[RotateC[TriangleC[0, phi, psi], 8phi],
8],
PolygonC[RotateC[TriangleC[0, phi, 0], 9phi], 9],
Text["color 0", {.35, .1}],
Text["color 1", {.35, .4}],
Text["color 2", {0, .6}],
Text["color 3", {-.3, .4}],
Text["color 4", {-.4, .1}],
Text["color 5", {-.45, -.1}],
Text["color 6", {-.36, -.4}],
Text["color 7", {0, -.45}],
Text["color 8", {.35, -.4}],
Text["color 9", {.4, -.1}]
};
ShowMe[obj]
```

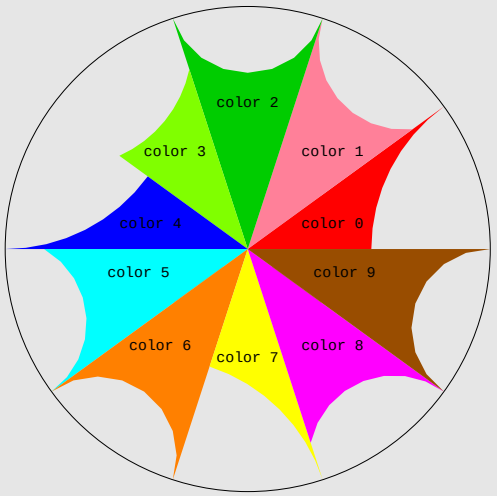

RightangledPentagon[a,b] returns the vertices of the rightangled pentagon with edges of length a on the imaginary axis and b on the real axis. There is a warning, when a and b are not compatible (because the geodesics orthogonal to the axes intersect). **drawPentagon[a,b]** shows the pentagon.

RightangledPentagon[.6, .5];
Print["vertices = ", %];
drawPentagon[.6, .5]

vertices $= \{0, 0.5, 0.555584 + 0.283348i, 0.20051 + 0.639127i, 0.6i, 0\}$

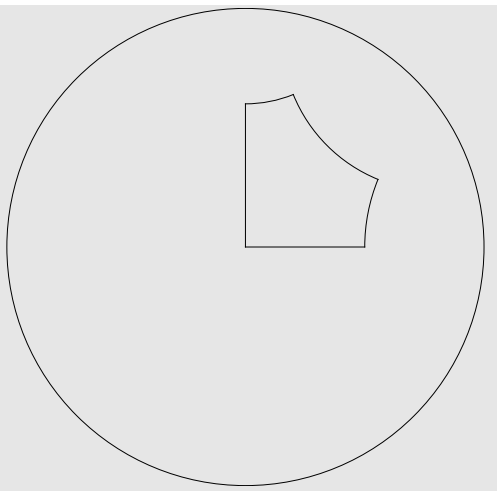

RightangledHexagon [b1,b2,b3] returns the vertices of the rightangled hexagon with every second edge of prescribed hyperbolic length b1,b2,b3. All not exreme values are accepted. **drawHexagon [b1,b2,b3]** shows the hexagon.

RightangledHexagon[1.2, .8, 1.];
Print["vertices = ", %];
drawHexagon[1.2, .8, 1.]

vertices $= \{0, 0.537, 0.702 + 0.437i, 0.639 + 0.545i, 0.255 + 0.706i, 0.631i, 0\}$

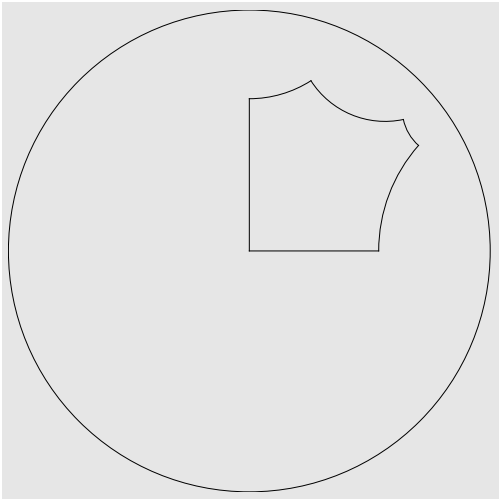

RightangledHexagon uses exceptionnaly an hyperbolic measure. The programm knows of course only points in R^2. **hDistC[z,w]** computes the hyperbolic distance between the Euclidean points z and w anywhere in the disk. It is easy to reverse the instruction, but it usually does not make much sense, as one would have to assign the position of one point and the direction to the other.

TranslateRightC[poly,p1,p2] translates the list of vertices poly with the vector (p1,p2) to the right when p1 < p2 lie on the real axis. **TranslateLefC[poly,p1,p2]** translates in the opposite direction. So -TranslateLeftC can be used instead of TranslateRightC. Here an edge of the hexagon is translated along itself to the right in red and to the left in blue.

```
hexa = RightangledHexagon[1., 1.2, .8];
p1 = hexa[[2]]; p2 = hexa[[3]];
obj = {
GraphPolyC[hexa, 4],
GraphPolyC[TranslateRightC[hexa, p1, p2], 0],
GraphPolyC[TranslateLeftC[hexa, p1, p2], 2],
{RGBColor[0, 1, 1],
ArcC[p1, p2, MidpointC[p1, p2]],
PointC[p1], PointC[p2]}
};
ShowMe[obj];
```

RotateC[poly,alpha,n:1,centr:0] returns the rotation of the list of points (poly) with the angle alpha, n-times (default value 1), around the point centr (default value the origin). Here the hexagon is rotated 2 times with Pi/3 around a vertex. Of course this is rotating by 2Pi/3, but "n" is fine for loops when using instructions like Do, Table, etc.

```
rotcent = .3e^(i5Pi/3);
hexa = RightangledHexagon[.8, .5, .9];
rothexa = RotateC[hexa, Pi/3, 1, rotcent];
circles = Prepend[
Table[hCircleC[rotcent, hDistC[hexa[[i]], rotcent]],
{i, 6}], Dashing[{0.01}]]//Chop;
obj = {
GraphPolyC[hexa, 0],
GraphPolyC[rothexa, 2],
```

```
circles,
PointC[rotcent]};
ShowMe[obj];
```

HoroRotateC[poly,p,phi] returns the rotation with angle phi along horocycles touching the unit disk in p. This hyperbolic move without Euclidean equivalent is the link between translation and rotation.

```
p = e^(i Pi/4); phi = Pi/3;
tri = TriangleC[Pi/5, Pi/7, Pi/2];
horotri = HoroRotateC[tri, p, phi];
circles =
Prepend[Table[ThreeptcircC[p, tri[[i]], horotri[[i]]],
{i, 3}], Dashing[{0.02}]];
obj = {
PolygonC[tri, 0],
PolygonC[horotri, 2],
circles,
PointC[p, 10, .03]};
ShowMe[obj]
```

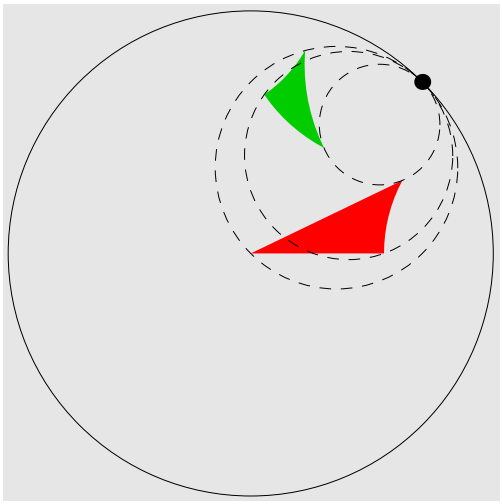

STess[n,m] returns the edges of the tessellation with the polyon of n edges turning m times around the vertices. This small tessellation limits to the central tile and its immediate neighbours. **MTess[n,m]** extends to the first crown of tiles around the central tile. **XLTess[n,m]** extends further to two crowns of tiles. All three tessellations are displayed by **ShowSTess**, **ShowMTess**, **ShowXLTess**. **TranslateSTess** and **RotateSTess** allow to translate or rotate for getting another viewpoint. **ShowTranslateSTess** and **ShowRotateSTess** display the moves. Corresponding instructions do the same for the medium and the large tessellations.

CleanList[x] eliminates most duplicates from a list. Here is a tessellation of 5 pentagons arranged 5 times around the vertices. The tessellation is translated along the vector (p,q) and rotated by the angle phi around the point p. The gain of time when cleaning the list is usually not significant. The intention behind this example is to show **how to move a tessellation around the disk**.

```
rough = XLTess[5, 5];
Print["length of original list = ", Length[rough]];
clean = CleanList[rough];
```

```
Print["length of cleaned list = ", Length[clean]];
p = -.1e^(iPi/3); q = .2e^(iPi/8); r = .5e^(iPi/4); phi = Pi/3;
d1 = TranslateRightC[Flatten[clean], p, q];
d2 = RotateC[d1, phi, 1, r];
d2 = Partition[d2, 3];
movedtess = EdgetoArcC/@d2;
ShowMe[movedtess]
```

length of original list = 1875

length of cleaned list = 1874

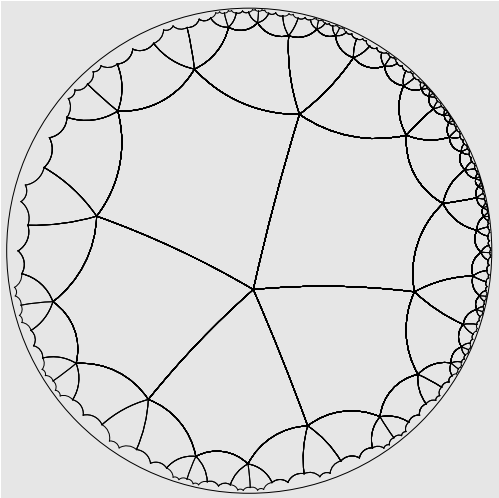

VertextoArc [vlist] returns the graphic instruction for the arcs joining the points of vlist.

Moeb3ptsC[z1,z2,z3,w1,w2,w3] returns the matrix of SL(2,C) mapping any 3 points of R^2onto any 3 other points of R^2. So far the points define two geodesic lines this Moebius mapping will be an hyperbolic move.
FixptsC[matrix] returns the fixpoints of a matrix.
MatonPtC[mat,z] returns the image of the point z when applying the matrix mat of SL(2,C). **MatonEdgeC[mat,edge]** does the same with edges i.e. a list of 3 points, so defining specially an hyperbolic move.
As an example a copy of a triangle is made, so that the second edge is reversed and glued on itself. Identifying the second edge after reversing returns the matrix form of an hyperbolic move. Applying this matrix to the triangled returns the copy. FixptsC confirms that the midpoint of the edge is the fixpoint of the matrix.

```
tri = TriangleC[Pi/5, Pi/7, Pi/2];
mid = MidpointC[tri[[2]], tri[[3]]]
mat = Moeb3ptsC[
tri[[2]], mid, tri[[3]],
tri[[3]], mid, tri[[2]]];
MatrixForm[mat]
copy = MatonEdgeC[mat, tri]//Chop;
fp = FixptsC[mat][[1]]
obj = {
PolygonC[tri, 0],
PolygonC[copy, 2],
PointC[fp]};
ShowMe[obj]
```

$0.571609 + 0.16659i$

$$\begin{pmatrix} -2.09832 - 1.3322676295501878^{*\wedge}\text{-}15i & 1.77103 + 0.516149i \\ -1.77103 + 0.516149i & 2.09832 + 1.3322676295501878^{*\wedge}\text{-}15i \end{pmatrix}$$

$1.24373 - 0.202172i$

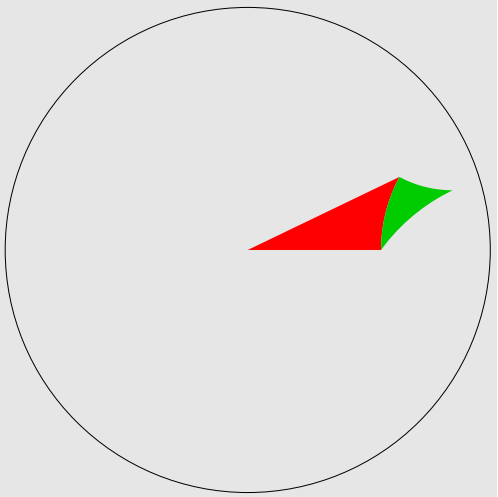

LineC[z,w,color] does the tedious job of converting into the instruction for the Euclidean line (z,w) in R^2, **PointC[z,color,g]**. In the same spirit PointC[z,g] returns the graqphic insruction for a point with PointSize[g], defaultvalue g=0.02. Like ArcGeoC, GraphpolyC and PolygonC the color option offers 10 colors.

LineC $\left[5.5e^{i\text{Pi}/3}, 1.8e^{i\text{Pi}/8}\right]$
PointC $\left[.5e^{i\text{Pi}/5}\right]$
PointC $\left[.5e^{i\text{Pi}/5}, .03\right]$

Line[{{2.75, 4.76314}, {1.66298, 0.68883}}]

{PointSize[0.02], Point[{0.404508, 0.293893}]}

{PointSize[0.02], Point[{0.404508, 0.293893}]}

CutLineCircC[z,w,c,R] computes in R^2 the intersection of the line supporting z and w with the circle with center c and radius R. Both points are returned, {Null,Null} if the line does not cut the circle, the tangency point if the line touches.
Cut2circlesC[c1,R1,c2,R2] and **Cut2linesC[z,w,u,v]** are analogous instructions for Euclidean constructions in R^2.

```
z = .5e^(iPi/3); w = .3e^(iPi/4);
c = .2 + .3I; R = .1;
s = CutLineCircC[z, w, c, R];
Print["Intersection = ", s];
Show[Graphics[{
LineC[z, w],
Circle[{Re[c], Im[c]}, R],
PointC[s[[1]], 0, .03], PointC[s[[2]], 0, .03],
PointC[z], PointC[w]
000900090009}, AspectRatio → Automatic]]
```

Intersection = $\{0.242699 + 0.390426i, 0.21014 + 0.200515i\}$

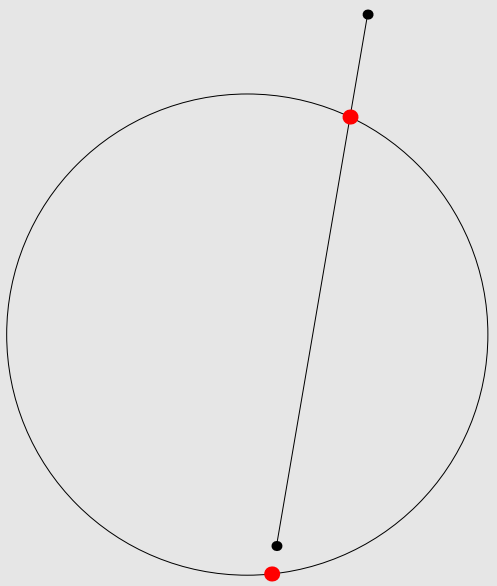

Cut2circlesC[z,w,c,R] computes in R^2 the intersection of the circles with center c1, resp. c2 and radius R1 resp. R2. Both points are returned, {Null,Null} if the circles do not cut, the tangency point if the circles touch each other.

Cut2geoC has been replaced in this issue by the more confortable CutGeosC. Geocenter C, GeoradiusC and ThreePtGeoC are also obsolete.

Here is an exercice using the instructions CutGeosC, AngleC, PointC,ArcgeoC, GraphPolyC, RegPoly and ShowMe. We turn the Mercedes star and turn it with Pi/3, so as to get an hexagon as intersection. We compute the angle phi of the hexagon in the point p and draw the regular hexagon in red for confirmation.

```
p = CutGeosC [-(-1)^(5/6), i, -i, (-1)^(1/6)] ;
phi = AngleC[-i, i, p];
obj = {
PointC [-(-1)^(5/6)] , PointC[i], PointC [-(-1)^(1/6)] ,
ArcgeoC [-(-1)^(5/6), i] ,
ArcgeoC [-(-1)^(1/6), i] ,
ArcgeoC [-(-1)^(1/6), -(-1)^(5/6)] ,
ArcgeoC [(-1)^(1/6), (-1)^(5/6)] ,
ArcgeoC [-i, (-1)^(5/6)] ,
ArcgeoC [-i, (-1)^(1/6)] ,
{RGBColor[1, 0, 0], AbsoluteThickness[3],
GraphPolyC[RegPoly[6, phi/180Pi]]},
PointC[p, 0, .03],
Text[{phi"°"}, {.05, 0}]};
ShowMe[obj]
```

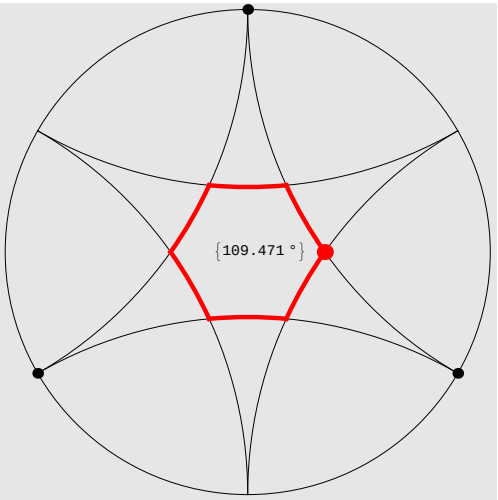

HalfRegPoly[n,phi,psi] returns the halfregular polygon with n edges and alternating angles phi and psi. Here a small tessellation with angles $\pi/3$ and $2\pi/3$ and a free number of edges n $\geq$ 6 .

```
n = 12;
poly = HalfRegPoly[n, Pi/3, 2Pi/3];
If[
EvenQ[n] == False||n < 6,
Print["choose n even and ≥ 6"]; Abort[],
copies = Table[RotateC[poly, Pi/3, i, poly[[j]]],
{i, 5}, {j, 2, n + 1, 2}];
pavage = Map[GraphPolyC, copies, {2}];
ShowMe[pavage]]
```

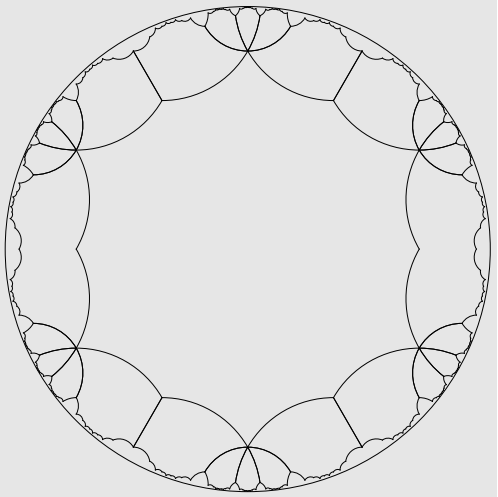

The disk can also be tessellated with regular "ideal" polygons, whose vertices are at infinity on the unit disk, the angle is zero.
with ideal n-edged polygons turning m times around the vertices. For n = 4 the surfaces is the 1-punctured torus.
InfTess[n,m] returns and **ShowInfTess[n,m]** displays the tessellation for n edges and m copies around the vertices of the central tile. A widely used representative is the 1-punctured torus with n = 4 and any m.

```
ShowInfTess[4, 10]
```

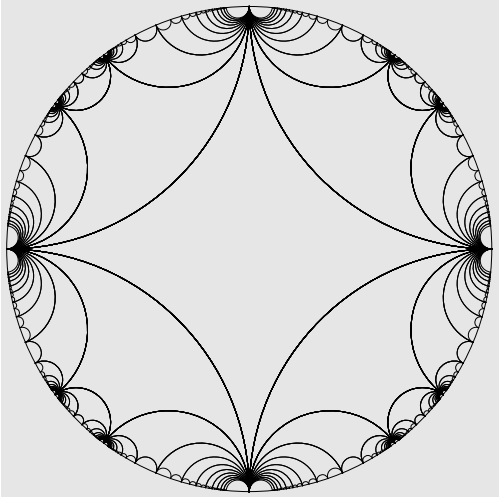

Using n = 3 returns a modular group tessellation, the vertices of each triangle are a triple of rational neighbours $\frac{p}{q}$ $\frac{p+q}{r+s}$, $\frac{r}{s}$ (Cayley fractions)

```
p = InfTess[3, 10];
obj = {
Apply[ArcC, p, 2],
Text["0/1", {−.5, .95}],
Text["1/4", {−.04, 1.05}],
Text["1/3", {.15, 1.05}],
Text["2/5", {.31, 1.01}],
Text["1/2", {.52, .92}],
Text["3/5", {.75, .76}],
Text["2/3", {.88, .65}],
Text["3/4", {.97, .5}],
Text["1/1", {1.03, .05}]
};
ShowMe[obj]
```

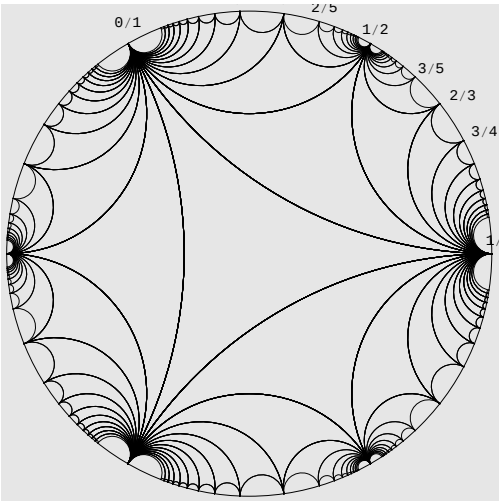

PolygonC[x,color,lev], the hyperbolic version of Polygon, is the graphic instruction for a filled closed polygon given by the list x of vertices. It uses Polygon over a discretisation taking lev-times the Euclidean midpoints. Default value is lev = 3.
Here is the description of the three hyperbolic moves as mirroring against two geodesics.

The regular quadrilateral is mirrored against the first geodesic to the dashed quadrilateral. Mirroring anew against the blue geodesic returns the rotation around the crosspoint of the geodesics. The red parallel geodesic infers a horocycle rotation around the common point at infinity. The green ultra parallel geodesic generates a translation along the common perpendicular as unique invariant line.

```
quadri = RotateC[RegPoly[4, Pi/3], Pi/3, 1, -.7];
z = e^(i 2π/2.8) //N; w = e^(i 3π/2.2) //N; y = e^(i π/12) //N;
u = e^(i π/3) //N; v = e^(-i π/6) //N;
obj = {
GraphPolyC[quadri],
ArcgeoC[z, w],
ArcgeoC[y, -y, 0],
ArcgeoC[w, -w, 2],
ArcgeoC[u, v, 4],
{Dashing[{.01}],
GraphPolyC[MirrorC[quadri, z, w]]},
PolygonC[MirrorC[MirrorC[quadri, z, w], y, -y], 0],
PolygonC[MirrorC[MirrorC[quadri, z, w], w, -w],
2],
PolygonC[MirrorC[MirrorC[quadri, z, w], u, v], 4]
};
ShowMe[obj]
```

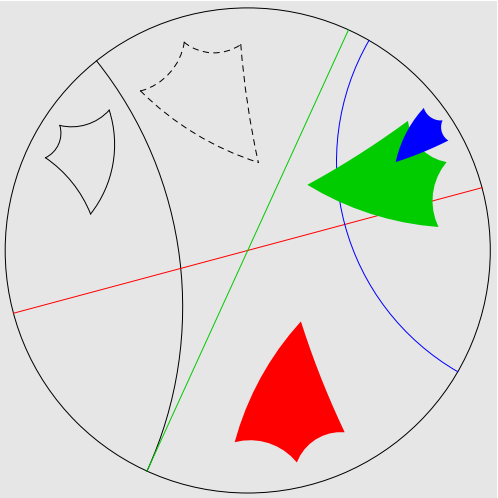

Appendix C.

Pinacotheca

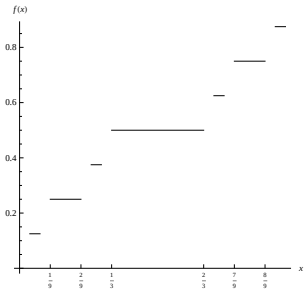

About_Cantor Created by Stan Wagon. Cantor sets, Cantor function.

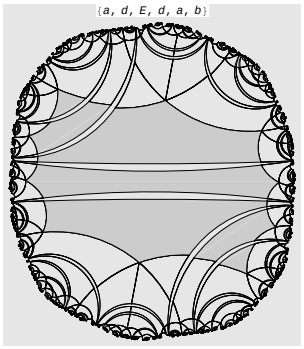

***** Big_Quake_Georama** Hundreds of simple geodesics of one up to six letters. Random or chosen selection. Choice of fineness of tiling. All Möbius moves.

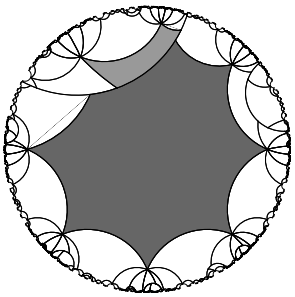

Bubbles_Equake_octo Tessellation of an earthquake in the octagon model.

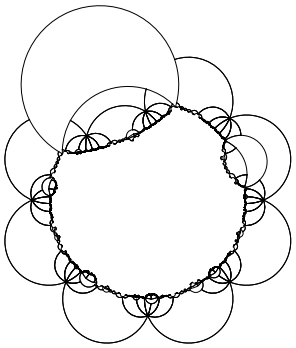

Bubble_Graft_Inv_octo $\mathbb{C}P^1$ Tessellation in the octagon model showing the grafted inner and the pruned outer Poincaré disk.

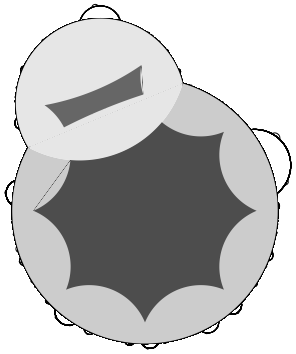

Bubble_Graft_octo $\mathbb{C}P^1$ Classical tessellation of grafting in the octagon model. Alternatively tessellation with Poincaré disks 'Mickey Mouse ears'.

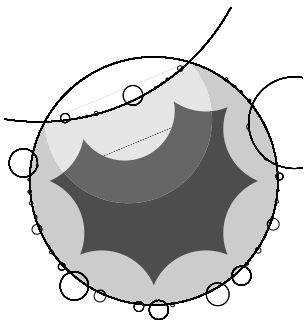

Bubble_Prune_octo $\mathbb{C}P^1$ Classical tessellation of pruning in the octagon model. Alternatively tessellation with Poincaré disks 'Mickey Mouse inside out ears'.

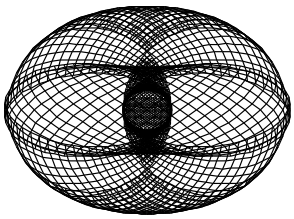

Comp_Surf_Ekki Created by Dr. Ekkehard-H. Tjaden. Visualizes the tile of the decagon model in $\mathbb{S}^3$.

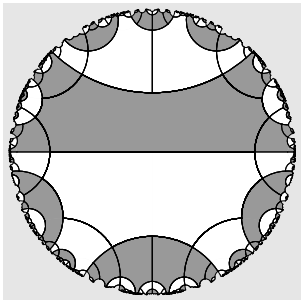

Double_Pants Black & white or colored tessellation of a pretzel as doubled pair of pants.

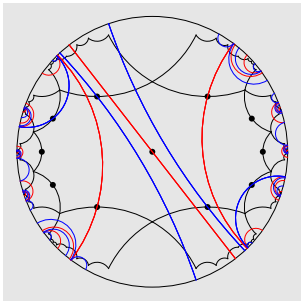

Duelling_geos An extension of Lamination with a view to shows a sequence of laminations through two simple geodesics with an increasing number of leaves.

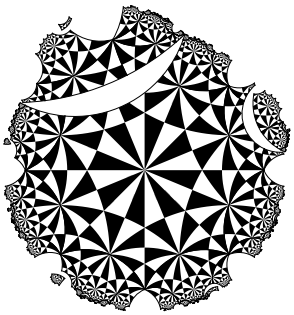

***** Earthquake_96_tri** All Möbius moves on the tessellation where the octagon is made of 96 black and white triangles.

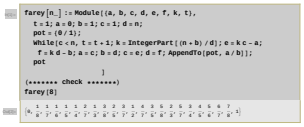

```
farey[n_] := Module[{a, b, c, d, e, f, k, t},
  t = 1; a = 0; b = 1; c = 1; d = n;
  pot = {0 / 1};
  While[c < n, t = t + 1; k = IntegerPart[(n + b) / d]; e = k c - a;
   f = k d - b; a = c; b = d; c = e; d = f; AppendTo[pot, a / b]];
  pot
  ]
(******* check *******)
farey[8]
```

Farey_play Several instructions for computing Farey sequences of given length, denominator or finding the neighbours of a fraction.

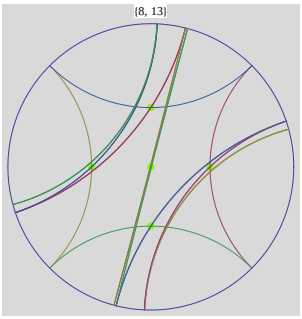

Farey_torus Visualizes simple geodesics on the 1-punctured torus. Choose a real number. Choose a fraction in the proposed Farey-sequence. Can compute quickly very long words.

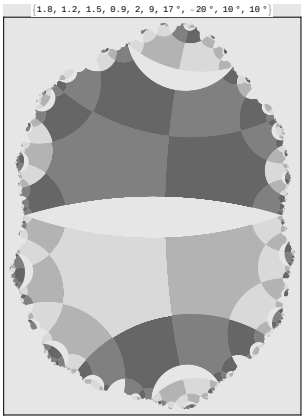

***** Flying_fractals** Visualizes a Möbius move along the real axis. Uses the 14-gon pretzel model. The tile is made of fronts and backs of two pairs of pants, each four part in a different color. Parameters to select: length of every second edge of the hexagonal subtile, break condition for the fineness of the tiling,all 9 possible side pairings, angles for grafting, pruning, twisting to the right or to the left, rendering in 4-colors or in gray tones.

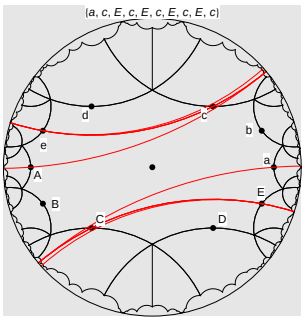

Geo_Finder_deca Visualises closed geodesics on the decagon model of the pretzel. Zooming is possible. Enter any word as 'choice' or load the database 'Allchoice' listing preselected simple geodesics. Returns a complete diagnostic of the word, specially simple or intersecting, Birman Series test, separating or not.

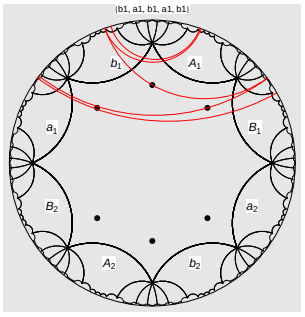

Geo_Finder_octo Visualizes closed geodesics on the octagon model of the pretzel. Returns simple or intersection points.

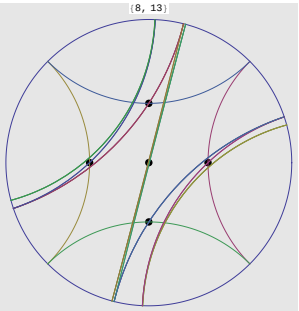

Geo_Finder_torus Visualizes closed geodesics on the 1-punctured torus. Zooming is possible. When entering a real number a Farey suite is returned. Very long words can be tested.

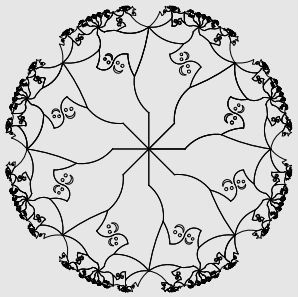

Hyperbolic_ghosts Tessellates the octagon with non geodesic tiles. Choose a point in the triangle and draw your irregular tile.

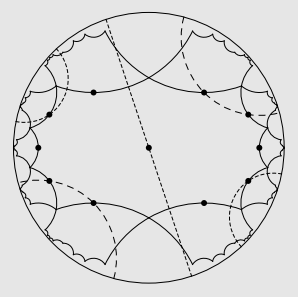

Lam_2geos_deca Tests a lamination with two simple geodesics in the decagon model of the pretzel.

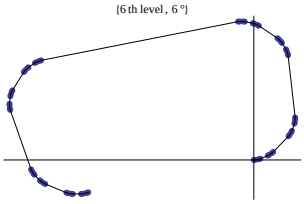

Lamination_measure Removes the gaps of a Cantor function for getting a Dirac-measure. Implements this measure on transversals to a lamination from a simple closed geodesic.

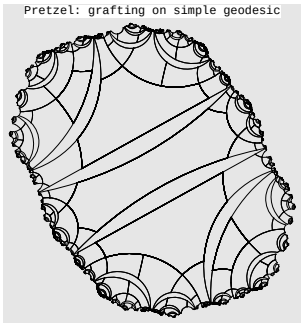

Pretzel_Grafting_tess Tessellation of grafting along a 4-leaved geodesic in the 14-gon model.

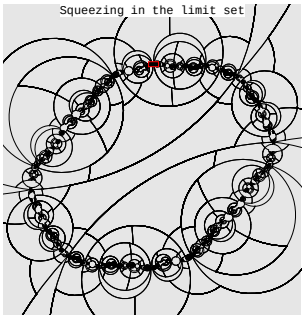

Pretzel_Pruning_tess Tessellation of pruning along a 4-leaved geodesic in the 14-gon model. Also inner and outer tessellation on $\mathbb{C}P^1$.

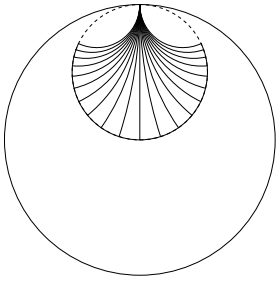

Pseudosphere_disk $\mathbb{C}P^1$ Mapping of a layer of the pseudosphere onto the Poincaré disk.

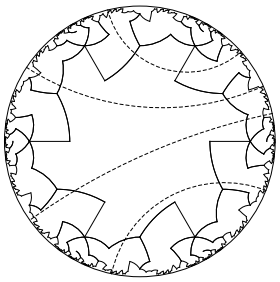

$S3$**_comic_tess** Tessellation from a not convex polygon in the decagon model of $\mathbb{S}^3$. 4-leaves simple closed geodesic.

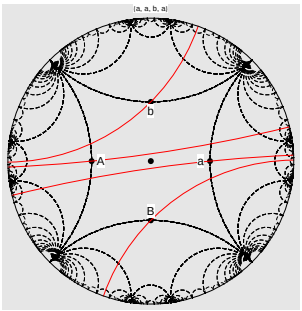

Simple_geos_torus . Has additional features to Geo_Finder_torus. One can test any (not too long) words. The self intersections are returned. All alternative words obtained by permutation of the letters are reported simple or not.

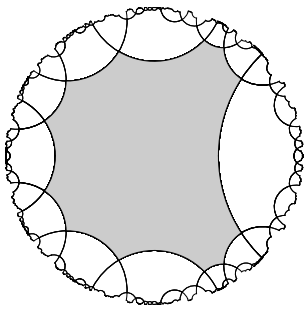

Tess_dodeca_skew Tessellation in the dodecagon model, where the hexagonal subtile has three different every alternate edge lengths.

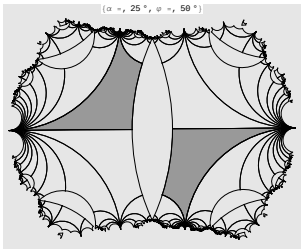

***** Torus_fractal** Möbius moves along a vertical 1-leaved geodesic of the 1-punctured torus. Rendering in harlequin for sake of beauty or in gray for observing the limit happenings.

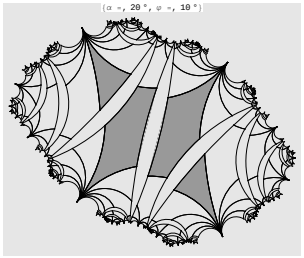

Torus_surgery Möbius moves along a $(1, 2)$ geodesic of the 1-punctured torus.

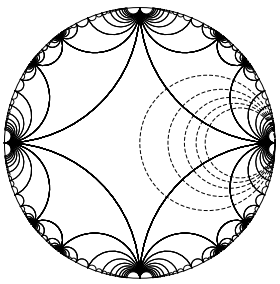

Traktrix_etc Visualization of the tractrix and of horocycles in the tiling of the 1-punctured torus.

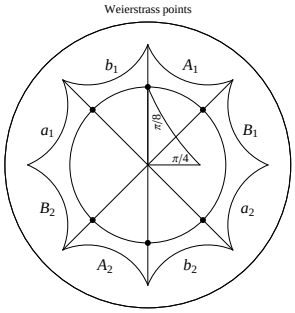

Weierstrass_octo Exact localisation of the Weierstrass points on the octagon.

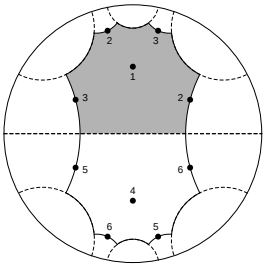

Weierstrass_pts Doubling of a perforated torus to locate Weierstrass points.

Bibliography

[1] R. Benedetti, C. Petronio: Lectures on Hyperbolic Geometry, *Springer-Verlag, 1992*

[2] Alan F. Beardon: The Geometry of Discrete Groups, *Springer-Verlag 1983*

[3] Joan Birman, Caroline Series: An Algorithm for Simple Curves on Surfaces, *J. London Math. Soc. 2. 29. 1984*

[4] Francis Bonahon: Geodesic Laminations on Surfaces, *American Mathematical Society, 1997*

[5] Francis Bonahon: Closed Curves on Surfaces, *University of Southern California, 2000*

[6] Francis Bonahon: Earthquakes on Riemann Surfaces and on Measured Geodesic Laminations, *Transactions of American Mathematical Society, 1992*

[7] David A. Brannan, Matthew F. Esplen, Jeremy J. Gray: Geometry, *Cambridge University Press, 1999*

[8] Keith Burns, Marion Gidea: Differential Geometry and Topology, *Chairmann & Hall, 2005*

[9] H.S.M. Coxeter: Crystal symmetry and its generalizations, *Royal Society of Canada(3), 51 (1957), 1-13*

[10] Canary, D.B.A.Epstein, P. Green: Notes on Notes of Thurston, *Cambridge University Press, 1987*

[11] Martin d. Crossley: Essential Topology, *Springer-Verlag, 2005*

[12] D.B.A. Epstein: Analytical and Geometric Aspects of Hyperbolic Space, *Cambridge University Press, 1984*

[13] R. Fricke, F. Klein: Vorlesungen über die Theorie der automorphen Funktionen, *Teubner, Leipzig, 1912*

[14] William Fulton: Algebraic Topology, *Springer-Verlag, 1995*

[15] Alfred Gray: Modern Differential Geometry of Curves and Surfaces, *CRC Press, 1994*

[16] Chaim Goodmann-Strauss: Compass a´nd Straightedge in the Poincaré Disk, *Amer. Math. Math. Monthly 108, 38-49, 2001*

[17] Andrew Haas, Perry Susskind: The Geometry of the Hyperelliptic Involution in Genus Two, *Proceedings of The American Mathematical Society, Vol.105 nb. 1, 1989*

[18] Klaus Jänich: Topologie, *Springer-Verlag, 1980*

[19] Ravi S. Kulkarni, Ulrich Pinkall: A Canonical Metric for Möbius Structures and its Applications, *Springer-Verlag Mathematische Zeitschrift, 1994*

[20] Wolfgang Kühnel: Differentialgeometrie, *Vieweg Studium, 1999*

[21] John McCarthy, Athanase Papadopoulos: Fundamental domains in Teichmüller space, *Annales Academiae Scientarium Fennicae Mathematica Volumen 21, 1996*

[22] Curtis T. McMullen: Complex earthquakes and Teichmüller theory, *Journal of American Mathematical Society, 1996*

[23] Wilhelm Magnus: Non Euclidean Tessellations and Their Groups, *Academy Press, 1974*

[24] Benoit Mandelbrot: Self-Inverse Fractals Osculated by Sigma-Discs and the Limit Sets of Inversion Groups, *The Mathematicla Intelligencer, Springer-Verlag, 1983*

[25] Greg McShane: Simple Geodesics and A Series Constant over Teichmuller Space, *UMPA Ecole Normale Supérieure, Lyon, 1995*

[26] Greg McShane: Weierstrass Points and simple Geodesics, *London Mathematical Society, 2004*

[27] Greg McShane: Simple Geodesics on Surfaces of Genus Two, *Annales Academiae Scientiarum Fennicae Mathmatica, vol. 31, 2006*

[28] David Mumford, Caroline Series, David Wright: Indra's Pearls, *Cambridge University Press, 2002*

[29] Tristan Needham: Visual Complex Analysis, *Oxford University Press, 1997*

[30] Bernd Oberknapp, Konrad Polthier: Visualization and Mathematics, *Springer Verlag, 1997*

[31] Erich Ossa: Topologie, *Vieweg Studium, 1992*

[32] Henri Poincaré: Analysis Situs, *Journal de l'École Polytechnique ser 2, 1 pages 1-123, 1895*

[33] Caroline Series: Geodesics with Bounded Intersection Numbers on Surfaces Are Sparcelly Distributed, *Topology - Vol. 24, 1985*

[34] John Stillwell: Geometry of Surfaces, *Springer-Verlag, 1992*

[35] John Stillwell: Classical Topology and Combinatorial Group Theory, *Springer-Verlag, 1993*

[36] William P. Thurston: Three-Dimensional Geometry and Topology, *Princeton University Press, 1997*

[37] Stan Wagon: Mathematica® in Aktion, *Spektrum, Akad. Verlag, 1993*

Index